Department of Precision and Microsystems Engineering

Localization and Transport of Biomolecules on 2D Hexagonal Boron Nitride Surfaces

Trey Cranney

Report no : 2022.019
Coach : Dr. Dong Hoon Shin
Professor : Dr. Sabina Caneva
Specialisation : MSD-MNE
Type of report : Master's Thesis
Date : 13 June 2022

Delft University of Technology

High Tech Engineering Thesis

Localization and Transport of Biomolecules on 2D Hexagonal Boron Nitride Surfaces

Author:
Trey Cranney

Supervisors:
Dr. S. Caneva
Dr. D. H. Shin

in partial fulfilment of the requirements for the degree of

Master of Science

in Mechanical Engineering

to be defended publicly on Monday June 27, 2022 at 02:30 PM.

Abstract

This report will investigate the manipulation of biomolecules on 2D hexagonal boron nitride (hBN) crystal surfaces. The goal of this research is to explore the potential for a device that utilizes the interaction between biomolecules and hBN as a new approach to protein sequencing. Our hypothesis is that molecules adsorbed to hBN surfaces can be unfolded and moved at a controlled velocity through the use of shear horizontal surface acoustic waves. These surface acoustic waves utilize acoustoelectric effects that create forces on polarizable molecules. Until this point, the use of surface acoustic waves for manipulation of molecules has not been explored in the framework of single-molecule sequencing. Along with this, the surface interaction between biomolecules and hBN has been investigated primarily with simulations, while experimental confirmations are still lacking. To address this gap in the field, we conducted experiments to fluorescently image lambda DNA, M13mp18 DNA, and α-synuclein proteins adsorbed to hBN surfaces and analysed their free diffusion behavior. We subsequently designed, fabricated and characterized shear horizontal surface acoustic wave devices compatible with measurements in fluid and with an inverted fluorescence microscopy setup. Here, we studied the behavior of the same molecules adsorbed to an hBN surface when subject to acoustic actuation. It was found that limited diffusion effects were visible for α-synuclein proteins and M13mp18 DNA. However, it was possible to observe fragmented lambda DNA freely diffusing on the hBN surface. When acoustically actuated it was found that α-synuclein proteins and M13mp18 DNA located on the hBN surface could not be manipulated. Lambda DNA molecules that were in contact with the hBN surface could be manipulated through acoustic actuation. These findings open up further research opportunities for the use of shear horizontal waves in manipulation of molecules on 2D material surfaces.

Contents

1 Introduction

Proteins play a critical role in a myriad of biological functions in an organism. While DNA is regarded as the "instructions" upon which an organism operates, proteins are the workforce behind many of these complex operations. These proteins do everything from copying DNA to producing muscle motion.[1] Protein analysis can provide critical information about the underlying biological processes that are occurring in every living organism. By knowing the sequence of amino acids that make up a protein it is possible to determine the structure of said protein. This structure is what dictates the function that a protein serves in physiological processes.[2] The field that studies the composition of proteins and how this composition affects biological functions is referred to as proteomics.[3]

Currently, the depth and coverage of protein sequencing is lacking compared to the routinely used whole-genome profiling that is possible with DNA sequencing methods. Proteomics is still awaiting the leap in innovation that took place in the DNA sequencing field.[4] This lag in sequencing capacity is clearly visible in the missing proteome or 'dark' proteome. This missing proteome refers to proteins that have never been measured before but for which we have evidence from transcription data.[3,5] Up until this point only around 56% of the predicted human genome has been mapped to a full-length protein despite having sequenced the human genome nearly thirty years ago.[5] The lack of rapid and parallel sequencing methods for proteins has resulted in this large gap in our knowledge about the proteome and must be addressed in order to truly understand, and potentially predict, the biological functions and malfunctions of the human body.

In order to work towards creating rapid parallel sequencing methods for proteins, it is important to first consider the unique challenges presented by the nature of proteins. If it was possible to directly apply DNA sequencing methods to proteins, then the proteome would have already been sequenced. The main challenges that are limiting the use of existing technology for proteomics are as follows:

1. **Dynamic range**. No known amplification process such as polymerase chain reaction (PCR) exists for proteins which restricts the available concentration to what is found in cells. The protein concentration ranges from picograms per milliliter (interleukin) to milligrams per milliliter (albumin).[1,6] This means that protein sequencing devices must have extremely large dynamic ranges upwards of 10^9 in order to comprehensively sequence the proteins in a single cell.[1] It also means that the detection limit of protein sequencers must be very low in order to detect proteins with low concentrations. If this detection limit is high it means millions of cells worth of proteins would need to be analyzed in order to detect the lowest concentration proteins.[6] In order to truly map the human proteome, sequencing even the lowest concentration of proteins is critical.

2. **Charge**. DNA inherently has a negative charge that allows for relatively simple control of the motion of the particle via electrophoresis for instance. Proteins have a mixture of positive and negative local charges resulting in a low or neutral global charge that depends on the protein composition. This mixed charging makes controlling the sequencing process through electrophoresis much more difficult.[4] The differences between proteins and DNA mean that existing DNA sequencing methods often will not function for proteins. However, the methodologies behind DNA sequencing technologies can be applied to protein sequencing technologies to create a base of work to build upon.

3. **Composition**. Proteins are composed of over 20 different amino acids while DNA is only composed of four bases. It is a large challenge to be able to distinguish 20 distinct output signals regardless of the read-out method used.[1] This means that the readout of a protein sequencer is inherently more complicated than a DNA sequencer.

Through a combination of existing genomics technologies and the rapidly advancing field of proteomics, it will become possible to open new avenues into synthetic biology, drug discovery, and even personalized medicine.[3] However, there is still a large amount of innovation that must occur. The driving goal of this field is to develop a method for highly sensitive high throughput sequencing of proteins.[1] This goal requires the development of new technologies that build upon the success of DNA sequencing methodologies, but are applicable to the unique characteristics of proteins.

2 Protein Sequencing State of the Art

In order to determine a suitable research question that will contribute to the advancement of the proteomics field, it is first critical to discuss the current state of the art sequencing methods. There are many different approaches that can be used to sequence proteins. These methods range from well-established methods to theoretical concepts. Figure 1 summarizes the various possible platforms for protein sequencing.

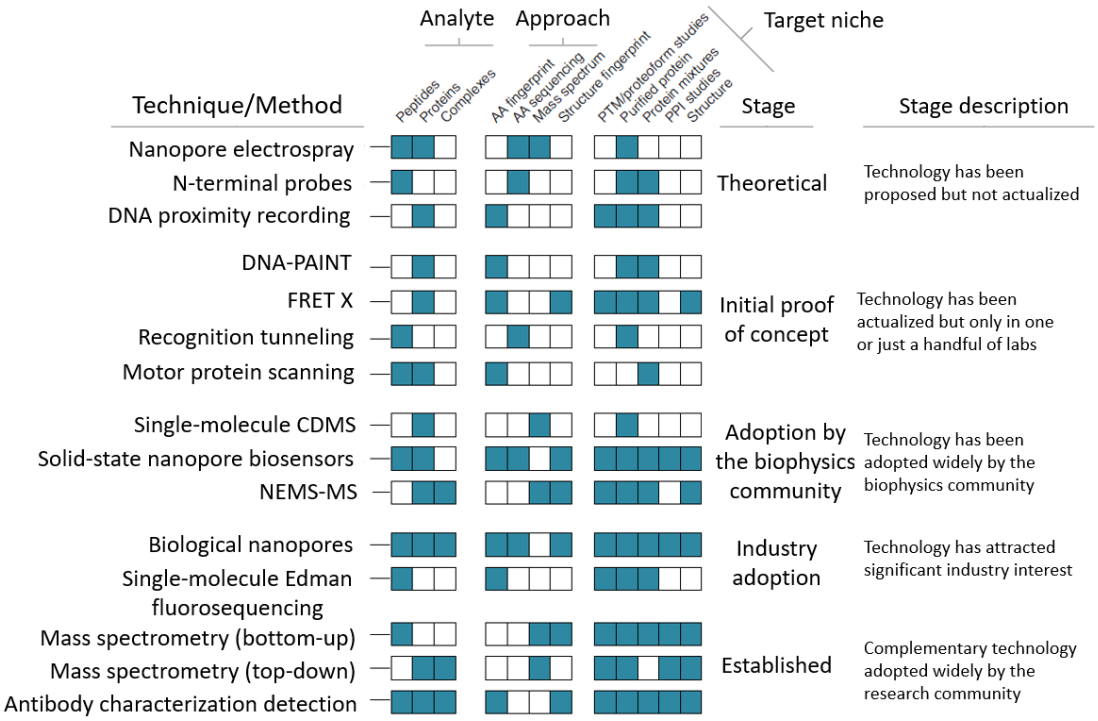

Figure 1: Overview of protein sequencing methods and their development status. Adapted from Alfaro et al. (2021).[4]

As can be seen in Figure 1, there are many different approaches to protein sequencing but only a few have reached a point of wide spread adoption. Well-established sequencing and analysis methods such as Edman degradation, immunoassays and mass spectroscopy have reached maturity and are widely implemented. However, these methods each have their limitations that restrict their ability to quickly and accurately analyze the proteome.

2.1 Current Protein Identification Methods

I will begin by discussing the features and limitations of three technologies that are currently widely used for protein analysis: Edman degradation, immunoassays, and mass spectroscopy.

1. **Edman degradation** is a process that allows for the ordered identification of a chain of amino acids from the N- to the C-terminus.[7] This is accomplished through a cycling chemical reaction that labels, cleaves, and identifies one amino acid at the end of the protein. Edman degradation is an extremely useful tool that allows for single molecule sequencing of peptides. This process usually has very low error which allows for reliable sequencing results.

   However, there are large drawbacks to this process. The first of these drawbacks is the fact that Edmand degradation is limited to the analysis of high purity peptides of a length shorter than 50 amino acids. This means that large proteins must be broken up into many peptides for analysis. Another drawback is that each degradation cycle can take upwards of 45 minutes, which results in extremely long measurement time for a single protein.[1]

2. **Immunoassays** have been extensively adopted as a semi-analytical method of detecting proteins. Immunoassays depend on the use of either polyclonal or monoclonal antibodies to recognize specific parts of a protein.[8,9] Generally, the sample to be analyzed is exposed to a wide set of different antibodies in order to detect the presence of different peptide sections. By exposing the sample to a large number of antibodies it is possible to determine the protein composition and concentration.

   The main challenge facing the use of immunoassays for analytical analysis is the low specificity of the method. For this technology to be of use for analytical evaluation of proteins, the immunoassays must be designed with high specificity to prevent cross-reactions with multiple target proteins.[9]

3. **Mass spectrometry** is the gold standard for proteomic analysis that measures the mass to charge ratio of charged peptides or proteins.[4] This is achieved by digesting proteins into peptides that are then put through a chromatography process in order to separate them according to hydrophobicity and charge.[1] This method is a bulk technique and is not yet capable of true single-molecule sequencing.[6] In theory, mass spectrometry can measure molecules that in attomolar concentration.[3] In practice, the measurement range is restricted by how rigorous the separation is. The level of separation of the digested peptides directly affects the resolution of the process.[3,6] Generally peptide mapping using mass spectrometry requires concentrations in the picomolar range.[3] As mentioned in section 1 this minimum detection limit is insufficient to identify low abundance proteins. Mass spectrometry also is restricted in its dynamic range. State of the art mass spectrometers have a dynamic range of around 10^4 to 10^5.[1] In order to comprehensively analyze human plasma samples it was found that a dynamic range of 10^9 is required.[1,6]

2.2 Nanopore Sequencing Advantages and Challenges

It is clear that the protein identification methods currently at our disposal have inherently restricted capabilities. As such, many new and experimental protein sequencing and analysis methods are under development. One of the most promising research directions is based on nanopore technologies[4]. This approach builds upon the success in DNA sequencing with

nanopore membranes. In a typical DNA nanopore experiment an insulating membrane containing a nanometer sized hole is placed in between two electrolyte filled cavities.[10] A potential is then applied across the membrane which induces an ionic current through the pore. This ionic current is measured and as strands of DNA pass through the pore, fluctuations are recorded, which correlate to the DNA nucleotides passing through the pore, thereby allowing for the sequencing of the molecule.[1,11] A similar sequencing concept to this can be used to sequence proteins. An illustration of this concept is shown in Figure 2.

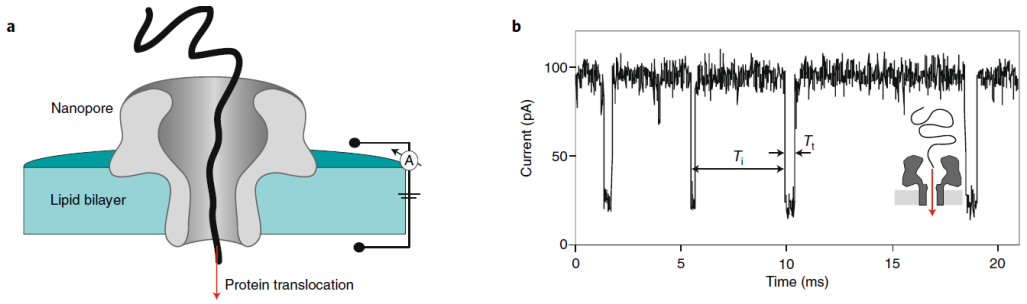

Figure 2: **a)** Schematic of a biomolecule translocating through a nanopore and **b)** characteristic ionic current signal from several translocation events.[1]

As previously discussed, DNA and proteins have differences that challenge the direct application of DNA sequencing technologies for proteins. In the following sections, these challenges are outlined.

2.2.1 Controlled Translocation

DNA has a global negative charge but proteins have a wide range of local charges that often result in a low or neutral global charge. Because of this lack of global charge, the transport of the protein through the nanopore is not easily induced. The translocation of a protein can be driven by either electrophoretic force or electro-osmotic force. As each protein experiences a different translocation force due to their individual charge profiles it is necessary to modify proteins to enable easier translocation through the pore. A modification that is commonly made is to use sodium dodecyl sulphate (SDS) as a denaturant. SDS will both unfold proteins and wrap them with a homogeneous negative charge through the use of attached sulphate groups. This allows the proteins to be translocated across the nanopore in a more controllable manner.[12] A second method used is the attachment of a negatively-charged oligonucleotide strand to one of the terminus of a protein. The attached oligonucleotide allows the protein to be dragged through the nanopore using electrophoretic forces. This approach was successfully demonstrated for solid-state nanopores and increased the number of translocation events.[3,13] Both of these methods are displayed graphically in Figure 3.

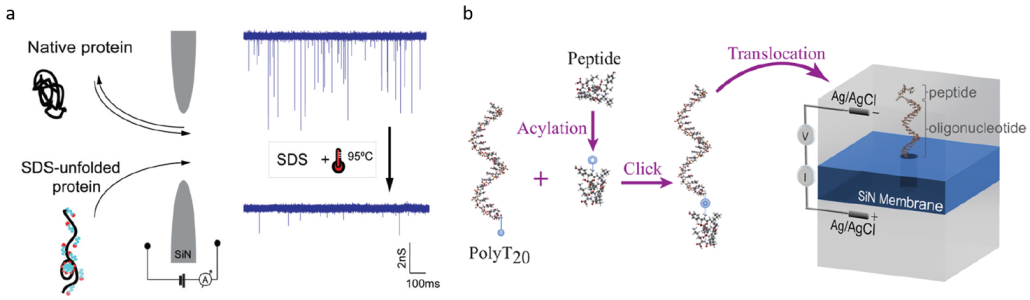

Figure 3: **a**) Translocation of native and SDS-coated protein and respective current traces.[12] **b**) Attachment of oligonucleotide strand to the peptide for guided translocation.[13]

In both cases it was found that while translocation through the solid-state nanopore is achieved, it occurs in under 1 millisecond. This translocation speed is too fast to accurately sequence a protein. In order to make nanopore-based sequencing feasible (i.e. with sufficient temporal resolution), it is critical that a method of slowing down translocation be developed. By being able to control the speed of translocation it will be possible to accurately read the different amino acids of the molecule as they pass through the solid state nanopore.[1]

2.2.2 Protein Folding

Another large difference between proteins and DNA is the degree of folding that proteins inherently display. Proteins fold locally and globally into secondary and tertiary structures that facilitate different biological functions.[14] Currently it is possible to sequence digested peptides through nanopores due to their lack of stable tertiary folding. However, in order to sequence full length proteins, it is necessary to use an unfolding method.

Multiple chemical and physical methods for protein unfolding has been proposed and analyzed. The most commonly used method is the use of strong denaturing chemicals such as SDS or guanidine hydrochloride.[1] This chemical unfolding of proteins is best suited for use in solid-state nanopores as biological nanopore are prone to denaturing.[1] This often restricts the use of biological nanopores to short peptide sequencing. For sequencing full length proteins new methods of controlled translocation speed through solid-state nanopores must be explored.

2.2.3 High Fidelity Signal Output

One of the main challenges for the implementation of nanopores in protein sequencing is the method of signal output and analysis. In DNA sequencing there are only four unique signals that must be distinguished, while in protein sequencing there are 20 unique signals that have to be differentiated. In terms of signal output, there are three main methods for identifying proteins. The first is through traditional ionic current measurement of a linearized protein, the second is through fluorescence time-traces, and the third is through ionic current measurements of folded proteins with lipid tethers.[4] These three processes are schematically shown in Figure 4.

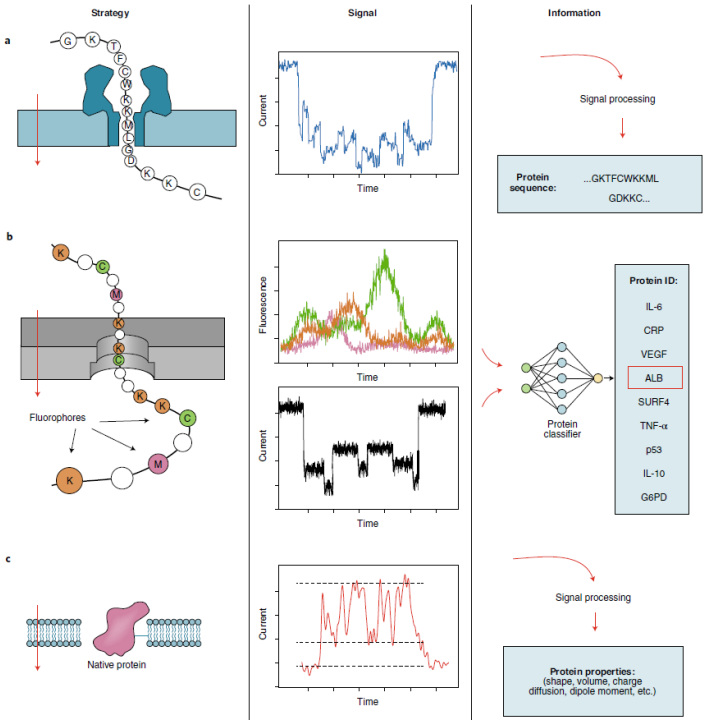

Figure 4: Signal output methods for 3D nanopores using ionic currents (a and c) and fluorescence time traces (b) for sensing proteins characteristics (e.g. dynamics etc.).[4]

In Figure 4a, the traditional form of single amino acid sequencing using the ionic current of the protein passing through the nanopore can be seen. This method is attractive due to its straight forward implementation in solid-state nanopores. However, this method can also be challenging due to the difficulty in distinguishing a unique current level for all 20 amino acids. A large limitation to distinguishing these current measurements is the inability to control translocation speed of particles through a nanopore. Very fast translocation, as is often seen in solid-state nanopores,[14,15] can result in a noisy transient output signal that can be difficult to analyze.[15] The third method presented in Figure 4c works on a similar premise as the ionic current sequencing method. However, in this method the protein is left in its native form and is tethered into a pore using lipids. This method allows for analysis of the shape, volume, charge diffusion, and dipole moment.[4] However, this measurement does not allow for the sequencing of the amino acids in the protein which limits its usefulness to this study.

The second method that was presented in Figure 4b is the use of fluorescence signals to create a fingerprint of the protein. In this method fluorescent molecules are attached to a specific subset of the amino acids of the protein and are used to generate an output fluorescence signal as they pass through the nanopore. This method is advantageous as it is a very fast process and can be massively parallelized.[1] However, this method of output is limited by the number of available fluorescent markers. There are fluorescent markers that can be attached to some but not all of the 20 different amino acids. Despite this, it has been shown that even using just three fluorescent markers it is possible to identify 95% of the proteins in the human proteome with high confidence.[4,16] While this method is not true sequencing, it allows for protein identification from partial sequence information.

3 Interaction between Biomolecules and 2D Materials

Flat 2D nanochannels are a very new technology that may be able to address some of the challenges that traditional 3D nanopores face. The premise of this technology is to apply the unique properties of 2D materials to the challenges found in 3D nanopores. These nanochannels can consist of heterostructures made of two or more in-plane materials or can be made with a single material. The structure and materials that are chosen dictate the behavior and performance of the nanochannels.

3.1 2D Materials

One class of materials that is especially interesting for the fabrication of nanochannels are crystalline 2D materials. These are layered crystals that hold unique mechanical and electrical properties as a result of their atomically thin nature and unusual electronic band structures. Nanofabrication techniques such as reactive ion etching and ebeam lithography enable the generation of narrow constrictions and channels in a wide variety of 2D materials such as graphene, hBN, WS_2, MoS_2, $MoSe_2$, and WSe_2.[17] Of these, graphene and hexagonal boron nitride (hBN) can be of particular interest due to their interactions with biomolecules and their bio-compatible nature.[18,19]

Both hBN and graphene possess similar crystal structures. While graphene is a planar hexagonal lattice made of sp^2 hybridized carbon atoms, hBN consists of a planar hexagonal lattice arrangement of boron and nitrogen atoms. It has been found that the lattice mismatch of hBN and graphene is only 1.5%.[20] This means that these two materials can be nearly seamlessly stitched together into heterostructures.[21,22] The interlayer forces of both of these materials are weak van der Waals forces, which means that it is possible to produce atomically thin layers of hBN and graphene through the use of mechanical exfoliation. Using exfoliated crystals and deterministic stamping, atomically thin flakes of these 2D materials can be accurately positioned and integrated onto larger functional devices.[20,23]

Both graphene and hBN have unique interactions with biomolecules that are of interest for sequencing. It has been observed that the components of both DNA and proteins will actively adsorb onto hBN and graphene surfaces.[24,25] During this adsorption, the van der Waals forces and hydrophobic interactions of biomolecules towards hBN and graphene is believed to result in structural unfolding on the crystal surfaces in the case of hBN.[19,24,26] The unfolding of biomolecules onto the surface of these 2D crystals is a unique and potentially exploitable phenomenon.

The effect of graphene and hBN on biomolecule fluorescence should also be noted. Fluorescence of a biomolecule is important as it can be used for both motion tracking and sequencing purposes. As such, it is undesirable for the materials used in a sequencing setting to quench the fluorescence of the biomolecule being analyzed. For hBN it has been found that fluorescence is not actively quenched when biomolecules are adsorbed to the surface.[27] It is also possible to generate single photon emitters on the surface of hBN that can serve as a readout method for fluorescent tags attached to a protein.[28,29] On the other hand, previous work has shown that graphene does in fact suppress the fluorescence of many biomolecules.[30,31] This is due to non-radiative coupling between between the emitter (e.g. fluorophore) dipole and electron-hole pair excitations in graphene..[32] Therefore, the application of graphene in a device that requires fluorescent readout can be detrimental to performance as graphene acts as a very efficient energy

sink.[33]

3.2 Nanochannels

One of the most important functions of a nanopore is the localization of the biomolecule that is to be analyzed. Without trapping and localization of the molecule it is very difficult to deterministically study its structure and properties. In 3D nanopores, this localization is implemented using the geometry of the pore.[1,3] As a molecule passes through this pore, it is possible to analyze the composition of the molecule if it is linearized and threaded from one end to the other.

It may be possible to exploit biomolecule unfolding from 2D material interaction to assist with localization during translocation of a nanopore. Utilizing graphene, this concept has been simulated for use in a traditional solid-state nanopore configuration as seen below in Figure 5.

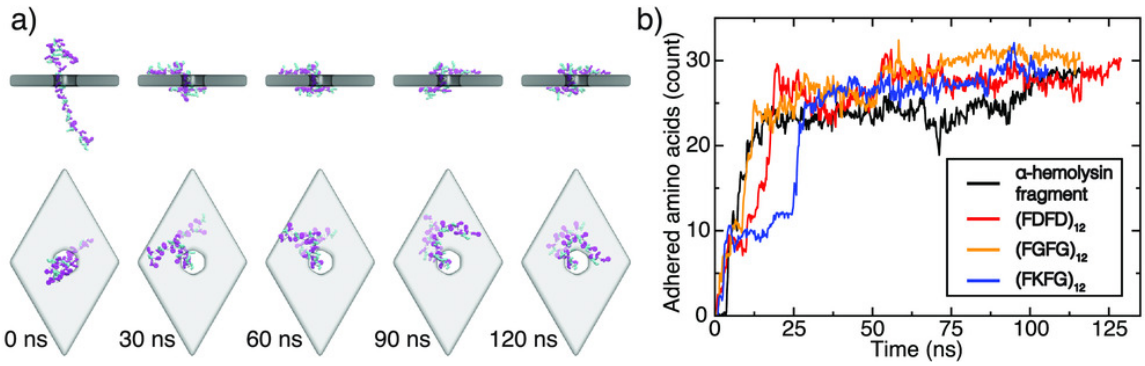

Figure 5: **a)** Molecular Dynamics simulation of graphene nanopore with biomolecule translocating through pore **b)** Simulation of number of adsorbed amino acids to graphene surface[34]

In this Figure the peptides adsorb to the graphene surface and exhibit stepwise translocation when subject to a transmembrane bias or a hydrostatic pressure gradient.[34] The stepwise translocation of the peptides inherently restricts the translocation speed. Utilizing similar methodology it is possible to develop new sequencing techniques that have different form factors than traditional nanopores. One such method that utilizes the properties of 2D materials is the use of nanochannels made from hBN, graphene, or both. Our hypothesis is that 2D nanochannels can provide an alternative linearization and transport avenue that feeds directly into a sequencing output and is therefore of particular use for single molecule sequencing.

By exploiting the characteristics of graphene and hBN it is possible to develop systems that can constrain and control translocation of proteins and other biomolecules. One example of such a system is an hBN/graphene 2D nanochannel. A simulation of this proposed system can be seen in Figure 6.

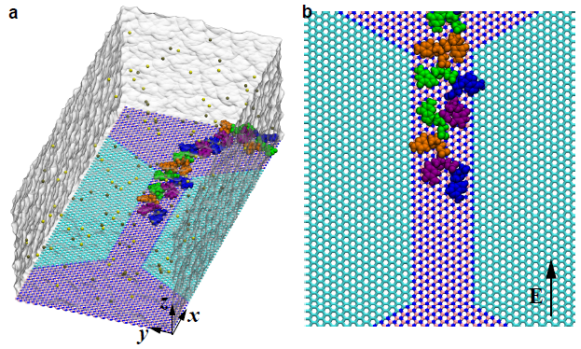

Figure 6: hBN nanochannel surrounded by graphene with DNA adsorbed to surface of the hBN.[17]

2D nanochannels in theory offer advantages over traditional 'bulk' solid-state nanopores in two main areas: 1) controlled unfolding before the biomolecules enter the pore region and 2) potential for controllable translocation speeds. The details of how these advantages can be achieved will be discussed in later sections. The goal of this report is to analyse the feasibility of implementing 2D hBN for use in a biomolecule sequencing platform.

3.3 Protein Adsorption

The first step to localize a protein on a 2D nanochannel is the binding of a protein to the device surface. It has been shown that proteins and other biomolecules can be preferentially adsorbed onto the surface of a 2D nanomaterial due to van der Waals interaction and hydrophobic interactions.[18,26,35] During this adsorption process, it is believed that amino acids and nucleotides will form $\pi - \pi$ bonds with the surface of hexagonal 2D materials.[24,35] From theoretical work, these bonds combined with spontaneous diffusion motion have been shown to result in unfolding of the structure of proteins that have been adsorbed to the surface.[26] This unfolding results in a planar configuration in which all of the parts of the molecule being analyzed are in contact with the 2D material. This means that many of the degrees of freedom for the molecules motion have been restricted.

The adsorption properties of proteins onto 2D surfaces is not the same between materials. Biomolecules will preferentially adsorb onto surfaces with lower average energetic interaction.[35] This was shown through simulation to be true for graphene and hBN heterostructures. It was found that for single-stranded DNA (ssDNA) this interaction energy is -23.2 kcal/mol per nucleotide for graphene and -29.3 kcal/mol per nucleotide for hBN.[35] A similar energy difference between the two materials of -230 kcal/mol for graphene and -330 kcal/mol for hBN was also be seen for proteins.[25,26] This shows that both ssDNA and proteins will preferentially adhere to hBN instead of graphene. The effect of this energy difference was tested in simulation using an in-plane graphene and hBN structure with an Aβ42 protein adsorbed onto the graphene surface. Figure 7 shows a representative depiction of this interaction.

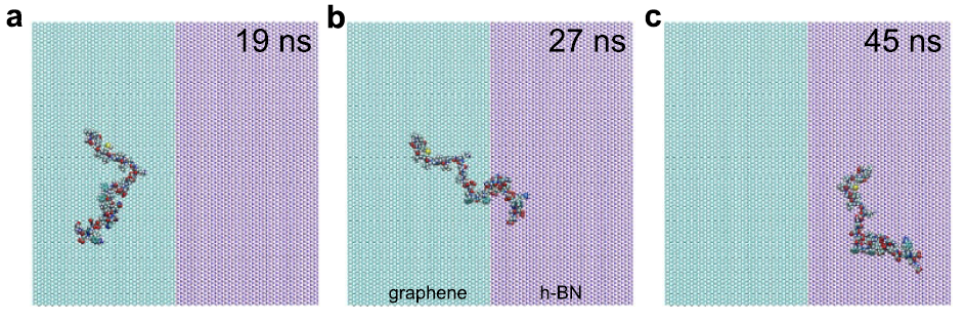

Figure 7: Split plane hBN-graphene biomolecule diffusion simulation[25]

In the simulation seen in Figure 7, it was found that the adsorbed Aβ42 strand rapidly diffused from the graphene surface to the hBN surface (on a scale of ns). It was also observed that the molecule did not return to the graphene surface.[25] This simulation shows that due to the energy difference between the two surfaces, the molecule diffused and remained confined to the hBN area. Such preferential motion was confirmed through multiple simulations and was also demonstrated for ssDNA.[35] This phenomenon shows great promise for enabling the localization of proteins onto an hBN surface.

3.4 hBN Nano-Ribbons

By exploiting the adsorption behavior seen in the previous section it is theoretically possible to localize and linearize proteins on a graphene-hBN surface. It has been proposed that by using a graphene-hBN-graphene sandwich heterostructure it is possible to confine a protein to a single hBN nanoribbon. This confinement is possible because there are less energy favorable materials on both sides of the hBN nanoribbon. Using these energy barriers, a protein will be confined in the hBN region. An illustration of this proposed in-plane heterostructure and its effect on biomolecules is shown in Figure 8.

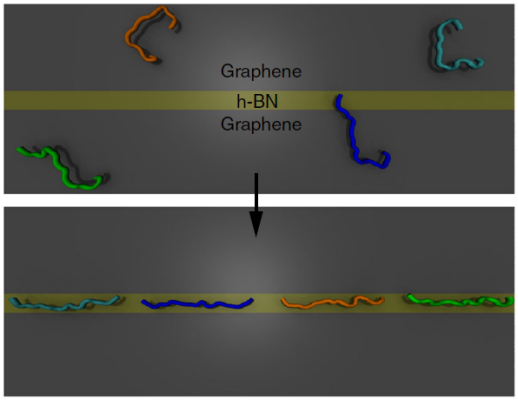

Figure 8: Graphene/hBN/Graphene in-plane heteorostructure as protein confinement concept[17]

The concept has been evaluated in molecular dynamics simulations for both ssDNA as well as proteins. These simulations focused on the speed at which biomolecules linearized as well as the forces applied to the molecules by surface interactions. In each of these simulations the molecule of interest was placed in its native folded state onto a graphene surface adjacent to the hBN nanoribbon. For all of the simulations it was found that, as expected, the molecule would

become unfolded as it adsorbed to the surface. It was also observed that the molecule would move from a disordered planar orientation to a linearized orientation on the hBN. Figure 9 shows these results for three different proteins.

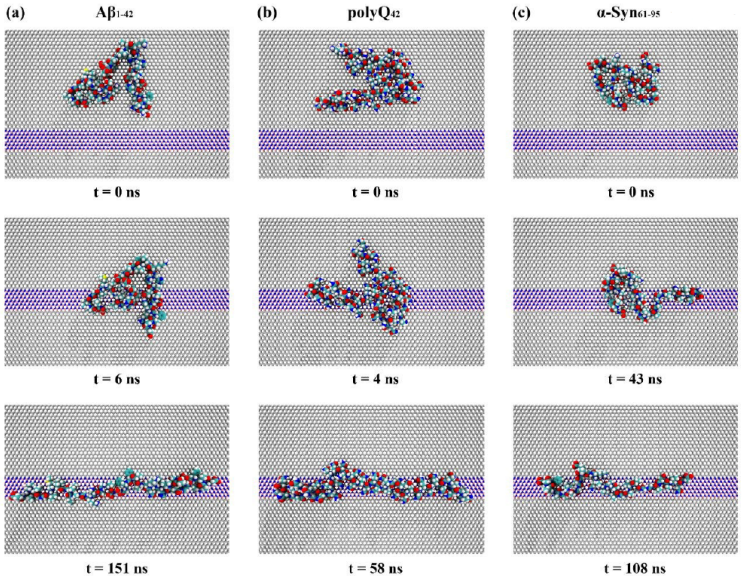

Figure 9: Linearization of three different proteins at different timestamps in Graphene/hBN/-Graphene in-plane heteorostructures.[25]

As can be seen from the simulation data in Figure 9, the proteins are localized and linearized as expected. It was found that during this process, the amino acids of the proteins were stretched.[25,35] This is important as it may allow for easier readout of signals during the sequencing process. Along with this, it was found that longer peptides experience higher confinement forces. This results in a higher probability density that the protein will be confined in the transverse direction.

The simulation work described above demonstrates that by using energy barriers associated with hBN nanoribbons it is possible to localize and linearize proteins, and that the linearization force actually increases for longer peptides.[25] This represents an interesting alternative to translocation through traditional 3D nanopores that rely on chemical denaturing agents to unfold proteins. By being able to localize these biomolecules, hBN nanoribbons open up the possible use of 2D nanochannels as a quantitative sequencing method.

As aforementioned, one main challenge facing the use of hBN/graphene heterostructures is that graphene exhibits strong fluorescence quenching.[30,31] This means that graphene may quench the fluorescence from the molecules that are being analyzed. Without this fluorescence it is difficult to track translocation of the molecules. Likewise, the use of fluorescence as a sequencing readout method is challenging if graphene surfaces are present in the device. Due to this quenching behavior of graphene, it is necessary to consider a nanochannel system that depends solely on the molecule adsorption and localization properties of hBN nanoribbons.

It is currently unknown if the use of graphene is a necessary component for the linearization of biomolecules. It is possible that any energy barrier will work in the same manner. It is feasible that hBN nanoribbons without adjacent graphene regions will still be able to constrain and linearize the molecules being analyzed. Additionally, edge effects of hBN layers can potentially

serve as an energy barrier that can constrain a biomolecule to the nanoribbon.[36] This behavior has not yet been simulated for the proposed hBN nanoribbon system. This research proposal will explore the potential use of hBN nanoribbons as a localization method from an experimental standpoint.

Until this point the advantages of using hBN for 2D nanochannels has been theorized and simulated in relation to heterostructure based systems. In order to show the feasibility of a single material hBN based system, it is necessary to test both the adsorption of biomolecules to an hBN surface as well as the transport of molecules on an hBN surface, we aim to lay the groundwork for further development of hBN nanoribbon based devices through these baseline experiments.

4 Techniques for Localization and Transport of Biomolecules

Localization of a protein is only the first step in the sequencing process. In order to determine the composition of the molecule, it is essential that the molecule be transported through a sensor. In 3D nanopores, this is generally accomplished through the use of electrophoretic forces between two reservoirs separated by a membrane. This method of electrophoresis for the transport of proteins in a 2D nanochannel is not a feasible transport mechanism due to the lack of separate reservoirs. However, due to the planar nature of the 2D nanochannel, it is possible to exploit transportation methods that cannot be used for traditional translocation. Three specific avenues of interest are the use of optical tweezers, electrophoresis, and surface acoustic wave (SAW) devices.

4.1 Optical Tweezers

One of the most widely implemented manipulation methods in single-molecule biophysics is the use of optical tweezers. This method uses a high power laser system and optical apparatus to create a optical 'trap' that a particle will become fixed inside of. This method can be used to localize and transport microscopic particles. The size of the particle that can be manipulated with a standard optical tweezer apparatus ranges from a few hundred nanometers to a few micrometer.[37] As most biomolecules are much smaller than this range, it is difficult to directly manipulate them with optical tweezers. Often biomolecules are attached to larger particles that are then manipulated using the optical tweezers. One use of this technology is for the threading particles through solid-state nanopores. By optically manipulating the beads that the biomolecule is attached to, it is possible to restrict the speed at which the molecule translocates the nanopore. An illustration of this concept can be seen in Figure 10.

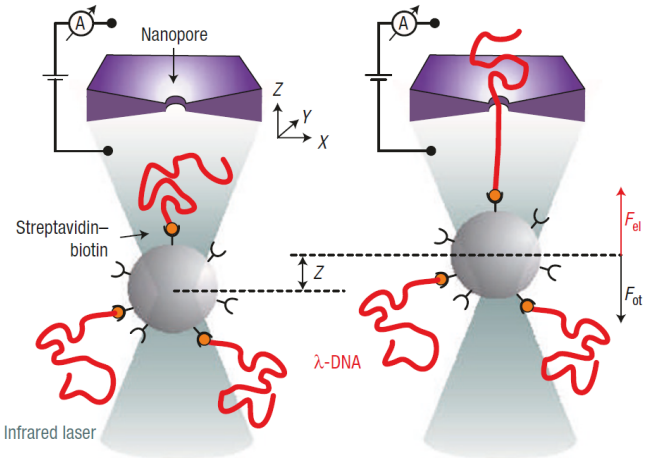

Figure 10: DNA strand attached to a microbead and translocated through a nanopore.[38]

.

Optical tweezers face several challenges for implementation with the proposed 2D nanochannels. One major issue is that this method cannot directly manipulate the biomolecule on the surface of the nanochannel. This issue is a result of varying orientations of guide particles that could result in only partial biomolecule adsorption to the nanochannel. This requires the system to employ guide particles that may cause the biomolecule being analyzed to not properly attach to the hBN surface. A secondary issue is the fact that optical tweezers can generate a large amount of localized heating.[39] This heat generation has the possibility of damaging both the nanochannels as well as the molecule being analyzed. These challenges make the use of optical tweezers difficult for the translocation of biomolecules in this system.

4.2 Electrophoresis

Electrophoresis as a method for transport is a very appealing concept due to its relative simplicity. By applying a potential on both ends of the nanochannel an electropheretic force is generated on any charged particles adsorbed to the surface. In multiple simulations of 2D nanochannels, this method is used to translocate ssDNA at a constant speed.[35] This translocation is accomplished by applying a voltage of between 0.2 V and 1 V which is easily achievable in an experimental setup. Translocation speeds of around 0.5 nm/ns to 3 nm/ns were achieved through the constant application of this voltage.[17,35] These velocities are well suited for sequencing applications.[1] However, in simulations, the electrophoretic transport of proteins requires orders of magnitude higher applied electric field strength than DNA. Also, a constant velocity may not be achievable due to the lack of global charge in proteins.[25] Those make manipulation of unmodified proteins with electrophoresis experimentally infeasible. In order to use this method of transport it would be necessary to use one of the protein modifications as mentioned in section 2.

4.3 Surface Acoustic Waves

A largely unexplored transport method for single biomolecules is the use of SAW for the transport of proteins along a 2D crystal surface. SAW in micro devices are generally produced by applying an electric field to a piezoelectric material. When this electric field is applied to the device, the piezoelectric material deforms and produces a mechanical stress, which is in

turn converted into a standing or travelling surface wave. This behavior is the result of the inverse piezoelectric effect. A SAW device typically consists of metallic interdigitated transducers (IDTs) formed on a piezoelectric material. IDTs consist of a set of connected metal fingers that are interspaced with a mirrored set of connected metal fingers. To generate the electric field used to deform the substrate, an alternating current signal is applied between the two sets of fingers. Importantly, the structure of the IDTs determines the characteristics of the generated wave such as bandwidth and direction of propagation.[40,41] One type of SAW device that is of particular interest is the two-port SAW device which consists of two sets of IDTs that are separated by an area called the delay line.[42] An image showing this delay line SAW design can be seen in Figure 11.

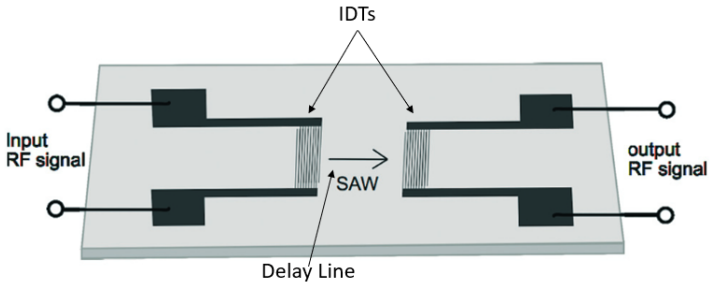

Figure 11: A schematic illustration of a delay line SAW device.[42]

By using two sets of IDTs that have the same signal frequency and phase it is possible to create a standing wave in the delay line. By slightly shifting the phase of the input signals, a travelling wave is generated. The piezoelectric material used for the device has an influence on the type of wave that is generated.[43,44] The most commonly used wave type for SAW devices is the Rayleigh wave in which the mechanical displacement is perpendicular to the plane of the substrate. This type of wave is useful for movement of particles or cells suspended in a fluid but is not well suited for in plane manipulation of particles as a result of energy loss to the liquid.[42] This type of wave is also not suitable for transport of proteins along the surface of a 2D crystal because of its fluid streaming effects.[44] It has been shown that acoustic streaming results in removal of non-specifically bound proteins on a surface.[45] A possible wave type that can be used for transport of proteins on a surface is a shear horizontal wave. These shear horizontal waves have an in-plane deformation instead of an out of plane deformation. An illustration of the differences between these two types of waves can be seen in Figure 12.

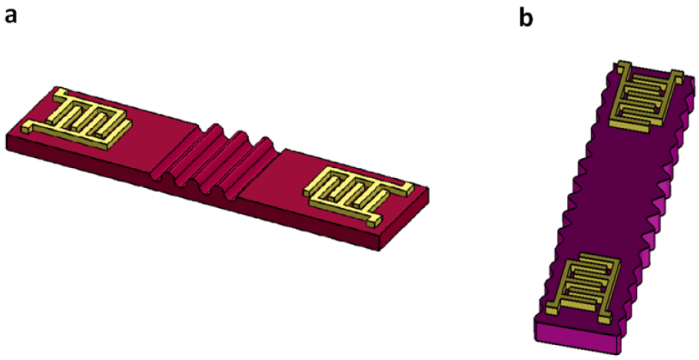

Figure 12: a) Rayleigh wave in a SAW delay line, b) Shear horizontal wave in a SAW delay line.[40]

The type of SAW generated by a device is dependent on the material and crystal orientation of the piezoelectric substrate. Some materials such as Y-128 lithium niobate ($LiNbO_3$) are especially efficient for use in generating Rayleigh waves. The most common material that is found to have a high efficiency for generating shear horizontal acoustic waves is Y-36 lithium tantalate ($LiTaO_3$).[44] As such, this material was selected for further analysis in this report.

Using Y-36 $LiTaO_3$ it has been shown that it is possible to concentrate, pattern, and transport biomolecules that are attached to a supporting lipid membrane.[43,46] This includes the manipulation of DNA and proteins. In these studies the authors were able to show small scale patterning of the molecules and even demonstrated a moving pattern of molecules.[43,46] The motion of this moving pattern will be referred to as a 'beating' wave in this report. It was noted that different proteins being patterned using this method would migrate to the nodes or the antinodes of the SAW. This patterning and separation of proteins under SAW actuation can be seen in Figure 13

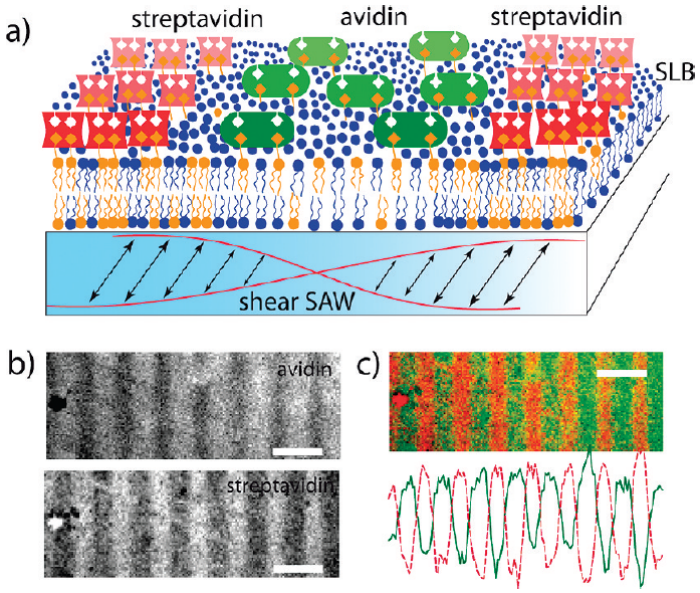

Figure 13: a) Schematic of patterning and separation of avidin and streptavidin molecules, b) Patterning of each protein type, **c**. Migration of protein to nodes and anti-nodes.[46]

Originally it was speculated that the force driving the patterning of these molecules was an acoustoradiative force. The observed migration of proteins to the nodes and anti-nodes of the SAW leads to the possibility that the proteins under evaluation where actually undergoing patterning due to a dielectrophoretic effect instead of the assumed acoustoradiative force. This possibility was strengthened by a study in which carbon nanotubes under SAW actuation where found to be aligned with the electric field of the SAW device instead of the mechanical wave.[47] Through further investigation, it was found that this phenomenon was most likely caused by acoustoelectric forces.[44]

4.3.1 Acoustoelectric Transport

Generally, in a SAW device, acoustoradiative forces dominate the manipulation of particles. However, in a shear horizontal wave device, the acoustoelectric forces are the dominant force.[44] Acoustoelectric forces are generated from the presence of a SAW driven evanescent electric field

near a polarizable particle.[40,44] This evanescent field is generated as a reaction to the deformation of the piezoelectric substrate. Using these fields it is possible to induce dielectrophoresis in molecules that do not have a uniform charge or are not charged.[48,49] This is ideal for the manipulation and translocation of proteins due to their varied local charge distributions.

Dielectrophoresis can occur when an alternating current is applied to a SAW device. The rapidly changing localized electric field induced by the standing SAW creates an alternating potential near a particle in a solution. The charge carriers inside the particle and in the solution are moved to alternating sides of the particle. A slight delay in the speed at which these charge carriers move results in a net dipole.[40] An illustration of this concept can be seen in Figure 14.

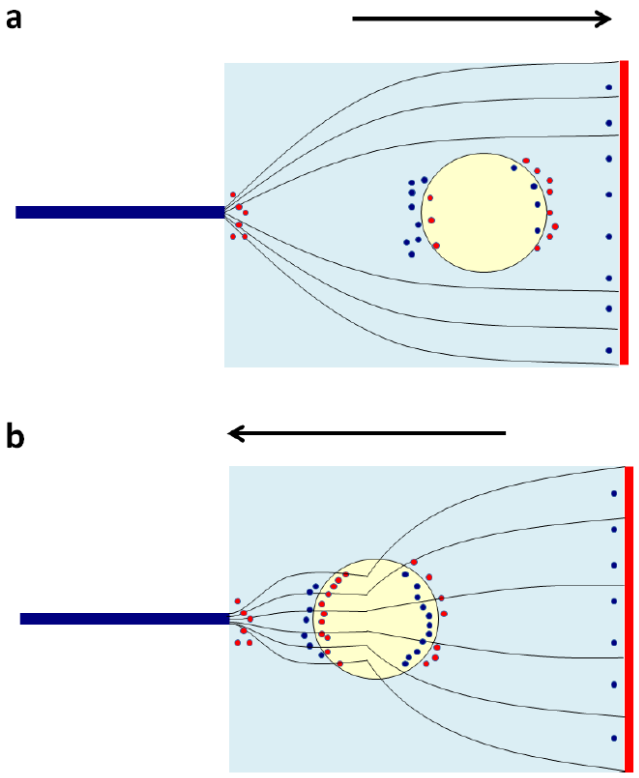

Figure 14: a) Polarization of a particle using negative dielectrophorsis, b) Polarization of a particle using positive dielectrophorsis.[40]

This net dipole results in polarized particles that will move when an electric field is applied. Therefore, the electric field generated by a standing SAW will create a force towards the negative or positive nodes of the electric field. This will concentrate particles into nodes and anti-nodes depending on their dielectrophoretic characteristics.[44,47] These characteristics are dependent on multiple different parameters such as particle size, ionic concentration in the solution, and applied frequency.[40,50] Figure 15 shows the standing SAW patterning of polarized particles that have different dielectrophoretic characteristics.

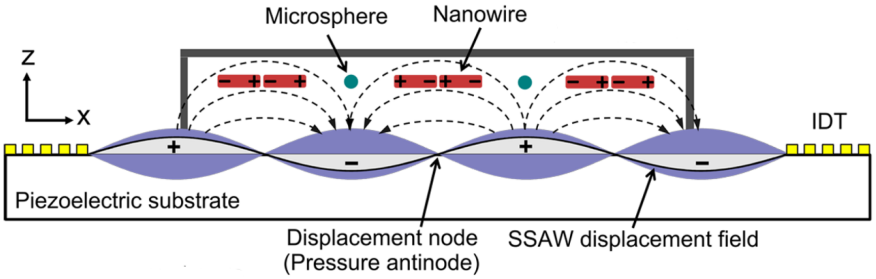

Figure 15: Patterning of polarized particles in a standing SAW device.[47]

It has been shown that dielctrophoretic forces generated by SAW can pattern many different nanomaterials. Using a Y-41 $LiNbO_3$ substrate it was possible to pattern nanomaterials include: DNA, exosomes, graphene flakes, quantum dots, proteins, and dextran molecules.[44] By shielding parts of the substrate and observing no patterning effect in these areas, it was found that this patterning was entirely induced through electrical effects. The patterns generated using this approach can be seen in Figure 16.

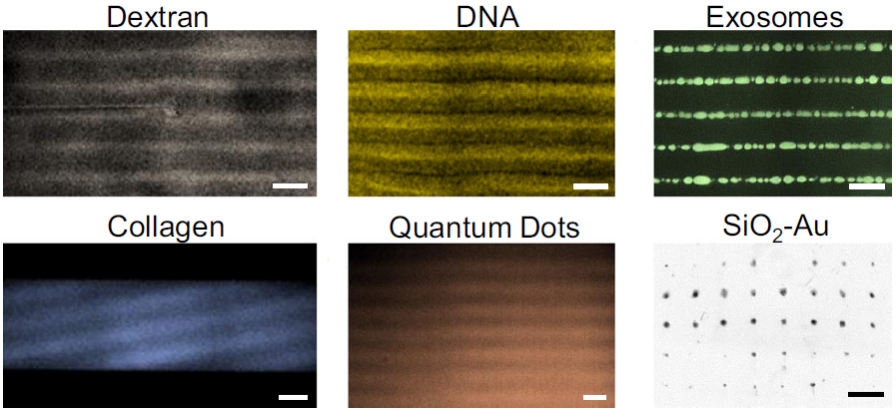

Figure 16: Various types of nanoparticles patterned by acoustoelectric forces.[44]

These patterning experiments were conducted directly on a piezoelectric substrate without the aid of a supporting lipid membrane. This shows the patterning is not an effect of the lipid behavior but is a result of the SAW actuation itself. Thus, we hypothesize that acoustoelectric forces can be used to also generate patterns on a hBN surface without the need of a supporting lipid layer.[44]

We speculate that a constant transport velocity can be achieved by employing a scrolling SAW to molecules adsorbed on hBN surfaces. This could enable the controlled movement of proteins through a sensor allowing for clear single amino acid fluorescence sensing. The speed of this motion will be dictated by the scrolling speed of the SAW.

4.4 Comparison between Protein Transport Techniques

It is important to directly compare the advantages and disadvantages of the three different biomolecule transport methods discussed in this section. A figure comparing the characteristics of these transport methods can be seen below in Figure 17.

Manipulation Method	Direct Manipulation of Biomolecules	2D material Compatibility	Protein Compatibility	Implementation Complexity
Optical Tweezers	No direct manipulation possible, carrier particles required	Localized high temperatures can damage 2D materials	Proteins must be bound to carrier particles so protein modification necessary	High cost for experimental setup
Electrophoresis	Direct manipulation of charged particles possible	Easy integration with 2D materials	Proteins must be modified to have a uniform charge for manipulation	Simple electrode setup with low driving voltages
Surface Acoustic Waves	Manipulation of large variety of particle sizes and charges possible	Largely unstudied interaction with 2D materials	No protein modification necessary for unfolding or manipulation	Simple electrode design with readily available signal input sources

Figure 17: Comparison of biomolecule manipulation techniques for 2D nanochannels.

It can be seen in Figure 17 that optical manipulation and electrophoresis have downsides that restrict their implementation into the proposed nanochannel device. SAW devices are a very promising technology but has not been thoroughly studied for this application. The possibility of using shear horizontal SAW to achieve transport of biomolecules on hBN surfaces will be experimentally explored in this project.

4.5 Characterization of Transport

In order to be able to characterize the efficiency of a transport method, it is necessary to be able to see spatial variations with sufficient resolution. As most biomolecules are on the nanometer scale, it is impossible to view them using traditional optical microscopy.[51] As such, it is necessary to detect the molecules using a different method. One simple and widely implemented method for detecting the location of biomolecules is the use of fluorescent tags.

Fluorescent tags are molecules that can be attached to different locations on a biomolecule such as DNA or proteins and emit a certain frequency of light when excited by a light of sufficient energy.[52] By placing these tags on mobile molecules it is possible to track the position of this light emission as a means of determining translocation direction and speed. This can be further analysed by object tracking software that allows for frame by frame plotting of biomolecule movements.[53,54] Using this method, it should be possible to determine whether biomolecule transport is driven by diffusion or by surface acoustic waves.

Using fluorescent tags it may also be possible to observe the unfolding and linearization of biomolecules on an hBN surface. By attaching many fluorescent tags to very long molecules, one could discern the shape and folding of the molecule in real time. This approach was used to study conformational changes in long DNA strands and was able to show different types of folding, coiling and unfolding. The study showed that by attaching a DNA strand with multiple fluorescent tags to a surface and unfolding it using a shear flow, it was possible to see the various possible shapes of the molecule.[54] Figure 18 shows different experimentally observed configurations of a DNA strand, including coiled and nicked geometries.

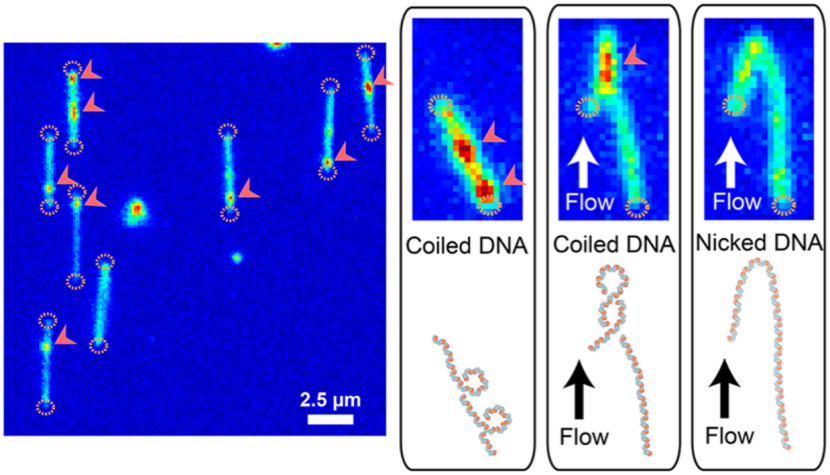

Figure 18: Fluorescent molecule tagged DNA unfolding due to shear flow. The colour shows the concentration of fluorescent molecules:Red is high concentration while dark blue is low concentration.[54]

In this thesis, we will use a similar fluorescence-based imaging technique to investigate the behaviour of the biomolecule in space and time. By tracking the motion of the fluorescent biomolecules under SAW actuation, the efficiency of the transportation method can be evaluated for statistically significant data sets given the large field of view in fluorescence microscopy.

5 Research Proposal

The overarching goal of this project is to investigate the potential for SAW driven unidirectional transport of individual biomolecules along an hBN surface. Understanding this transport will enable the implementation of hBN based protein sequencing methods. The state-of-the-art presented in previous sections indicates that 2D hBN sequencing methods could offer significant advantages over existing materials and platforms for protein sequencing applications. In order to focus the scope of the proposed research, it is necessary to make some initial experiment design decisions. These decisions are as follows:

1. **Materials.** As seen in Section 3 there are a plethora of potential materials that can be used to create a 2D material nanochannel. Of these materials, the most widely simulated and studied combination is hBN-graphene heterostructures. However, it was shown that graphene's fluorescence quenching property makes it incompatible with the tracking of biomolecules with fluorescent tags. As such, the focus of this report will focus on the use of hBN for the constraint and transport of biomolecules.

2. **Manipulation method.** Three main manipulation methods are proposed for the translocation of proteins in Section 4. Of the three main manipulation methods for the transport of biomolecules introduced in Section 4, we have shown that the surface acoustic wave technique is the most promising for our application. As such, it was decided that SAW devices manufactured on Y-36 $LiTaO_3$ will be used for studying the transport of biomolecules on an hBN surface.

3. **Readout method.** Single-protein sequencing readout methods exist in many flavors and have specific sets of design requirements. As such, a separate project studying the

characteristics of fluorescence based optical readout will be undertaken. The finding of this separate project may be combined with the findings of this project at a later time.

5.1 Knowledge Gap

To the best of our knowledge, the combination of biomolecule adsorption to 2D hBN and SAW driven manipulation of biomolecules is entirely new and has not been attempted by other groups. This novelty aspect also means that there is very little literature than can be used for baseline experiments. As such we have found several points that require certain assumptions to be made in order to design an experimental methodology. One of the goals of this project is to fill these knowledge gaps through these experimental methods.

An obvious first major gap in the knowledge is related to the diffusion driven unfolding of molecules on 2D hBN surfaces. There is very little experimental data that shows this unfolding on 2D hBN surfaces will occur as shown in simulation. As such it is uncertain under what conditions this behavior will occur at all. It is also unknown if this phenomenon will be affected by variables such as aging or contamination. As such it will be necessary to analyze the diffusion of biomolecules on hBN surface under a wide range of conditions.

There is also a large gap in knowledge related to the use of SAW devices as a biomolecule transport mechanism. So far, there has been a lack of literature related to the in-plane manipulation of biomolecules that are adsorbed to a 2D material. As shear horizontal waves have been shown to pattern molecules attached to a lipid bilayer membrane,[43,46] we speculate that the same concept can be applied to biomolecules on hBN. It was also reported that shear horizontal waves can manipulate a wide range of molecules that are suspended in a fluid without significant fluid coupling.[44] Therefore, it is expected that such a negligible fluid coupling due to shear horizontal waves will not remove molecules from the surface.[55] However, there is no experimental data suggesting that shear horizontal waves can be used for manipulation of molecules adsorbed to the hBN surface.

5.2 Research Questions

Having acknowledged the gaps in our understanding of this system, we can now outline three main research questions:

1. *How are the diffusion dynamics of single molecules affected by the interaction with hBN surfaces?*

2. *Can we manipulate single molecules using non-invasive acoustoelectronic forces generated with SAW devices?*

3. *Can we demonstrate unidirectional single molecule transport and using combined hBN/-SAW devices?*

The planned experiments are designed to explore each of these research questions. The details of the experimental steps and methodology that will be used to answer these questions will be laid out in the following sections.

6 Experimental Methods

In order to investigate the research questions presented in Section 5.2, it was necessary to develop an experimental approach, divided into four main parts: **1)** SAW device design, fabrication, and characterization; **2)** hBN surface fabrication and experimental setup; **3)** adsorption and diffusion of biomolecules on hBN surfaces; and **4)** SAW-driven transport of biomolecules. The methodology for each of these steps will be illustrated below.

6.1 SAW Device Design

The first step in towards achieving SAW driven transport of biomolecules is the design of the SAW device itself. This SAW device must be designed in a way that optimizes the acousto-electric manipulation of the selected biomolecules. As such, we must first consider the biomolecules that are being manipulated. This report analyze the manipulation of multiple bio molecules including: lambda DNA, M13mp18 DNA, and α-synuclein. The details of each of these molecules and their characteristics can be found in section 6.8.

It has been shown that when the wavelength of a SAW device is much larger than the size of the particle being manipulated, the particles tend to aggregate.[56] This behavior is not ideal for single molecule sequencing application. In order to sequence individual biomolecules, it is necessary to prevent aggregation of large numbers of molecules in the nodes of the SAW. Using a SAW with a wavelength comparable to the size of the biomolecule increases the chances that single molecules will become trapped in SAW nodes.[56] This concept can be clearly illustrated below in Figure 19.

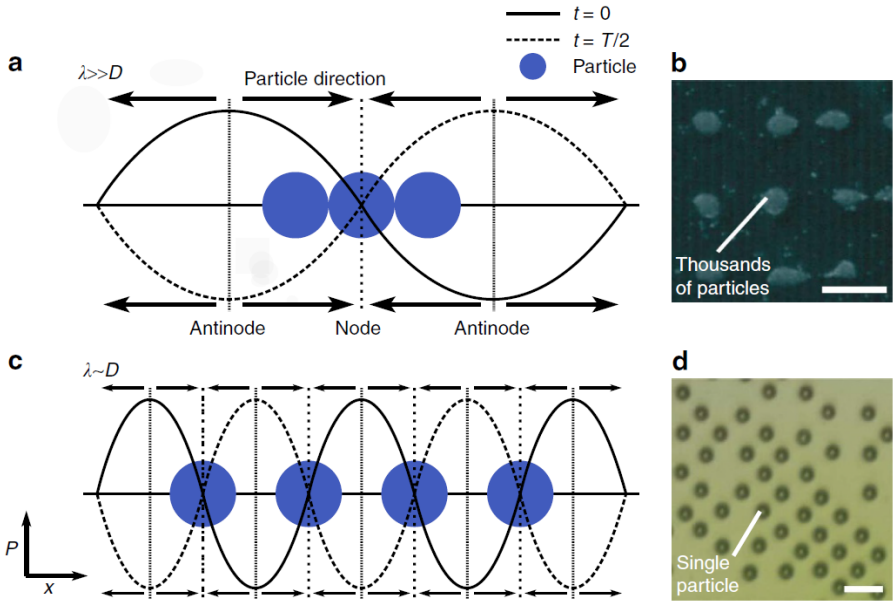

Figure 19: Difference in number of trapped particles for large and small SAW wavelengths.[56]

By having a SAW wavelength similar in size to the particle it is possible to manipulate lower numbers of particles in each SAW node. Lambda DNA has fully linearized length of approximately 7 μm[54] and M13mp18 DNA has a linearized length of around 3 μm. The length scale of these molecule dictates the selected acoustic wavelength of the SAW device. As such, the desired wavelength of the SAW device was set to be approximately $\lambda = 10\mu m$. The driving

frequency is determined by the speed at which sound moves through the selected piezoelectric substrate. The equation that dictates the driving frequency of the device can be seen below in equation 1.

$$f = \frac{v}{\lambda} \tag{1}$$

In this equation, f is the driving frequency, v is the speed of sound at the surface of the piezoelectric substrate Y-36° cut lithium tantalate, and λ is the desired acoustic wavelength. The speed of sound in lithium tantalate has been found to be 4160 m/s.[57] The remaining properties of lithium tantalate can be found in Appendix A. Using equation 1 and the value of the speed of sound in lithium tantalate, it was found that for a wavelength of 10 μm, the driving frequency of the SAW device should be 416 MHz.

Is is possible to determine the dimensions of the SAW device structures using the desired 416 MHz driving frequency. The pitch of the IDT fingers should be the same as the wavelength of the driving frequency in order to generate the desired surface acoustic wave.[40] As such, the pitch of the IDT fingers was set to $\lambda = 10\mu m$. The delay line length was set to $L_D = 500\mu m$. This value of L_D was selected so that the IDT phase center is in the same location as the geometric center of the SAW device.[58] The value of the electrode overlap was set to 104 μm. This value was selected so that hBN surfaces with a width of around 100 μm could fit in the propagation region of the SAW device.

The number of IDT finger pairs N and the thickness of the fingers τ were selected to minimize impedance mismatch of the IDTs with a standard 50 Ω signal source. The impedance of the IDTs is calculated by setting the resistance of the IDTs equal to the inverse of the radiation conductance.[59] The radiation conductance $G_a(f_0)$ can be calculated using:

$$G_a(f_0) = 8K^2 f_0 C_S N^2 \tag{2}$$

where K^2 is the electromechanical coupling constant, and the variable of f_0 is the synchronous frequency. The value of C_S is the static capacitance of each pair of IDT fingers and the number of finger pairs is represented by N.[59] By setting the value of $1/G_a$ equal to 50 Ω, the number of finger pairs and the finger thickness can be selected. As a result of this calculation, the number of finger base pairs N was selected to be 31 pairs, and the value of τ was selected to be 65 nm. An illustration of this final design can be seen below in Figure 20.

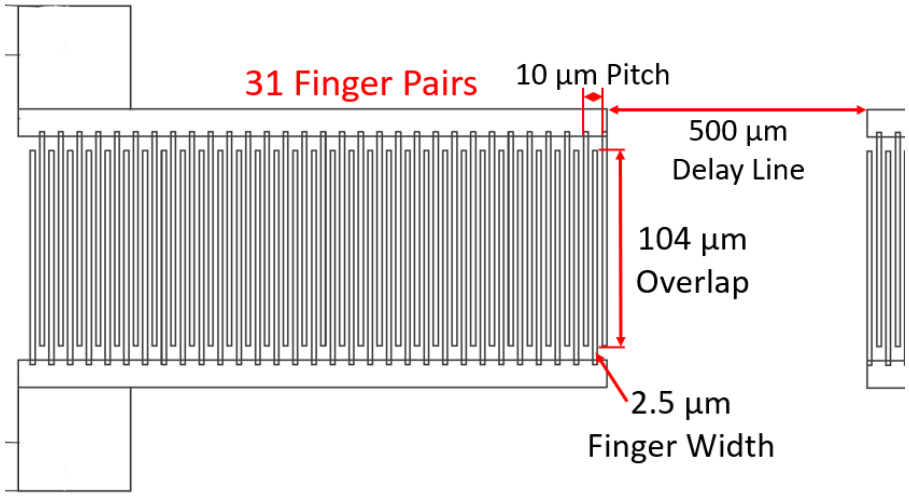

Figure 20: Schematic of SAW device idt design with critical dimensions labeled

The two leads connected to each IDT are connected to bond pads, which allows the SAW device to be connected to external control electronics. It was decided that these bond pads would have dimensions of 100 μm by 100 μm in order to allow enough space for bonding. In order to maximize the number of SAW devices that can fit on one chip, the bond pads were staggered. In total, four SAW devices can fit on the available 5 mm by 10 mm lithium tantalate substrates. The layout of this chip can be seen below in Figure 21.

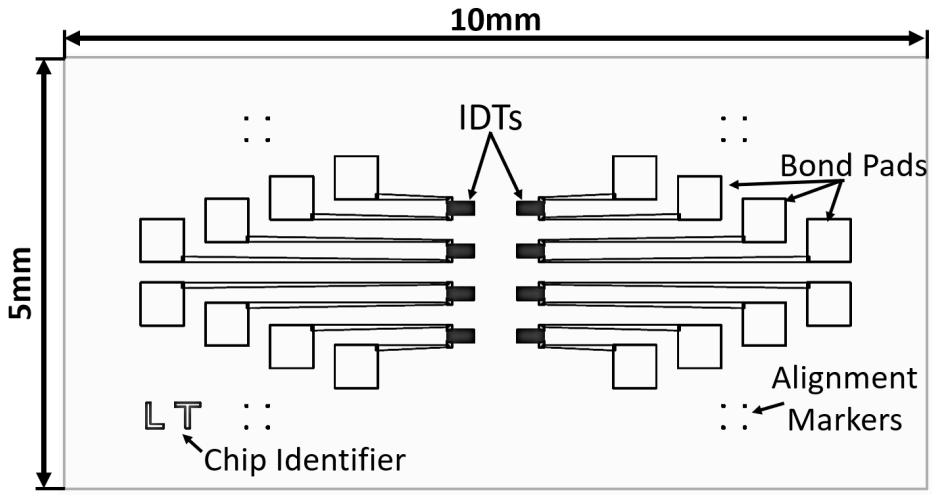

Figure 21: Schematic of SAW device IDTs with bond pads on piezoelectric substrate.

6.2 SAW Device Fabrication

The designed SAW device was fabricated onto a lithium tantalate substrate with a thickness of 500 μm. The wafer used for these substrates was polished on both sides and was selected for its optical transmission. The substrate was spin-coated with ebeam resist (AR-P 6200.9) and conductive polymer (Electra 92) before it was placed into a Raith Nanofabrication 5200+ electron beam lithography system for pattern exposure. The exposure dose administered to the substrate was adjusted based on the geometry of the SAW device to provide a uniform dose profile to the entire pattern. Following the pattern writing, the resist was developed by first washing the substrate in water to remove the electra layer, followed by a wash in pentyl acetate, MIBK:IPA (1:3) and IPA. These chemicals act to develop and remove the resist that was exposed to electron beam irradiation.

After the lithography process, a deposition of 5 nm of titanium and 60 nm of gold was placed onto the lithography defined SAW pattern. This was accomplished through the use of electron beam physical vapor deposition. The SAW substrate was then placed into a 60 °C bath of anisole for three hours to release the resist layer from the lithium tantalate. The substrate was then ultrasonically cleaned to remove the remaining resist from the device and reveal the SAW structures on the surface.

The final step of the SAW device fabrication process was the addition of a silicon dioxide passivisation layer on top of the SAW IDTs. This layer prevents Joule heating, electro-osmotic current, and damage to the SAW devices when exposed to a buffer solution. This SiO_2 layer was deposited using an radio frequency (RF) sputtering machine. The bond pads of the device were covered in a kapton tape shadow mask in order to prevent deposition of SiO_2 onto this region.

The complete SAW device fabrication process can be seen summarized below in Figure 22.

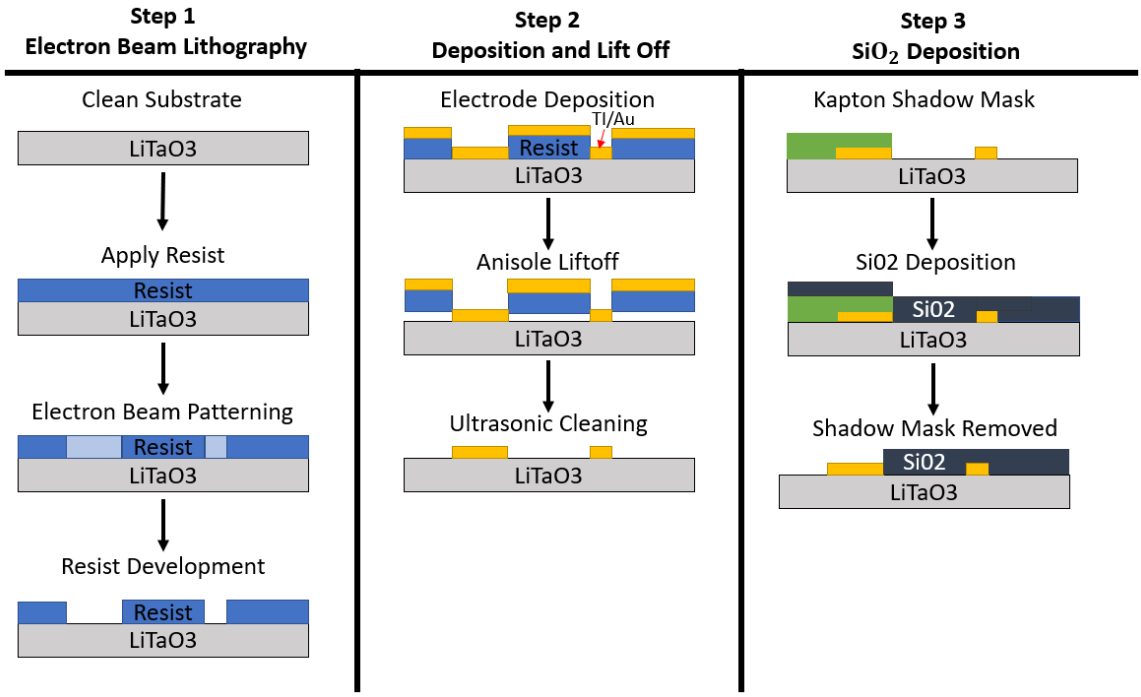

Figure 22: SAW device fabrication process.

Using this fabrication method, a total of seven usable SAW substrates were fabricated. Each substrate has a total of two to three usable SAW devices that have minimal defects. Varying thicknesses of SiO_2 passivisation layers were added to the substrates. A summary of the completed devices and their characteristics can be seen below in Table 1.

Table 1: Summary of fabricated devices and the thickness of passivisation layers

Chip Name	SI02 Thickness
LT-A1	297nm
LT-A2	0
LT-B2	370nm
LT-B4	140nm
LT-B7	0
LT-C1	198nm
LT-C2	180nm

6.3 SAW Device Characterization

A printed circuit board (PCB) was prepared to accommodate the SAW chip and provide standard SMA connectors for interfacing with test equipment. The connector pads of this circuit board were designed to minimize the impedance mismatch between the SAW device and the connectors. The SAW device was placed in a cut out located in the center of the PCB, and the

cover slip was attached to the bottom of the PCB using double sided tape. An illustration of this stacked configuration can be seen below in Figure 23. Once the SAW device was attached to the PCB, it was wire bonded to the PCB.

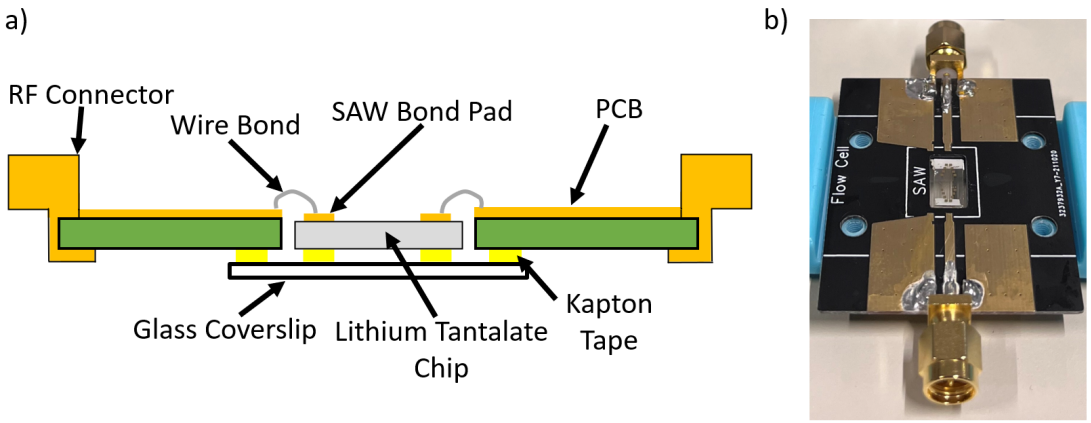

Figure 23: a) Stacked configuration of PCB with SAW device b) Realized PCB stack.

A characterization of the SAW device was carried out using a vector network analyzer (VNA). The VNA performs a frequency sweep at a set power level in order to determine the frequency behavior of the SAW device. Using this frequency sweep, we can determine the amount of power that is transmitted and reflected in the SAW device.[40] These parameters are expressed as S-parameters. The transmission power will be highest at the resonance frequency. By driving the SAW device at this resonance frequency it is possible to maximize the amount of power that can be used to transport biomolecules.

S-parameter measurements of each of the SAW devices were taken using a NanoVNA version 2. These measurements were first performed in air as a baseline. SAW devices with differing thicknesses of SiO_2 layers were tested. Representative results of these in air measurements can be seen below in Figure 24.

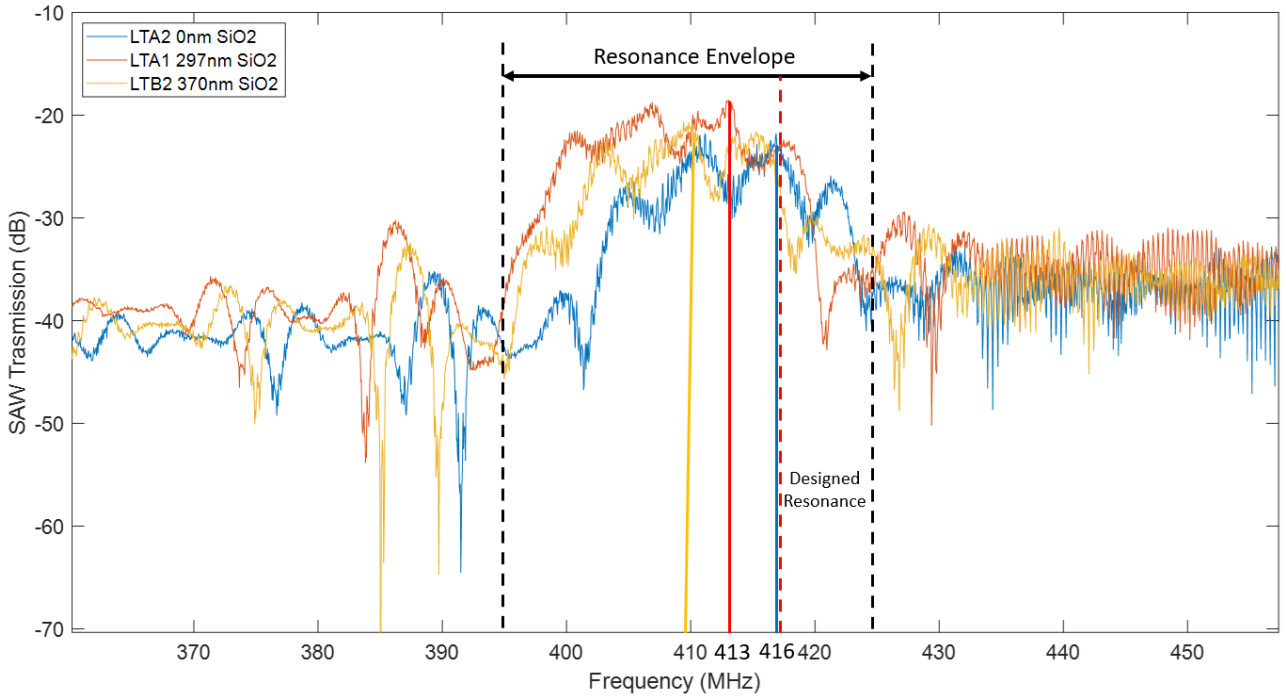

Figure 24: VNA transmission power measurement for three chips with passivisation layers of different thicknesses

The results in Figure 24 show that the frequency behavior of the SAW devices has some dependence on the thickness of the silicon dioxide passivisation layer. This shift in the frequency is caused by the SiO_2 changing the speed of the SAW wave.[60] As such, each of the devices will have a slightly different excitation frequency. It was found that all of the devices analyzed had a resonant frequency that resulted in a wavelength close to the desired 10 μm. This shows that while not perfect, the fabrication process resulted in SAW devices that are sufficient for the intended manipulation tasks.

It is also important to evaluate the transmission and reflection power of the SAW devices. A poorly connected or potentially incorrectly induction-matched device will result in very low transmission power. This transmission power is critical, as it is the driving force behind the patterning and manipulation of molecules on the surface. It was found that for most of the fabricated SAW devices operating at the peak resonance frequency, the value of the transmission S-Parameter was between -21 dB and -19 dB, which is similar to the measurement results in the literature..[40,59]

The S-parameters seen in Figure 24 were measured in air, which is not representative of the real experimental environment for manipulating biomolecules. As such, it was necessary to characterize the SAW devices when immersed in a fluid environment. Each SAW device was immersed in a buffer solution (10 mM Tris, 50 mM NaCl, pH 8.0) and were characterized using a VNA. These measurements were then compared to the air-based measurements. An example of this comparison for SAW device LTA1 can be seen below in Figure 25.

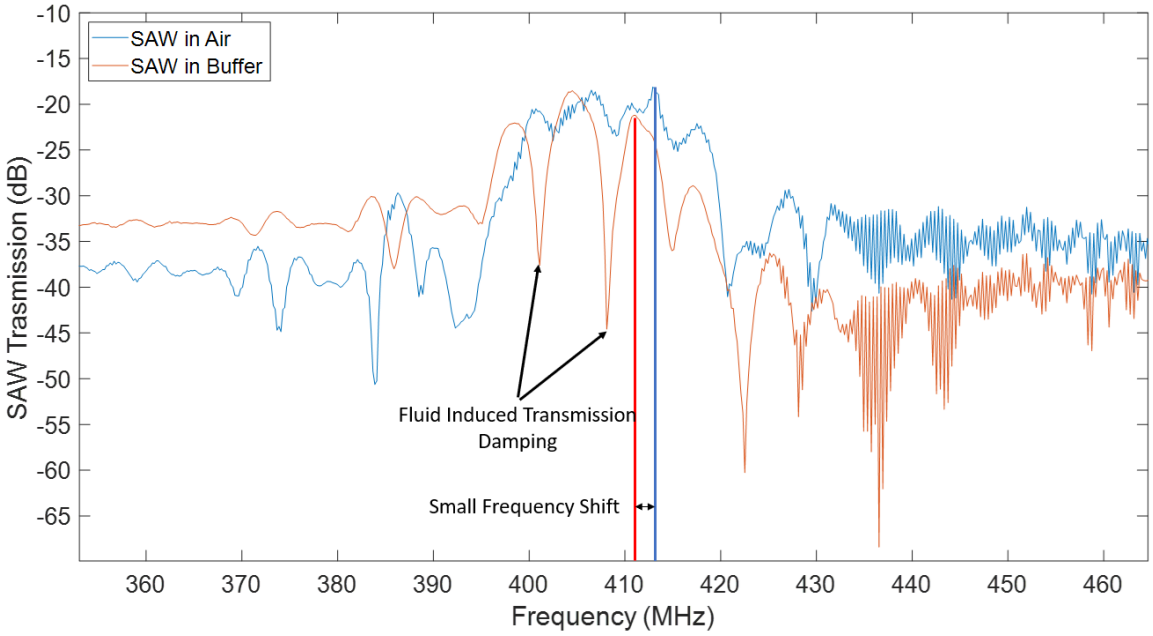

Figure 25: Transmission characterization of the same SAW device in air and in fluid

It can be seen in Figure 25 that the two frequency responses are similar. However, in the fluid-based measurement, the response has a notable damping that results in steep transmission drop off in certain parts of the plot. This is most likely due to coupling with the fluid at these frequencies. Despite this loss of power, at peak resonance, the transmission powers in both air and in fluid are comparable. This shows that the device is not losing power to the strong fluid coupling that out of plane SAW devices exhibit.[44,59] By driving the SAW devices only at resonance frequencies, it is possible to avoid losing substantial amounts of power to the fluid.

Using these VNA measurements, the driving frequencies and wavelengths of the SAW devices can be set for further experiments. However, before each experiment an in-liquid characterization was conducted to ensure that no changes have occurred. Using these repeated characterizations, it is possible to exactly select the resonance frequencies for biomolecule actuation.

6.4 2D Material Preparation and Transfer

After the fabrication and characterization of the SAW devices, it was possible to move on to designing the experimental setup. This experimental setup was designed to accommodate both molecule diffusion experiments as well as SAW driven molecule transport experiments. The first step in the experimental setup process is preparing a 2D hBN surface. There are two typical approaches for creating this 2D hBN surface.[61] The first is through the use of chemical vapour deposition (CVD) grown hBN crystals. This method is useful due to its tendency to create near atomically thin layers of hBN.[61] However, this CVD-grown hBN has been shown to have a lower quality crystallinity and significant surface contamination.[62] This makes CVD-grown hBN unsuitable for this application, as surface contamination can severely restrict the diffusion of molecules on an hBN surface. As such, it was necessary to consider a different source of 2D hBN surfaces.

The hBN source that was selected for this research was hBN crystals grown under a high-

pressure high-temperature (HPHT) environment. These crystals were provided by the National Institute for Materials Science in Japan. It has been shown that crystals grown in this way have a much higher purity than CVD-grown crystals.[62] However, these HPHT grown crystals are macroscopic crystals and are not thin flake crystals. As such, it is necessary to break off thin flakes of the hBN from the macroscopic crystals. In order to generate thin flakes of hBN a process called mechanical exfoliation is used. This mechanical exfoliation process exploits the fact that hBN layers are held together by weak van der Waals bonds.[61] When a mechanical force is applied to the crystal, these bonds are easily broken, which results in layers of the hBN crystal separating. When these layers separate from the larger crystals, they form thin flakes of hBN that have a range of sizes and thicknesses. These hBN flakes make ideal candidates for use as a 2D hBN surfaces in this research.

In order to create the mechanical force necessary to create the hBN flakes from the larger crystals, a tape exfoliation method was used. The first step of this process involves placing the HPHT crystals onto a piece of scotch tape. A second piece of scotch tape is placed over the crystals and is connected to the first piece of tape. The two pieces of tape are pulled apart resulting in exfoliation of the crystals. This process is repeated multiple times in order to generate more flakes. The second scotch tape piece is then taken and placed onto a SiO_2 substrate. The tape is left for a time before gently being lifted from the substrate resulting in the flakes exfoliating onto the SiO_2 surface. This transfer process is referred to as a direct hBN transfer. An illustration of the direct transfer process, and an example of the flakes generated, can be seen below in Figure 26

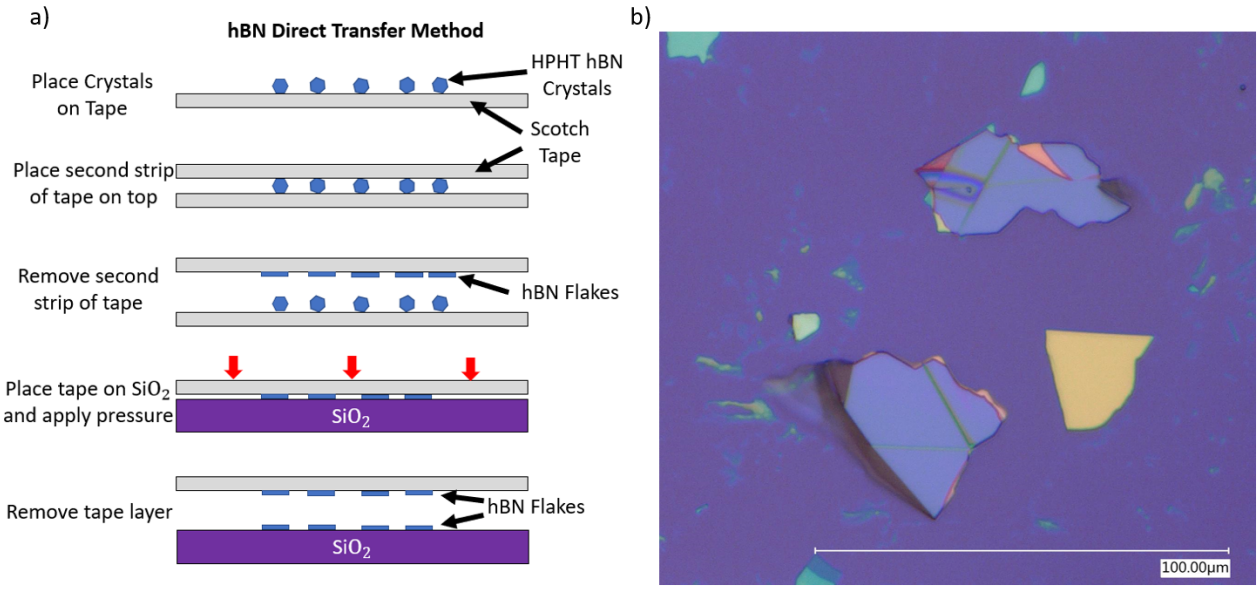

Figure 26: a) Mechanical exfoliation and direct transfer process to generate hBN flakes, b) example of hBN flakes generated using direct transfer.

Once the hBN flakes have been transferred onto the SiO_2 surface, it is possible to select a flake that is suitable for analayzing the interaction between biomolecules and the hBN surface. The preferred flake for the planned experiments is a large (around 100 μm), relatively thin flake (between 40 nm and 200 nm) that has a surface without many wrinkles. Having a large surface without wrinkles allows for a large area for molecules to adsorb onto. It also allows for a larger distance to move molecules along the surface using the SAW device. Having a thin flake is

critical, as thick flakes of hBN absorbs fluorescent light emitted by bio-molecules.[62]

In order to be able to systematically identify thin flakes, a quick method of estimating flake thickness was necessary. A number of flakes with varied thicknesses were measured using an atomic force microscope. These measurements were then correlated with the optical color of the flakes on a SiO_2 surface. By correlating the thickness with the color of the flakes, it was possible to quickly estimate which flakes were potentially viable options for molecule diffusion and manipulation experiments after the direct transfer process.

Once a suitable flake was located, it was necessary to transfer the flake from the SiO_2/Si substrate to the final substrate. To achieve this a method called "PPC bubble transfer" was used. The first step of this method is to create a polydimethylsiloxane (PDMS) bubble on a glass microscope slide. A thin layer of polypropylene carbonate (PPC) film is then placed over this PDMS bubble. This PPC layer is taped in place in order to create tension between the PPC and the PDMS. This bubble with PPC coating is then placed into a precision stamping setup. An example of the PPC bubble as well as the stamping setup used can be seen below in Figure 27.

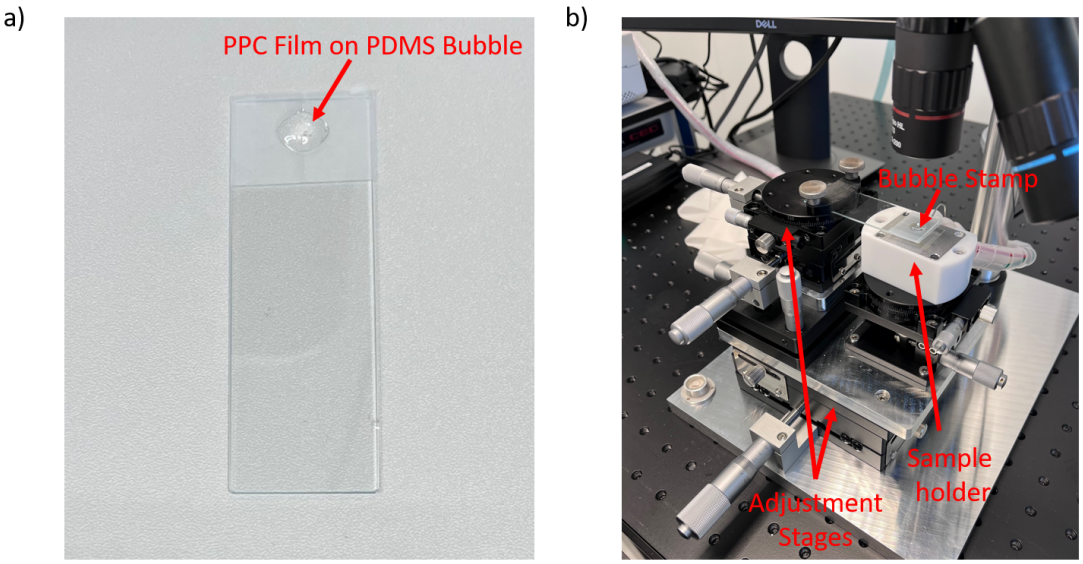

Figure 27: a) PDMS bubble with PPC layer, b) Precision Stamping setup

The SiO_2 substrate containing the direct transfer flakes is the placed in the stamping setup under the PDMS bubble. The bubble is then positioned over the desired flake. The bubble is then slowly lowered until the PPC film comes into contact with the flake and SiO_2 surface. This contact surface is then slowly released by moving the bubble away from the surface. During this release, the flake's adhesion to the PPC film becomes greater then its adhesion to the SiO_2 and is therefore released from the SiO_2 surface.[23] Once the flake is removed from the SiO_2, the final substrate is placed under the PDMS bubble. The position of the bubble is shifted so that the flake is over the desired final location. The bubble is then lowered until contact is made with the substrate surface. At this point the PPC layer is heated to 60°C in order to reduce the adhesion of the flake to the PPC film.[23] Finally the bubble is slowly raised until the PPC layer is released. As the PPC is removed, the flake is deposited onto the substrate. A diagram illustrating this PPC bubble transfer process can be seen below in Figure 28.

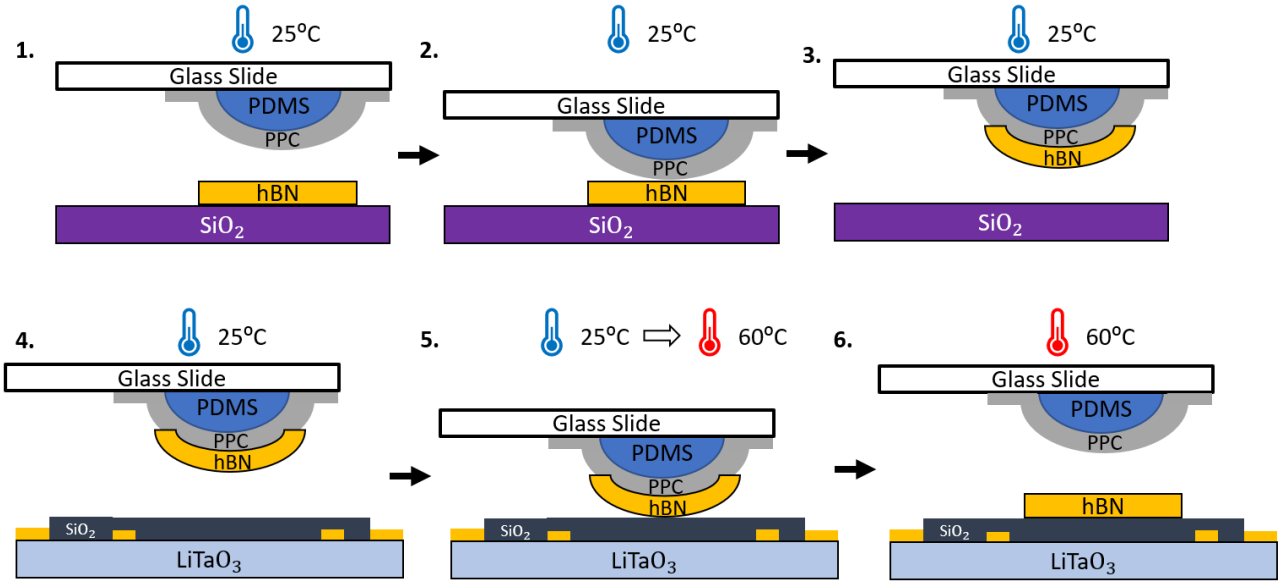

Figure 28: PPC bubble transfer process of hBN flake from SiO_2 onto SAW device

When transferring flakes onto the final substrate, it was found that thin flakes exhibit high transmission of light making them ideal for analyzing biomolecule motion. However, their low quantity and high adhesion to SiO_2 makes them difficult to transfer. The small size of the thin flakes also limits their use for molecule actuation cases. Thick flakes often are very large and are very abundant. However, due to their lower optical transmission thick flakes have limited usefulness for molecule actuation experiments. Due to these limitations, the ideal flake for the planned experiments is a large, thin flake. An illustration of two flakes after being transferred onto glass and SAW devices can be seen below in Figure 29.

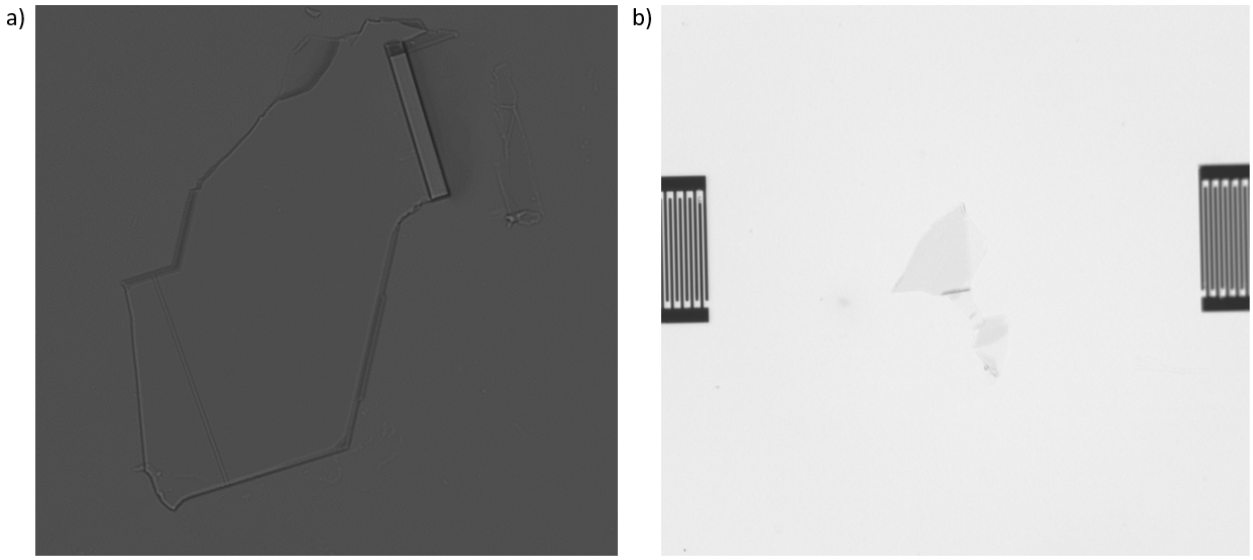

Figure 29: a) hBN flake on glass cover slip, b) hBN flake in delay line of SAW device.

Once a large, thin hBN flake has been located and transferred onto the final substrate, it is possible to move to the next step in the experimental setup. As the hBN on the surface of

the device can experience aging effects when exposed to air, it is important that this stamping process is completed directly before experiments. It was found that hBN flakes on the surface of the SAW device had no noticeable effects on the S-parameters of the device.

6.5 Flow Cell Assembly

Once a flake has been placed onto the SAW device, the PCB assembly (seen in Figure 23) can be built. The wirebonding of this PCB assembly is then tested in air using the VNA characterization process shown in Section 6.3. The PCB assembly is then placed onto a microscope adaptor and secured using double sided tape. A flow cell is then used to interface the buffer containing the biomolecules with the SAW device surface.

A custom flow cell was designed to deliver biomolecules to the surface of the SAW device. This flow cell is designed to only expose the IDT region of the SAW device to a fluid environment. Exposing the regions of the chip without SiO_2 to a fluid environment results in unwanted electrical coupling. Exposing these regions to fluid also has the potential to result in rapid contamination and physical damage. To achieve the necessary isolation, an O-ring was selected with a diameter that fits around the IDT region of the device. This flow cell was also designed to have both an inlet and an outlet to enable the possibility to flush buffer across the surface of the SAW device. The flow cell is secured to the SAW substrate through the use of a custom microscope adaptor. An illustration of the designed flow cell assembled with the microscope adaptor can be seen below in Figure 30.

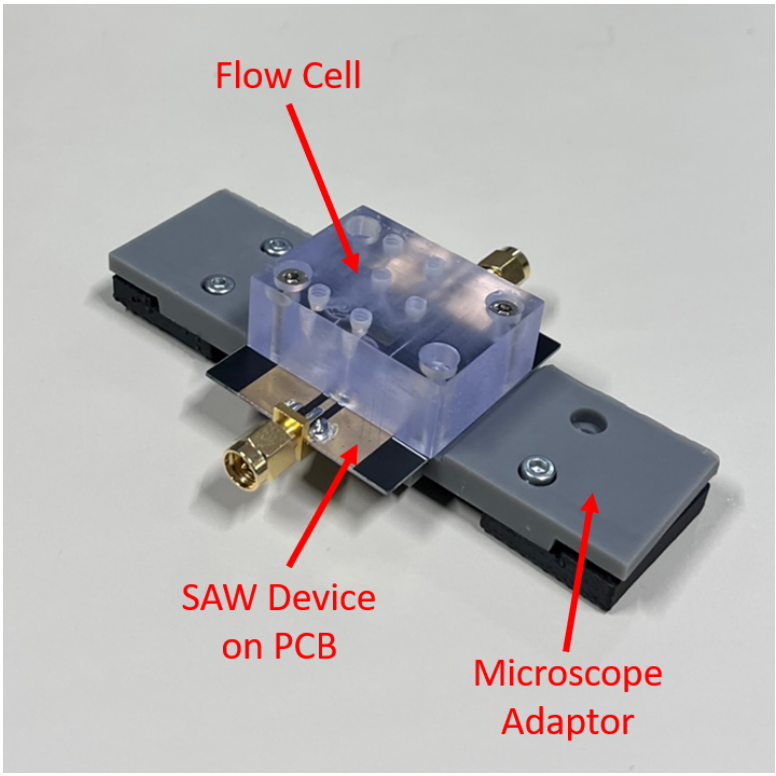

Figure 30: Flow cell assembled onto SAW device with microscope adaptor

In order to attach the flow cell to the SAW chip, a specific assembly order was required. The first step of this process was to place a 4 μL droplet of milliQ water onto the IDT region of

the SAW device. This droplet wets the SAW surface and prevents an air pocket from forming in the flow cell. The flow cell was then positioned over the IDT region and was slowly lowered into place. Once the O-ring made contact with the SAW chip, the flow cell and PCB assembly were secured using four bolts that pass through the flow cell into the microscope adaptor. An illustration of this assembly process can be seen below in Figure 31.

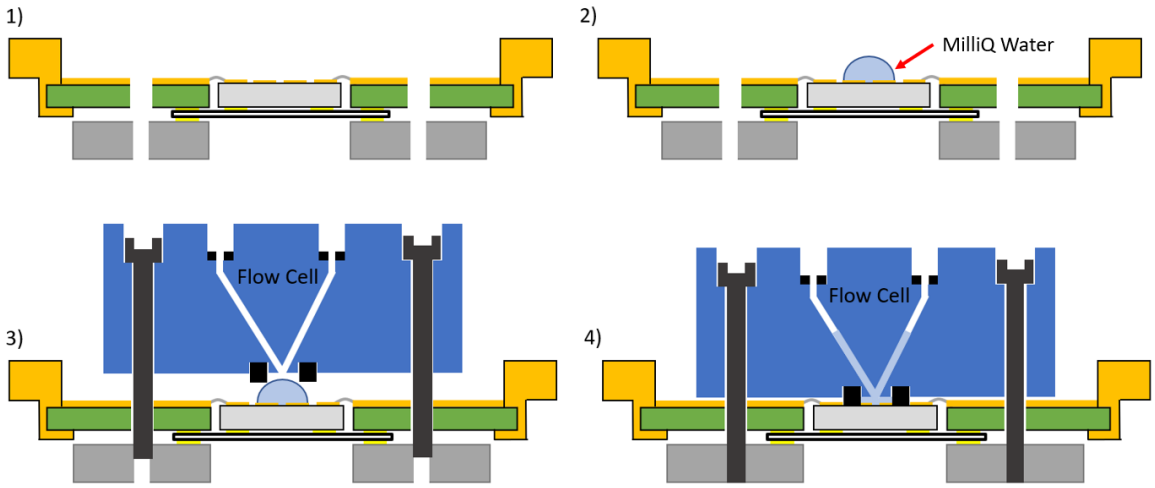

Figure 31: Assembly procedure for placement of flow cell

At this point the SAW is characterized again to ensure that the wire bonds were not broken by the O-ring contacting the SAW chip. Once the integrity of the wire bonds are confirmed, the SAW device is fully prepared for experimentation.

6.6 Optical Setup

The microscope that was used for measurements of biomolecule fluorescence was a Nikon Eclipse Ts2-FL inverted fluorescence microscope. This microscope is equipped with two LED laser sources at wavelengths of 525 nm and 470 nm. For the conducted experiments, the 525 nm light source was primarily used, as it is closest to the excitation wavelength of the Cy3 fluorescent dyes attached to the three different types of biomolecules as discussed in Section 6.8. In order to separate the fluorescence light from the reflected excitation light, a filter cube with a dichromatic mirror was utilized. A 60X magnification water immersion apochromatic objective lens was used for all experiments.

In order to load the SAW device and flow cell into the microscope, a custom microscope adaptor was developed. This adaptor was created as a means to secure the flow cell as well as to interface the assembly with the microscope. The adaptor is secured in place using a set of pressure clamps. Once the adaptor plate was secured in the microscope, a dark hood was placed over the top of the microscope in order to reduce background light. The microscope setup used in this research can be seen below in Figure 32a.

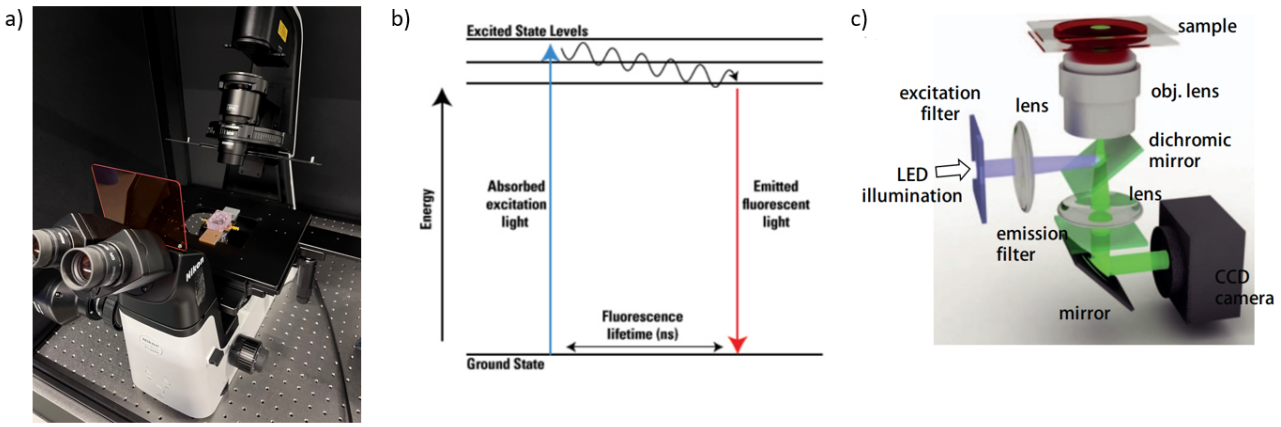

Figure 32: a) SAW device assembly mounted in fluorescence microscope, b) Excitation of fluorescent molecule energy states,[63] c) Optical path of fluorescence microscope. Adapted from Cho et al.(2013)[64]

This microscope is a wide-field epifluorescence microscope. When a fluorescent molecule is excited by the microscope's LED source, the energy state of the molecule drops back into an unexcited state, which releases a photon of a different wavelength, illustrated in Figure 32b.[64] The emitted photon travels through the microscope objective and a dichromatic mirror, which filters the excitation wavelength from the fluorescence, allowing for imaging of fluorescence in the sample.[64] An example of the optical path of an epifluorescence microscope can be seen in Figure 32c.

With this microscope, it is possible to directly measure the fluorescence near or on the surface of an hBN flake located on a SAW device. It is possible to determine if a molecule is on the surface of the device or in the bulk solution based on if the molecule is in focus or out of focus. This principle was tested using fluorescent polystyrene beads with a diameter of 1.5 μm. It was found that it is possible to differentiate beads that are directly on the SAW surface from those in the bulk solution.

6.7 SAW Electronics

In order to actuate the SAW device designed in section 6.2, it was necessary to implement a high frequency signal generation setup. As the driving frequency for the SAW device was set to be 416 MHz, it was necessary that all components of this setup should be able to operate at or above this frequency.

This experimental setup was designed to be able to generate both standing waves and beating waves in the SAW device. Two phase-coupled microwave signal generators, connected on each side of the SAW device, were used to create these waves. Phase-coupling was achieved using a 10MHz external reference signal from a signal generator(Rohde&Schwarz SM300). In order to measure the difference in phase between the two main signal generators, a digital oscilloscope (Rohde&Schwarz RTB2004) was used. An illustration of the signal generation setup can be seen below in Figure 33.

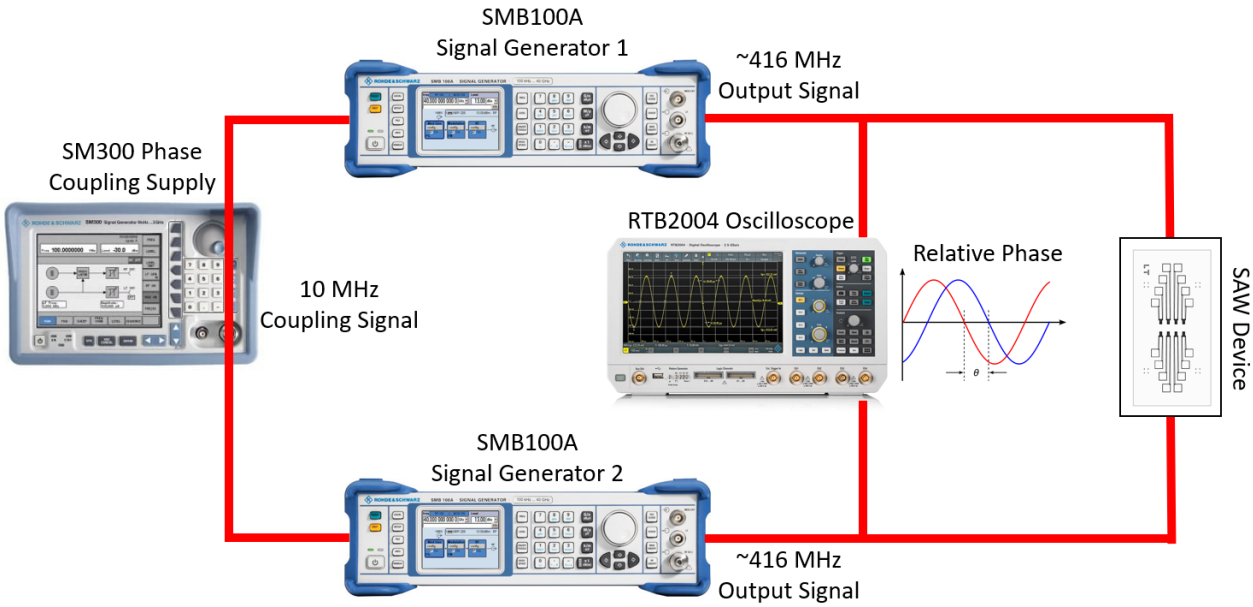

Figure 33: RF signal generation setup with SAW device connected

In order to generate a standing wave in the SAW device, the relative phase between the signal generators must be measured and adjusted to zero. Similarly, in order to generate a beating wave it is necessary to have the signals out of phase. The larger the relative phase, the faster the beating wave will travel.[46] The phase was measured and adjusted to create both types of waves in the molecule actuation experiments described in section 6.10.

6.8 Biomolecule Preparation

Before beginning experiments, it was necessary to prepare the biomolecules that will be analyzed in this research. Each of the selected molecules have unique characteristics that make them interesting as experimental subjects. The biomolecules used in this research are the following: lambda DNA, M13mp18 DNA, and α-synuclein. A description of these molecules and their characteristics can be found below.

1. **Lambda DNA**. This molecule is a DNA molecule comprising of both single-stranded and double-stranded segments of DNA. The total length of the molecule used was 20 kbp, which equates to around 7 μm when fully linearized.[54] This molecule is useful due to its large size and its bright fluorescent signal when multiple sites along the length of DNA are labeled. It has also been shown that it is possible to linearize this lambda DNA through induced flow.[65] It may be possible to observe this same phenomenon due to interactions with hBN and SAW actuation.

2. **M13mp18 DNA**. This molecule is a single-stranded Virion DNA that is isolated from an M13 lac phage vector.[66] This molecule has a length of 7.249 kbp, which is equivalent to 2-3 μm when fully linearized. This molecule is of interest as many biomolecule-hBN diffusion simulations have been conducted using single-stranded DNA.[35] Using these molecules it may be possible to compare experimental results to the simulated results of other research groups.

3. **α-synuclein**. This molecule is a presynaptic neuronal protein that is linked genetically to Parkinson's disease.[67] α-synuclein is composed of 140 amino acids and is a relatively small molecule compared to the lambda DNA and M13mp18 DNA. This molecule is of interest as the overall goal of this project is to be able to apply SAW-driven molecule manipulation to protein sequencing. However, it was found that the small size of this molecule presents challenges that will be discussed in a later section.

While both lambda DNA and M13mp18 DNA are relatively long molecules, they are only a few nanometers wide. As such, it is not possible to directly view the molecules using optical microscopy. As these biomolecules cannot be seen using optical microscopy it is necessary to use fluorescence microscopy. In fluorescence microscopy, fluorescent dyes attached onto a biomolecule are observed. Using this fluorescence measurements it is possible to image the behavior of single molecules.

There are many different labeling methods that can be used to prepare a molecule for fluorescence measurements. The biomolecules used in this report were all labeled with Cy3 fluorescent dyes: α-synuclein was labeled with monoreactive maleimide Cy3 dye, and M13mp18 DNA and lambda DNA with Cy3 fluorophores using Mirus Label IT Nucleic Acid Labeling Kit. For α-synuclein, only a single Cy3 dye was attached to each molecule. For M13mp18 DNA and lambda DNA, a Cy3 dye was attached every 20-60 base pairs. This means there are many dyes per molecule and as such, each molecule produces much more fluorescence than α-synuclein.

6.9 Biomolecule Surface Interaction Experiment

The first experiment conducted in this research was an observation of biomolecule diffusion on an hBN surface. In order to facilitate this experiment, hBN flakes were placed onto cover slips using the direct transfer and PPC transfer methods discussed in section 6.4. The cover slip was then secured to a microscope adaptor using adhesive tape. A flow cell was not used in this experiment in order to minimize the optical effects caused by additional material interfaces. The microscope adaptor loaded with the sample was then mounted onto the fluorescence microscope, as was illustrated in Section 6.6. Before any biomolecules were added to the cover slip, both bright field and fluorescence images of the hBN flake were taken..

For each diffusion experiment, the biomolecule of interest was prepared by diluting a feed stock with a 10 mM Tris, 50 mM NaCl, pH 8.0 buffer. Different concentrations of biomolecules were prepared for multiple test cases. For each experiment, a droplet of diluted biomolecule solution was carefully placed onto the region of cover slip in which the hBN flake was stamped. The microscope camera exposure time per a single frame was adjusted to be able to see the fluorescence signal of the molecules and videos were taken of the experiment. The results of these diffusion experiments can be found in Section 7.1.

6.10 Biomolecule Actuation Experiment

Actuation experiments of molecules on hBN flakes are critical for understanding if it is possible to transport biomolecules on a 2D hBN surface. The first step of this experiment was placing hBN flakes in between the IDTs of a SAW device, which was accomplished using the methods illustrated in Section 6.4. The SAW device was then assembled into the PCB assembly and wirebonded as illustrated in Figure 23. Finally the PCB was integrated with a flow cell and was mounted onto the fluorescence microscope.

The biomolecule for each experiment was introduced and incubated to the SAW device surface through the use of the flow cell assembly seen in Section 6.5. If it was found that many molecules remained in the bulk solution then the flow cell was flushed with buffer. Once the biomolecules were incubated and the number of molecules in the bulk solution was reduced, a measurement of the molecule diffusion on the hBN surface was conducted. This diffusion measurement provided a means to compare actuated and actuated motion of the particles on the surface.

Using the RF setup shown in Section 6.7, it was possible to conduct a number of experiments with SAW actuation. The first experiment consisted of actuating the SAW device with zero phase shift between the signal generators. Multiple different power levels were used in order to analyze how additional power affects actuation. In theory, the lack of a phase difference results in a standing wave. This standing wave was expected to result in trapping of molecules.

The second experiment that was conducted was a beating wave actuation of the SAW device. In order to generate a beating SAW, it was necessary to shift the relative phase between the two signal generators. The propagation speed of the wave is proportional to the amount of phase shift. As such, for each actuation experiment, a number of different relative phases were implemented.

7 Results and Discussion

7.1 Biomolecule Interaction with hBN

Before attempting to manipulate biomolecules on hBN, it was important to observe and analyze the unactuated behavior of the molecules. As discussed in Section 3, it has been shown that in molecular dynamic simulations, both single-stranded DNA and proteins tend to adsorb and diffuse on a hBN surface. This diffusion has also been shown, in simulation, to result in an unfolding of molecules onto a hBN surface.[17,35] At the time of this research, there has been very little experimental research conducted on this diffusion behavior. Due to the dearth of previous experiments in literature, these results will serve as a baseline for future work regarding this diffusion behavior.

7.1.1 Diffusion of α-synuclein on hBN

In order to conduct this analysis, hBN flakes were prepared and placed onto glass cover slips as discussed in Section 6.9. Before a solution of α-synuclein was place onto the hBN flake, bright field images as well as 525 nm fluorescence images were taken to serve as a baseline for later experiments. An example of these bright field and fluorescence images can be seen below in Figure 34a and Figure 34b.

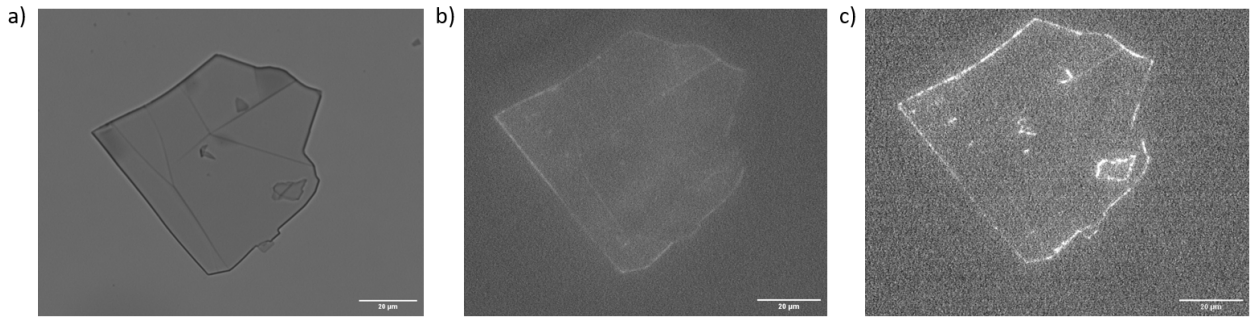

Figure 34: a) Bright field image of flake, b) 525 nm inital fluorescence image of flake, c) 525 nm fluorescence measurement after four minute incubation of 1 nM α-synuclein solution.

The flake used in this experiment was a large flake, with a diameter of approximately 72 μm. This flake was found to be relatively thin and had large areas without any folds, making it optimal for the diffusion experiment, as thinner hBN flakes have higher optical transmission of fluorescence. It can also be seen in Figure 34b that the flake has a overall low fluorescence compared to background fluorescence. The fluorescence that is visible is located on the edges of the flake. A lack of signal coming from the majority of the flake indicates that there is not a significant amount of contamination caused by the exfoliation process and transfer process, as some organic contamination is visible in 525 nm fluorescence images. This lack of visible contamination is important, as it has been observed that contaminants on the hBN surface greatly restrict diffusion of molecules.

A 1 nM concentration of α-synuclein was added onto the glass surface on top of the hBN flake pictured above. Once these molecules were added to the surface, they were left to incubate for four minutes. After incubation, it was possible to begin taking fluorescence measurements. The initial state of the flake after the introduction of the biomolecule can be seen in Figure 34c. The brightness seen on the flake visibly increases with the addition of the biomolecule, as demonstrated by comparing Figure 34c with Figure 34b. New bright spots are also now visible on the surface of the flake. This increase in brightness is a result of the fluorescence of the added α-synuclein.

As illustrated, it is very difficult to detect the fluorescent signal from single molecules of α-synuclein. This is most likely a result of the low sensitivity of the CMOS camera attached on our microscope, the presence of background fluorescence, and the intensity of the fluorescence light from a single molecule. Each α-synuclein molecule is only a few nanometers in diameter and only has a single Cy3 fluorescent label. As such, the signal from any single molecule is extremely limited compared to the fluorescence of larger lambda DNA, which has many thousands of Cy3 labels. This means that it was not possible to directly track the diffusion of α-synuclein on the surface of the flake with the current experimental setup.

A second surface interaction experiment was conducted with a 10 nM concentration of α-synuclein. This experiment was conducted to test the hypothesis that it may be possible to observe group behavior of a large number of α-synuclein molecules on the surface. Before adding the molecules to the surface, bright field and fluorescence images were taken once again for the purpose of post-experiment comparison. These images of the flake can be seen below in

Figure 35a and Figure 35b.

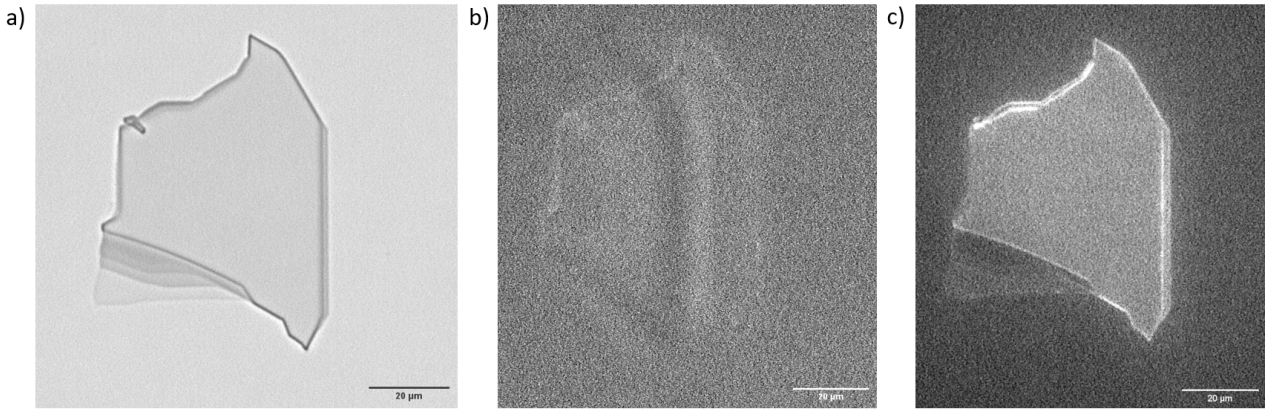

Figure 35: a) Bright field image of flake, b) 525 nm fluorescence image of flake, c) 525 nm fluorescence measurement after four minute incubation of 10 nM α-synuclein solution.

The flake use in this experiment was a large flake, with a width of 51 μm and a length of 69 μm. It can also be seen in Figure 35 that the flake has an overall low fluorescence compared to background. The initial fluorescence measurement that was taken after incubation of 10 nM a-synuclein can be seen in Figure 35c.

It is clear that the surface of this flake shows a much brighter fluorescence due to the higher concentration of α-synuclein. However, despite this brighter signal, it was still not possible to analyze the behavior of single molecules, as it is impossible to distinguish the light emitted by a single molecule. In order to evaluate the diffusion behaviour on α-synuclein, a higher resolution microscope or fewer brighter molecules are needed.

7.1.2 Diffusion of M13mp18 DNA on hBN

The interaction of M13mp18 DNA and hBN was also analyzed. In order to accomplish this, the same experimental setup was used as for previous diffusion experiments. This included the fabrication and stamping of an hBN flake onto a glass cover slip, before taking bright field and fluorescence images, shown in Figure 36a and Figure 36b.

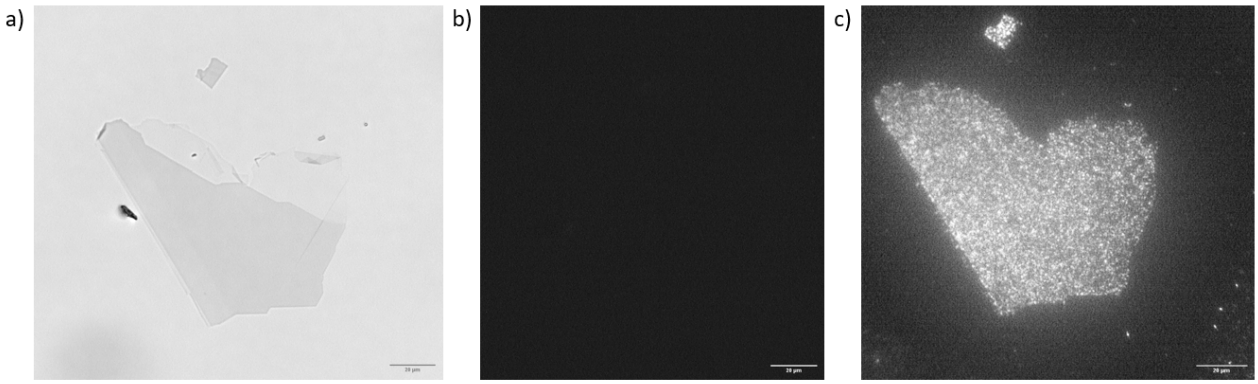

Figure 36: a) Bright field image of flake, b) 525 nm fluorescence image of flake, c) 525 nm fluorescence measurement after four minute incubation of 100 pM M13mp18 DNA solution.

This flake has a size of around 112 μm in width and 90 μm in length. This flake was found to be slightly thicker than many of the other flakes analyzed. It is important to note that there was very little fluorescence being emitted from either the center or edges of the flake, indicating the possibility that the hBN has little surface contamination and minimal defect sites, as the flake is not visible in Figure 36b.

A solution of M13mp18 DNA was prepared with a concentration of 100 pM. This solution was then introduced onto the surface of the hBN flake and was allowed to incubate for four minutes. After incubation, an initial fluorescence measurement was taken. The results of this measurement can be seen in Figure 36c.

The individual M13mp18 DNA molecules can clearly be seen on the surface of the flake. It was found that the 100 pM M13mp18 DNA solution resulted in a very high coverage of the flake surface with molecules although very few molecules of M13mp18 DNA seemed to be present on the glass surface near the flake. This indicates that the M13mp18 DNA preferentially adsorbed to the hBN surface. From the fluorescence present on the flake, it appears that the molecules on the flake have an even density distribution.

By evaluating how the molecules change in position between frames it is possible to determine their behavior on the hBN surface. As such, a video of this motion was taken and analyzed. In this analysis, it was found that these molecules begin to photo-bleach within minutes of introduction to the hBN flake. An illustration comparing the brightness of molecules on the surface at the beginning of the experiment and sixteen minutes into the experiment can be seen below in Figure 37.

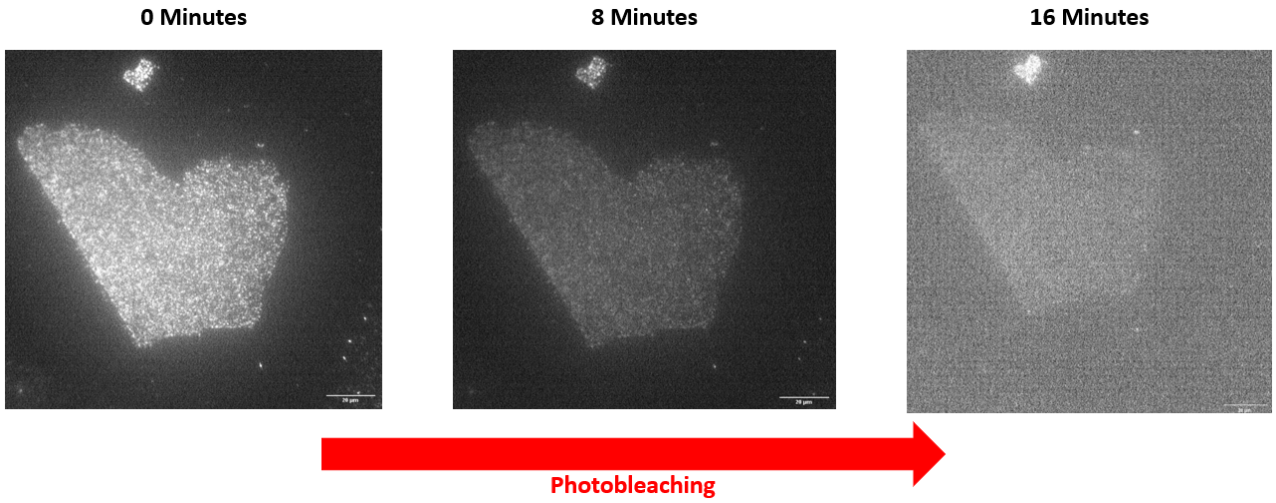

Figure 37: Comparison of 525 nm fluorescence from M13mp18 DNA before and after photobleaching.

This high rate photo bleaching is potentially a result of the unfolding of the M13mp18 DNA onto the hBN crystal surface. However, this behavior was not observed in either α-synuclein nor lambda DNA. As such experiments utilizing this molecule had to be conducted in a very short time frame in order to be able to observe and measure molecule motion.

Despite the original theory of surface diffusion, no significant diffusion motions of the M13mp18 DNA could be observed on the hBN flake through fluorescence microscopy observation over time. This could be a result of surface contamination that was not detected optically, the crowding of M13mp18 DNA on the hBN surface, or the strong interaction between the hBN surface and such a long DNA molecule. The high density of M13mp18 DNA molecules may have resulted in restricted diffusion of molecules due to the limited surface area for motion. It is also possible that surface defects or residue from the PPC transfer process resulted in the molecules "sticking" to the surface. In the future, this should be repeated with a smaller concentration of M13mp18 DNA molecules to rule out crowding effects.

It is also possible that the absence of the expected diffusion process of the single-stranded DNA is due to incorrect molecule dynamic simulations. It is possible that these simulations do not reflect how the molecules may actually behave. In these molecule dynamic simulations, the molecules freely diffused and unfolded onto the hBN surface. However, these simulations did not account for many of the crystal defects and manufacturing residues that are present on a real hBN flake. Additional simulation and experimentation may be necessary to understand the phenomenon and why the behavior of M13mp18 DNA differs from the simulated works.

7.1.3 Diffusion of Lambda DNA on hBN

The final molecule that was analyzed for surface interaction was lambda DNA. This molecule is of particular interest, as it is the brightest and largest of the molecules selected for experimentation. The SAW device was also designed to manipulate molecules with a size similar to these lambda DNA molecules. However, lambda DNA interaction with hBN has not been simulated in literature using molecular dynamics simulations. This means that while it may be easy to view these molecules, the observed behavior does not have a backing in literature. For

this reason, It was very important to observe unactuated molecule interaction with the hBN flake before SAW actuation was investigated to establish baseline interactions.

The bright field and fluorescence images of the hBN flake used for the first experiment can be seen below in Figure 38a and Figure 38b.

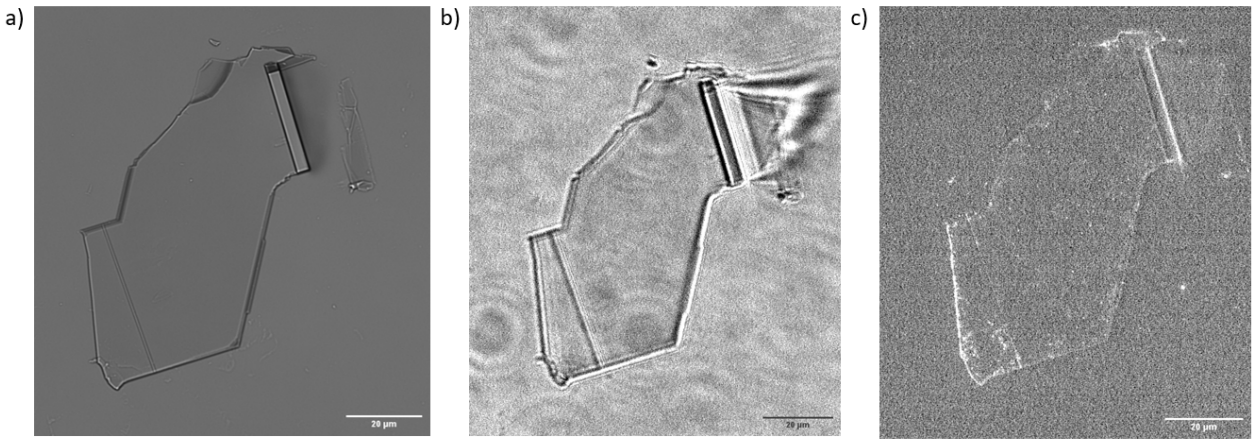

Figure 38: a) Bright field image of flake, b) 525 nm fluorescence image of flake, c) 525 nm fluorescence measurement after four minute incubation of 3 pM lambda DNA solution.

This flake has a size of around 40 μm in width and 70 μm in length, as shown in Figure 38. While the majority of this flake is thin, there is a portion of the flake that has been folded and is much thicker. As such, this section of the flake exhibited different behavior from the rest of the flake. It is also important to note that no significant fluorescence was seen in the center region of the flake, but there was some fluorescence emitted by the edges of the flake. It was decided that this flake was suitable for diffusion experiments.

A 3 pM concentration of lambda DNA was introduced onto the surface of the hBN flake and was allowed to incubate for before Fluorescence images of this flake were taken. The initial fluorescence of the molecules on the hBN flake can be seen in Figure 38c. The fluorescence image after incubation shows no significant increase of fluorescence in comparison to the background image. This indicates that the molecules that were deposited on the flake were so diffuse that they did not increase the overall fluorescence significantly. However, it is possible to see small, bright spots on the surface of the hBN flake in the image shown. These spots are lambda DNA molecules that were deposited from the solution. These bright spots on the surface of the hBN had only a 300 nm spot size. This means that these molecules are most likely not the intended full size lambda DNA molecules but are fragments of the lambda DNA that have broken off due to handling or fluorescent labeling, which could occur because lambda DNA becomes more unstable as more Cy3 labels are attached. As such, the behavior of these small fragments provides insight into the diffusion dynamics of molecules on the surface.

After measuring the initial fluorescence of the flake, a series of fluorescence measurements were taken to measure molecule motion. In these measurements, many of the small fragments of lambda DNA can be seen moving on the surface of the hBN flake. This behavior was observed mainly for molecules in the center of the hBN flake. An overview of the flake with the molecule paths tracked can be seen below in Figure 39.

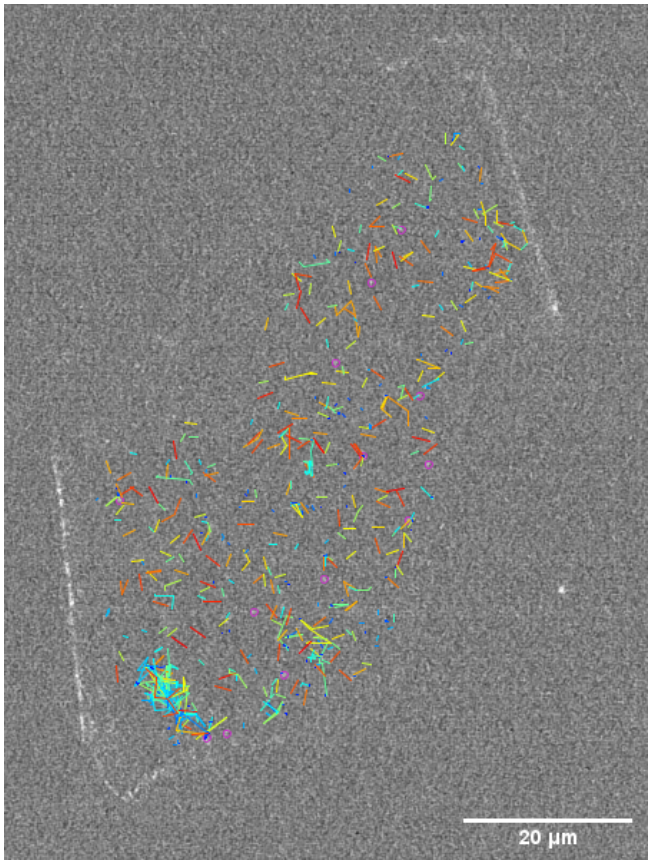

Figure 39: Tracking of lambda DNA fragment movements on the surface of an hBN flake.

During the tracking of the molecules' motion, it was found that the molecules tended to move sporadically in a small region of the flake. This indicates that the molecules are freely diffusing across the surface of the flake. This conclusion closely supports the results of the molecule dynamics simulations seen in Section 3. Molecules that were moving on the surface moved at a speed between 0.5 $\mu m/s$ and 4 $\mu m/s$ with an average of 1.47 $\mu m/s$. A plot of the molecule paths average measured diffusion speed can be seen below in Figure 40.

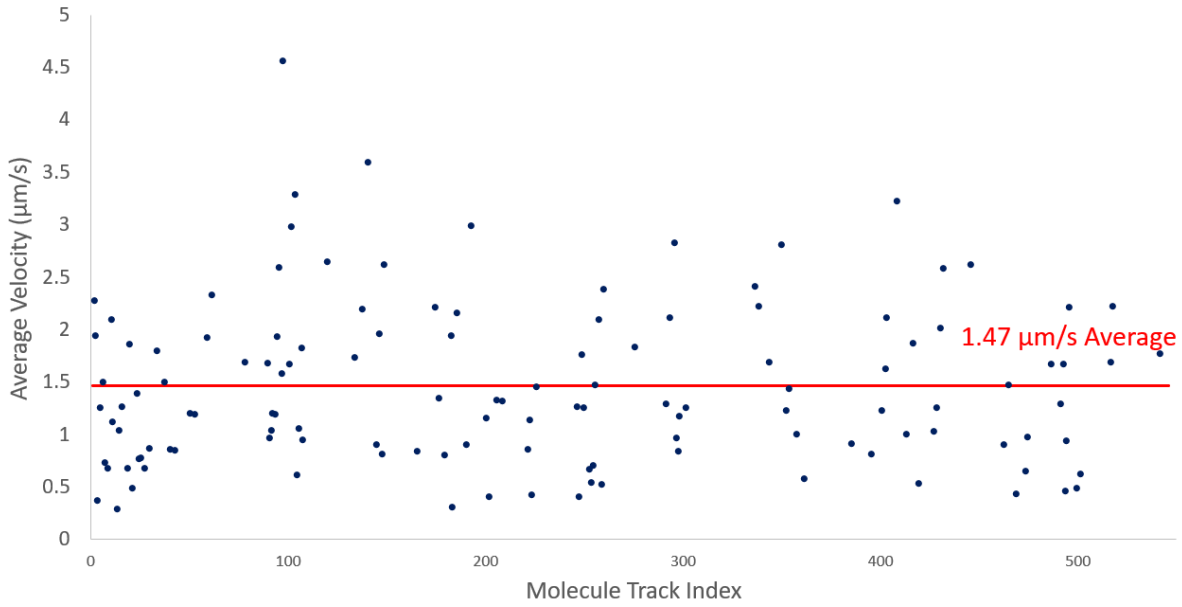

Figure 40: Average velocities of molecules tracked on surface.

It is important to note that not all of the lambda DNA fragments were shown to be in free diffusion. Many of the molecules appear to be stuck to either the edge of the flake or to specific spots in the center of the flake. This is most likely a result of surface contamination or from defects in the crystal that cause the DNA to remain stationary in specific locations on the chip. Overall, the results of this experiment support the possibility that lambda DNA will adsorb and freely diffuse on the surface of hBN. While it is not possible to see the length of the DNA fragments with the microscope used in the experiment, it can be speculated that this free diffusion of the molecules results in the unfolding of the molecule.

A second diffusion experiment was conducted under the same conditions but with a different hBN flake. Both bright field and fluorescence measurements were taken and can be seen below in Figure 41a and Figure 41b.

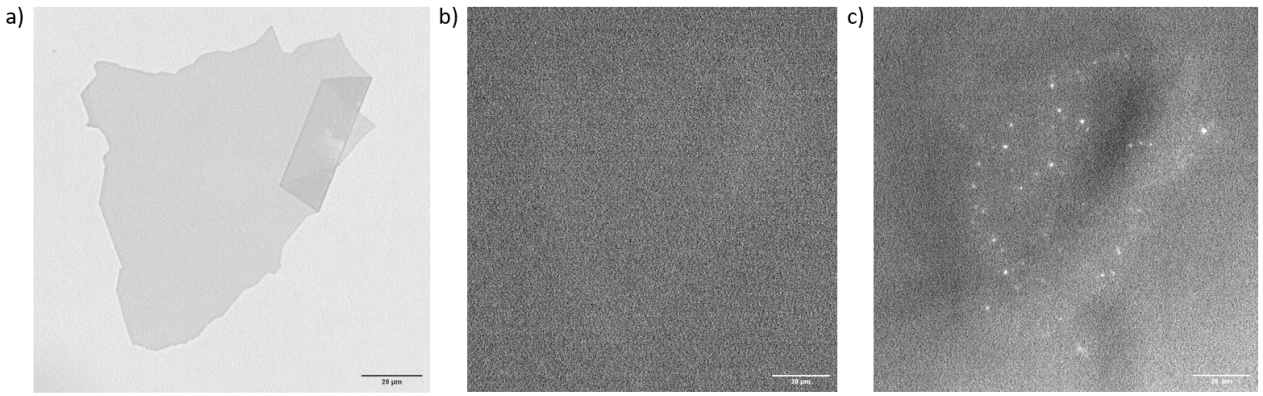

Figure 41: a) Bright field image of flake, b) 525 nm fluorescence image of flake, c) 525 nm fluorescence measurement after four minute incubation of 30 pM lambda DNA solution.

Figure 41 shows that this flake has a size of around 74 μm in width and 92 μm in length. the majority of this flake is a thin flat surface. However, there is a section that is folded in upon itself resulting in a much thicker area. It was found that the fluorescence emitted by this flake is very faint and is located primarily on the flake edges.

A solution of 30 pM lambda DNA was placed onto the surface of this hBN flake was allowed to incubate for four minutes before observation. Intial fluorescence can be seen in Figure 41c. The lambda DNA molecules are visible as light spots with a size of around 2.5 μm in diameter, the size that we expect from unlinearized lambda DNA. When analyzing experiment video, many lambda DNA molecules landed onto the flake surface throughout the course of this experiment. When these molecules landed, they appeared to stick to a single spot on the hBN flake. This sticking meant that no significant diffusion was observed on the surface. However, there was some flickering motion of the molecules that were on the surface.

It is possible that only one part of the lambda DNA was making contact with the crystal surface. This may be a result of the fact that lambda DNA is composed of both single-stranded DNA and double-stranded DNA. It is believed that the single-stranded DNA has a higher interaction with the hBN surface than double-stranded DNA. As such, the end of the lambda DNA molecules attached to the surface and the remainder of the molecule remained floating in the buffer. This phenomenon explains the flickering motion of the molecule around a fixed point on the crystal. However, it is also possible that the molecules are fully attached to the surface and the flickering is a result of localized diffusion.

A final diffusion experiment was conducted using lambda DNA. A hBN flake was created and transferred to the glass substrate using the same method as previously discussed. Both bright field and fluorescence measurements were taken and can be seen below in Figure 42a and Figure 42b.

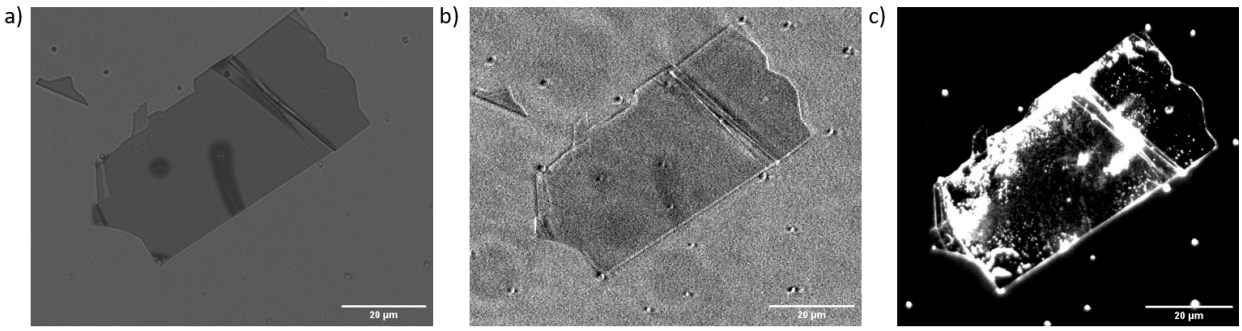

Figure 42: a) Bright field image of flake, b) 525 nm fluorescence image of flake, c) 525 nm fluorescence measurement after four minute incubation of 150 pM lambda DNA solution.

The flake used for this experiment was generally thin with a smooth surface of of 62 μm by 32 μm. However, it was also found that this flake was placed on top of defects in the glass cover slip. These defects resulted in a strained surface in the hBN that is clearly visible in bright field and fluorescence images. Despite these defects, the majority of the flake emits fluorescence that is similar in intensity to the background fluorescence of other flakes. A solution of 150 pM lambda DNA was placed onto the surface of this hBN flake. The lambda DNA was allowed to incubate for a four minutes before observation. An initial measurement of the molecule

fluorescence was then taken. This initial measurement can be seen in Figure 42c.

This initial fluorescence measurement is very different from the other measurements taken of lambda DNA. A much higher concentration of lambda DNA was placed onto the surface of this flake and as such, it was possible to see clumps of full sized lambda DNA instead of single molecules. These lambda DNA clumps are much brighter and larger than any of the previously tested molecules.

A video of the fluorescence emitted by the lambda DNA was taken in order to evaluate the surface behavior of the molecules. The video proved the ability to observe clumps of lambda DNA diffusing across the surface of the hBN flake. An illustration of this motion can be seen below in Figure 43.

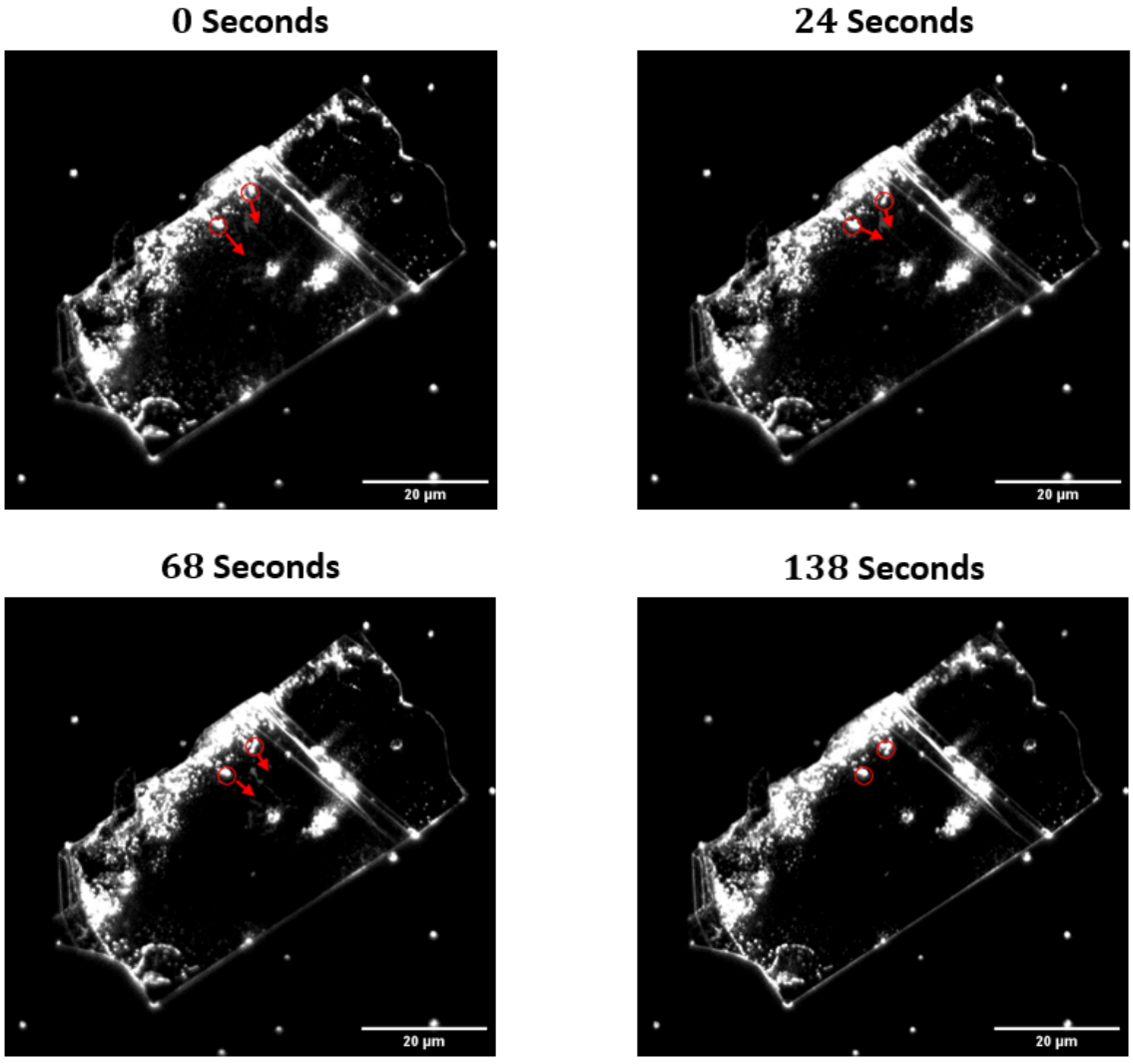

Figure 43: Time series/stamps of lambda DNA molecules diffusing on hBN surface.

It was found that some of the lambda DNA clumps were in fact diffusing on the hBN surface. The diffusion of these lambda DNA clumps was much slower than the diffusion of the small lambda DNA fragments. It was measured that the molecules seen shifting in Figure 43 where moving at a rate of approximately 0.02 $\mu m/s$. The diffusion shown in this experiment did not

demonstrate the expected random walking that was shown in molecule dynamics simulations. Instead, the molecules tend to migrate from high concentration regions near the edges of the flake towards the lower concentration regions in the center of the flake. This behavior is different from the behavior observed for the DNA fragments and single lambda DNA molecules. This change in surface interaction may be a result of the clumping of the molecules. This clumping may lead to decreased surface interaction and increased molecule mobility.

7.2 SAW Actuation of Molecules

Experiments to manipulate molecules using SAW devices were prepared in a manner as described in Section 6.10. For each actuation experiment, new hBN surfaces were generated and transferred onto SAW devices in order to limit possible surface contamination from previous experiments. The biomolecules used in each experimental work were then placed onto the hBN. Finally the SAW device was driven at different power levels and phase shifts in order to analyze the behavior of the molecules on the surface.

7.2.1 SAW Actuation of α-synuclein

The first biomolecule to be used for actuation experiments was α-synuclein. It was shown in previous sections that it was not possible to see individual molecules of α-synuclein using this experimental setup. However, it was believed that by using a SAW device, it may be possible to see some dynamic behaviour of a large number of α-synuclein. As such, an hBN flake was prepared and transferred onto a SAW device for initial imaging, shown below in Figure 44a and Figure 44b.

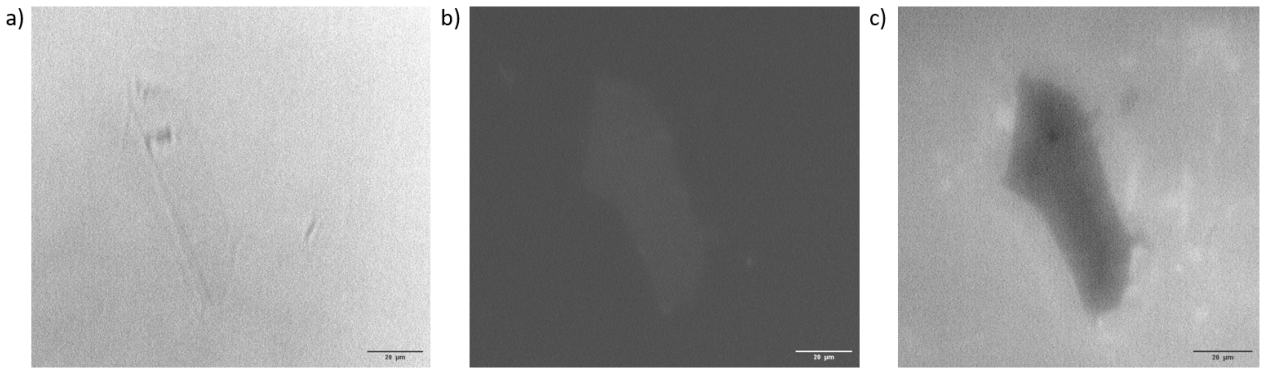

Figure 44: a) Bright field image of flake, b) 525 nm fluorescence image of flake, c) 525 nm fluorescence measurement after four minute incubation of 10 nM α-synuclein solution.

This flake had a size of around 80 μm by 30 μm. It was selected for this experiment because it was an relatively thin flake. This is important as the light emitted from α-synuclein has a low intensity and is mostly absorbed by the layers of material it must travel through to reach the microscope. In Figure 44b, it was found that after being transferred to the SAW device, the surface of the flake was emitting some fluorescence. This fluorescence may be a result of surface contamination or may simply be a result of the very thin nature of the flake. It was decided that this flake was still viable for use in the actuation experiment, despite this fluorescence.

A solution of 10 nM α-synuclein was prepared and was injected into the flow cell. These molecules were allowed to incubate for a four minutes before initial measurements were taken. These initial results can be seen in Figure 44c. In this initial fluorescence measurement, it was found that the background was much brighter then the hBN flake. This means that much of the light emitted by the proteins on the hBN surface is being lost or suppressed. Along with this, it is still not possible to see the signal from single molecules of α-synuclein.

The first actuation experiment was a standing wave actuation of the SAW device. This means that both IDTs were driven using an in phase sine wave. This results in a SAW whose nodes and antinodes are stationary. A series of standing wave experiments were conducted at different power levels. Fifteen frame z-projection images were taken after three minutes of actuation in each experiment. These z-projection images provide an average of the particle fluorescence over these fifteen frames. The images of the actuation experiments can be seen below in Figure 45.

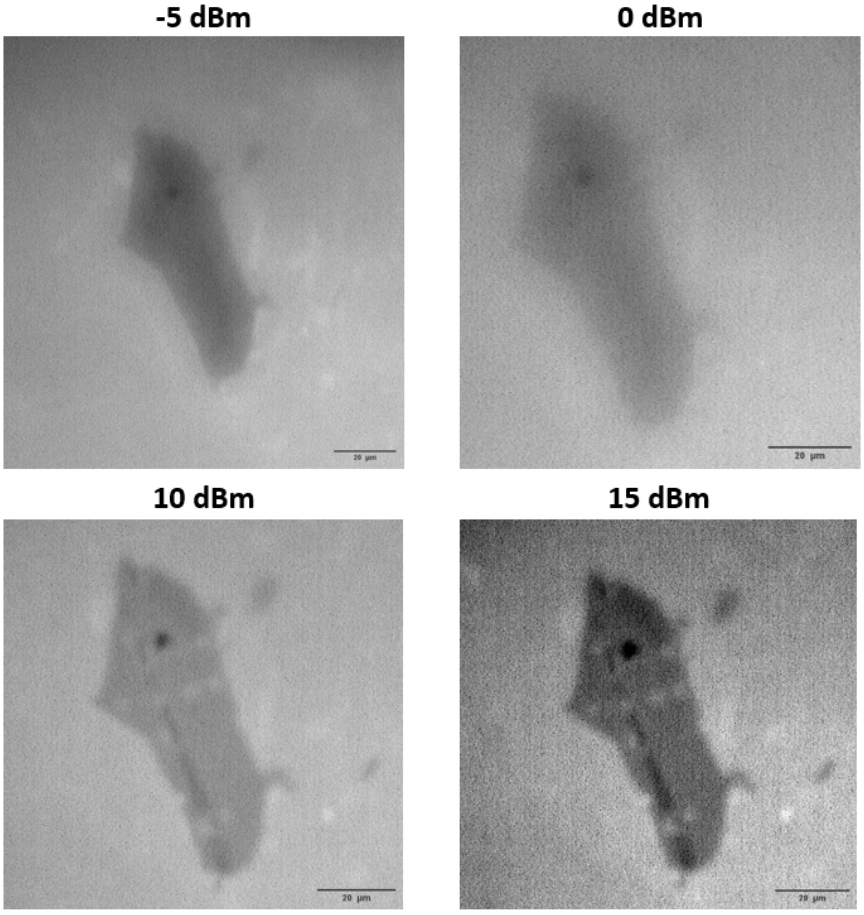

Figure 45: Standing wave actuation of α-synuclein on hBN at different power levels.

In the measurements of standing wave behavior, it was not possible to see motion of individual α-synuclein. Along with this, the molecules did not form ribbons of concentrated particles as expected, despite steady increases in input signal power. At some point between actuation experiments, a line of bright spots appeared on the hBN surface. These bright spots had a spacing of around 6 to 7.5 μm. The spots did not appear during an actuation of the SAW device and were not visibly affected by any actuation of the SAW device. As such, it is difficult to confirm if these spots are α-synuclein or if they are caused by another unknown factor.

The second experiment that was conducted was a beating wave actuation of the SAW device. This beating SAW was generated by changing the relative phase between the input signals. In this case, the relative phase between the input signals was set to 45 degrees. The power for the beating wave was set at multiple different levels and the SAW was actuated. The fifteen frame z-projection images of this actuation can be seen below in Figure 46.

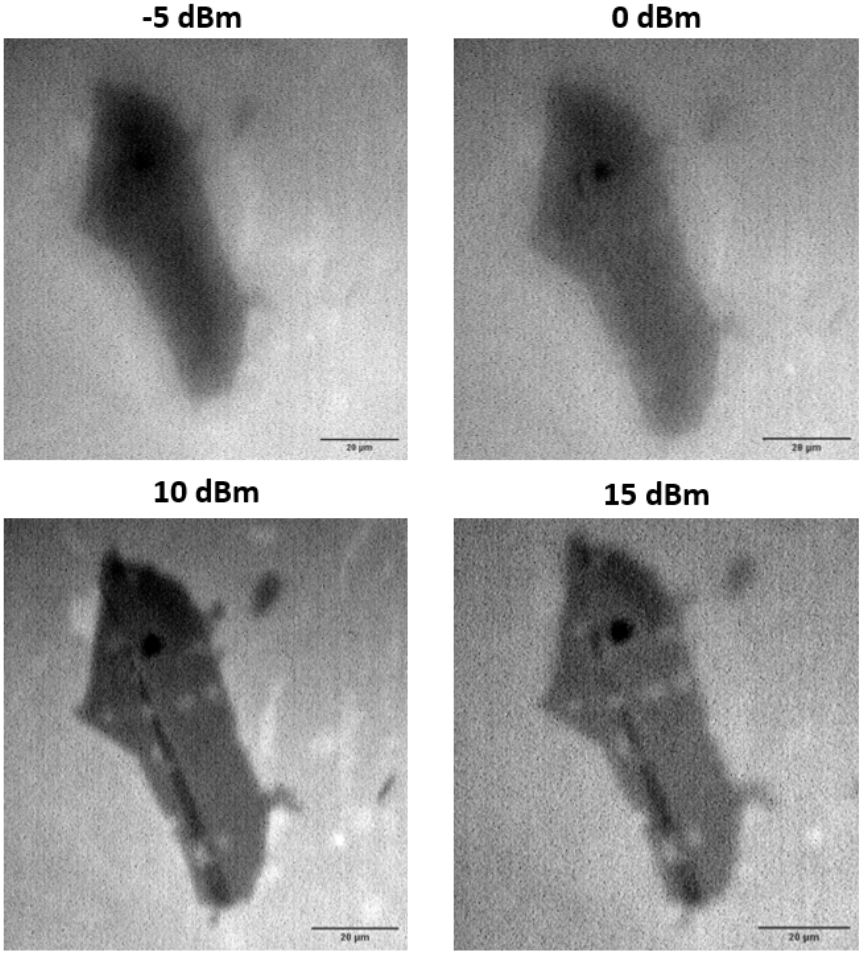

Figure 46: SAW actuation of α-synuclein on hBN with 45 degree phase shift.

The behavior of the molecules on the hBN does not appear to change when a beating wave is applied. No clear patterning nor movement of molecules on the surface could be seen. It was observed that particles in the bulk solution were being moved by the SAW device. However, these molecules were too large to be α-synuclein, so likely are contamination.

Overall, it was found that it was not possible to observe either patterning due to standing waves nor unidirectional motion due to a beating wave. This lack of observable manipulation of the biomolecules may mean that it is not possible to control the motion of α-synuclein with this current SAW design. The small size of α-synuclein may limit the amount of force that the 10 μm wavelength SAW can apply on the molecule.[44,68] It also may not be possible to observe this motion due to the experimental setup and limited microscope resolution. By repeating this experiment with single-molecule microscopy methods, it may be possible to see the behavior of single molecules under actuation.

7.2.2 SAW Actuation of M13mp18 DNA

The second biomolecule that was used for actuation experiments was single-stranded M13mp18 DNA. In earlier experiments, it was not possible to observe diffusion dynamics of M13mp18 DNA on the hBN flake. However, it was believed that it would be possible to observe motion of M13mp18 DNA when a SAW was applied. To test this hypothesis, a new hBN flake was prepared for experiments and imaged, shown in Figure 47a and Figure 47b.

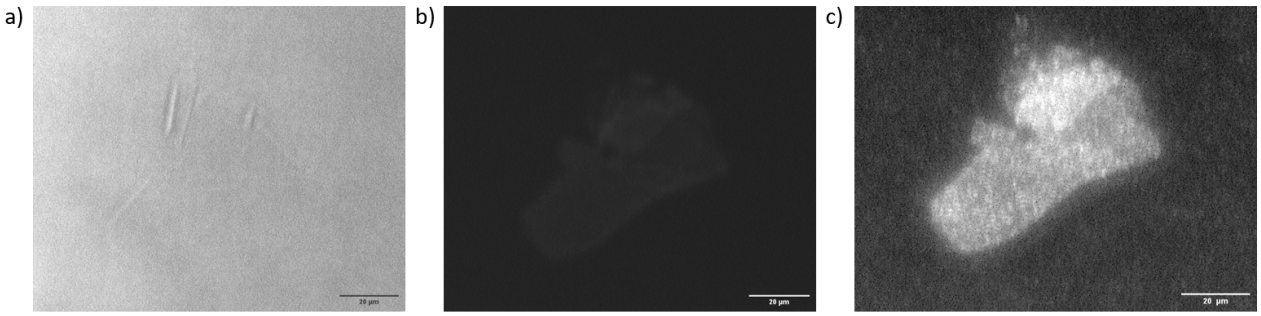

Figure 47: a) Bright field image of flake, b) 525 nm fluorescence image of flake, c) 525 nm fluorescence measurement after four minute incubation of 100 pM M13mp18 DNA solution.

The flake used for this experiment had a width of 30 μm and a length of 70 μm. This flake is one of the thinnest used during these experiments. This thinness is apparent as the flake is almost invisible in bright field images. As has been seen in the past, this flake emits more fluorescence due to it being so thin. It was decided that despite this initial fluorescence this flake was suitable for actuation experiments.

A solution of 100 pM M13mp18 DNA was prepared and was placed into the flow cell. This DNA was circulated through the flow cell and then was allowed to incubate for four minutes. An initial measurement of the flake surface was taken before actuation and can be seen in Figure 47c. Unlike in the previous α-synuclein experiment, it is possible to see the individual molecules of M13mp18 DNA on the surface of the flake, represented by individual fluorescent dots. Due to the large number of molecules on the surface, it is difficult to determine if these molecules are freely diffusing on the surface of the flake.

Once the molecules had been shown to be adsorbed to the hBN surface, it was possible to begin SAW actuation. The first tests that were conducted were standing wave tests at different power levels. The goal of these test were to determine if it was possible to generate a pattern of M13mp18 DNA on hBN using a standing SAW. The result of these actuation experiments can be seen below in Figure 48.

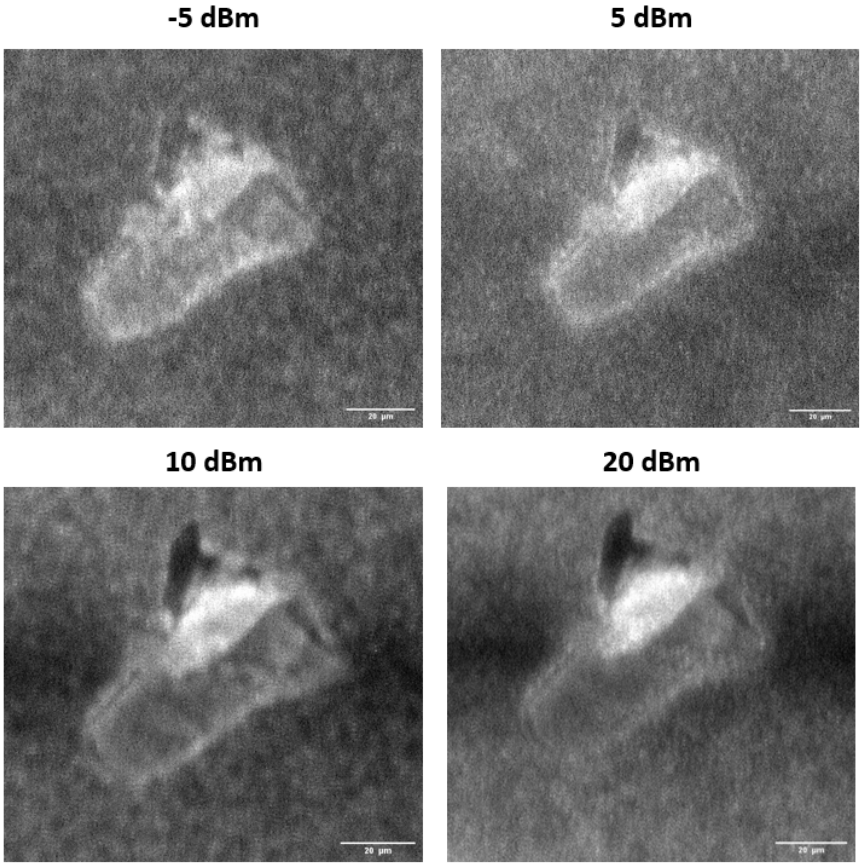

Figure 48: Standing wave actuation of M13mp18 DNA on hBN at different power levels.

Over the course of the standing wave actuation experiments, it was found that no patterning of the M13mp18 DNA was observable. Along with this, it was found that the molecules visible on the surface appeared to disappear between actuation experiments. This is most likely a result of the photobleaching that was shown in Figure 37. Another possible cause for this lack of visible fluorescence on the hBN may also be the removal of the molecules from the surface. However, this is most likely not the cause due to the fact that much of the fluorescence was lost between experiments and not during actuation. A phenomenon that was observed during this experiment was that when the SAW device was actuated, it increased the rate at which M13mp18 DNA molecules deposited onto the substrate and hBN surface. This indicates that the molecules are being pushed towards the surface of the SAW device by the actuation forces. This finding further supports the speculation that the molecules are becoming photobleached instead of being removed from the hBN surface by the SAW.

A second experiment was conducted in which the input signals for the SAW device were set with a relative phase shift of 45 degrees, which should result in a beating wave. This beating wave was applied to the M13mp18 DNA molecules that were adsorbed to the hBN flake used for the standing wave experiments. A comparison of the flake before and during actuation can be seen below in Figure 49.

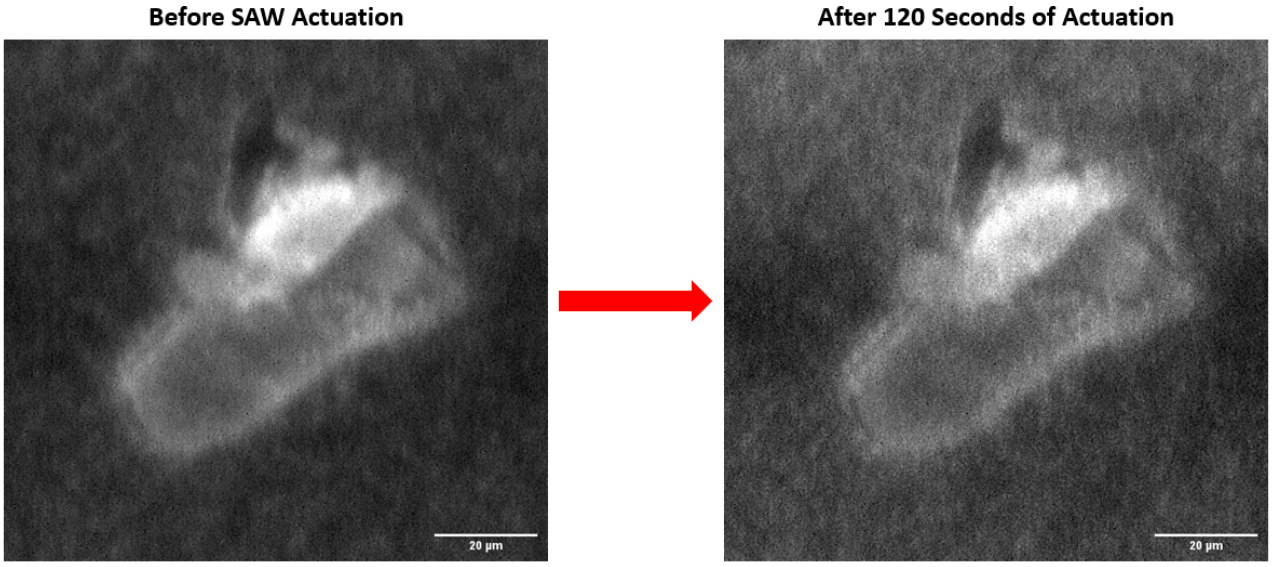

Figure 49: SAW actuation of M13mp18 DNA on hBN with 45 degree phase shift at 10 dBm power.

During this experiment, no measurable shift of M13mp18 DNA molecules could be detected on the hBN flake. The measurements that were taken showed very similar results to the previous standing wave experiment. These results may indicate that it is not possible to manipulate M13mp18 DNA with this experimental configuration.

A phenomenon that was observed in these experiments was the movement of M13mp18 DNA in the bulk solution. It was found that it was possible to see streaming of molecules. The molecules that were in the bulk tended to move from outside the delay line to the center of the delay line of the IDTs. This streaming always tended to move in one direction across the flake. This shows that the molecules in bulk are being unidirectional manipulated using the SAW device, but the molecules adsorbed to the surface appear to be unaffected.

7.2.3 SAW Actuation of Lambda DNA

The final molecule that was used for SAW actuation experiment was lambda DNA. Previously in diffusion experiments, this molecule showed great promise due to its large size and bright fluorescent signal. Fragments of this molecule also showed surface diffusion and surface interaction with hBN, making it an good candidate for further experimentation. A new hBN flake was prepared and bright field and fluorescence images of the flake were taken and can be seen below in Figure 50a and Figure 50b.

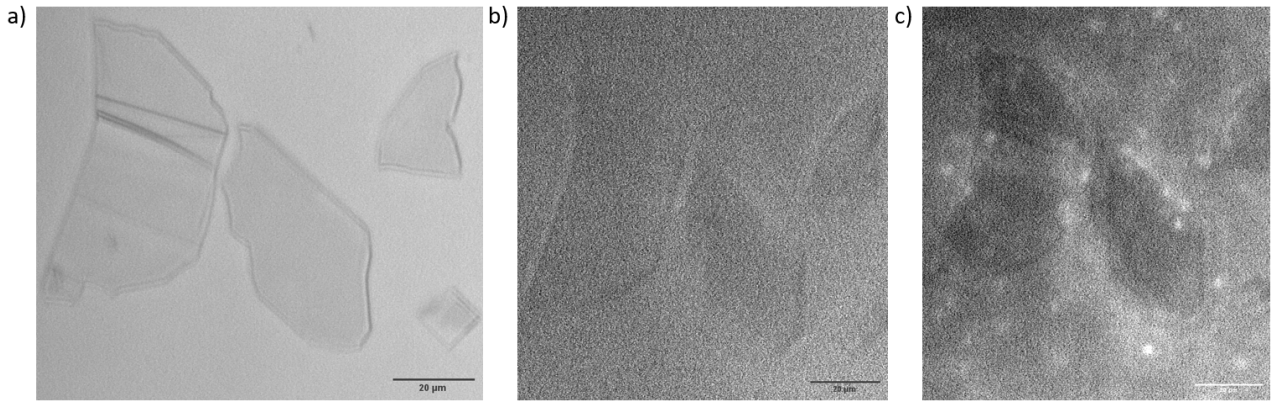

Figure 50: a) Bright field image of flake, b) 525 nm fluorescence image of flake, c) 525 nm fluorescence measurement after four minute incubation of 30 pM lambda DNA solution.

In this experiment multiple flakes were transferred at the same time onto the SAW device. The largest of the flakes has a size of 64 μm by 35 μm. The second largest flake had a size of 55 μm by 26 μm. These flakes had very little fluorescence compared to the background fluorescence. As such these flakes were suitable for actuation experiments.

A solution of 30 pM lambda DNA was prepared and was introduced into the flow cell of the SAW device. The lambda DNA molecules were circulated through the flow cell and then were allowed to incubate for a period of four minutes. Following this incubation, the first measurement of the molecules was taken. This initial measurement can be seen in Figure 50c. In this measurement, the lambda DNA can be clearly seen in the bulk solution as well as on the surface of the hBN and SAW device. The expected spot size of the molecules on the surface of the hBN is around 2.5 μm. Many of the molecules visible in this initial measurement were close to this spot size, meaning that they were very close to or in contact with the surface of the device.

After it was shown that the lambda DNA molecules were present and could be individually identified, it was possible to begin actuation experiments. Early in these experiments, one set of IDT wire bonds failed. As such, this experiment was conducted exclusively as a traveling wave experiment. In the first lambda DNA actuation experiment, a number of powers were used. It was found that power levels below 0 dBm did not cause noticeable motion of molecules in bulk or on the hBN surface. The experiment that presented the most interesting results was the actuation at 5 dBm. A snapshot of this lambda DNA motion under 5 dBm actuation can be found below in Figure 51.

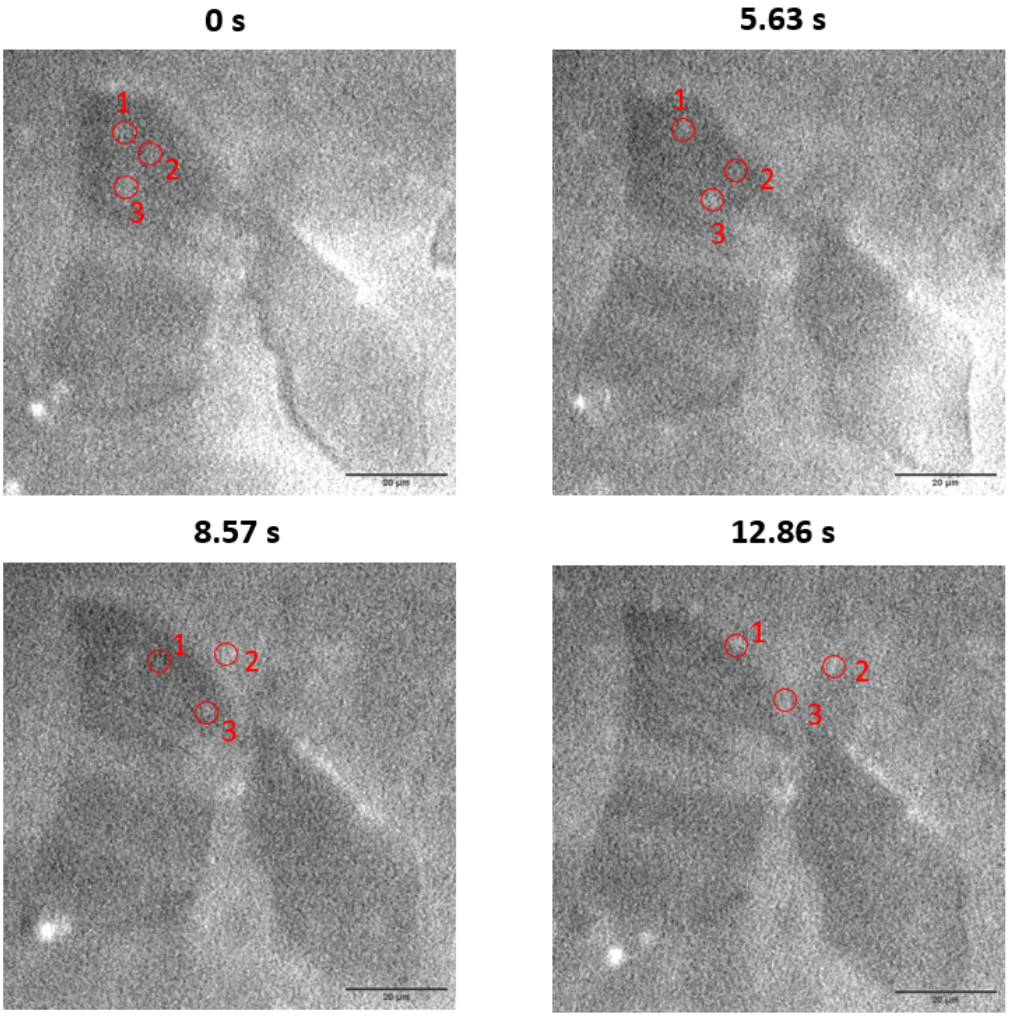

Figure 51: Time slices of lambda DNA under 5 dBm SAW actuation with three molecules tracked.

The SAW actuation of the lambda DNA at 5 dBm showed a very interesting result. The molecules in the bulk solution can be seen moving in a single direction due to the actuation. Along with this, it was possible to see molecules of the correct size that appear to be on the hBN surface also moving due to this actuation. These molecules were observed moving from outside the hBN flake and then moving onto the hBN flake when the SAW was actuated. After the actuation had ceased, these molecules appeared to remain on the hBN flake. During actuation, these molecules were found to generally travel in one direction. If they were outside the delay line, these molecules would move both towards the delay line and then towards one of the IDTs. For a 5 dBm actuation, the lambda DNA was found to travel at an average velocity of 2.83 $\mu m/s$ over the hBN surface. It was found that for higher power actuation very similar behaviour was observed but with a higher average velocity of the molecule.

It can be speculated that these lambda DNA molecules are exhibiting the desired unidirectional transport on the hBN surface. However, it is not possible to know with certainty that the molecules are actually attached to the surface. It is possible that this molecules are simply floating very near the surface or that only a single part of the molecule is attached. To investigate the true nature of this transport, it was necessary to conduct further experiments. As

such, a new flake of hBN was prepared and transferred onto the SAW device. The bright field and fluorescence images of this flake can be seen below in Figure 52a and Figure 52b.

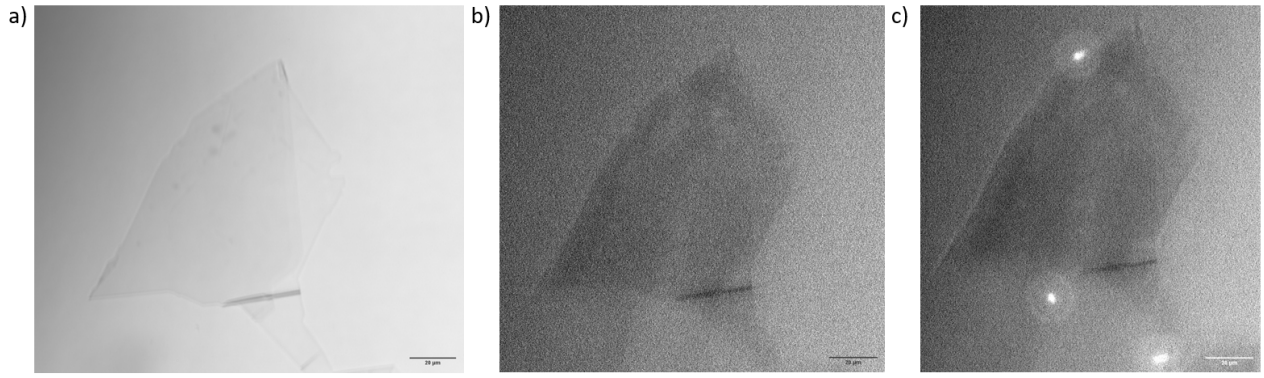

Figure 52: a) Bright field image of flake, b) 525 nm fluorescence image of flake, c) 525 nm fluorescence measurement after four minute incubation of 10 pM lambda DNA solution.

This flake has a size of 100 μm by 92 μm which is larger than many of the other flakes used. The fluorescence of the flake was found to be similar to background fluorescence and is therefore suitable for this experiment. A solution of lambda DNA with a concentration of 10 pM was prepared and introduced into the flow cell. These molecules were cycled over the hBN flake and then allowed to incubate. The initial measurement of the fluorescence was taken and can be seen in Figure 52c.

The initial fluorescence measurement shows that there is a significantly lower number of lambda DNA molecules both in bulk and on the surface. This is intentional because it limits the noise generated by a large concentration of molecules above the hBN. It also makes it much simpler to track single molecules when they do appear on or near the hBN flake.

The first experiment that was conducted using this flake was a standing wave experiment with a power level of 5 dBm. A snapshot of the motion observed during this actuation can be seen below in Figure 53.

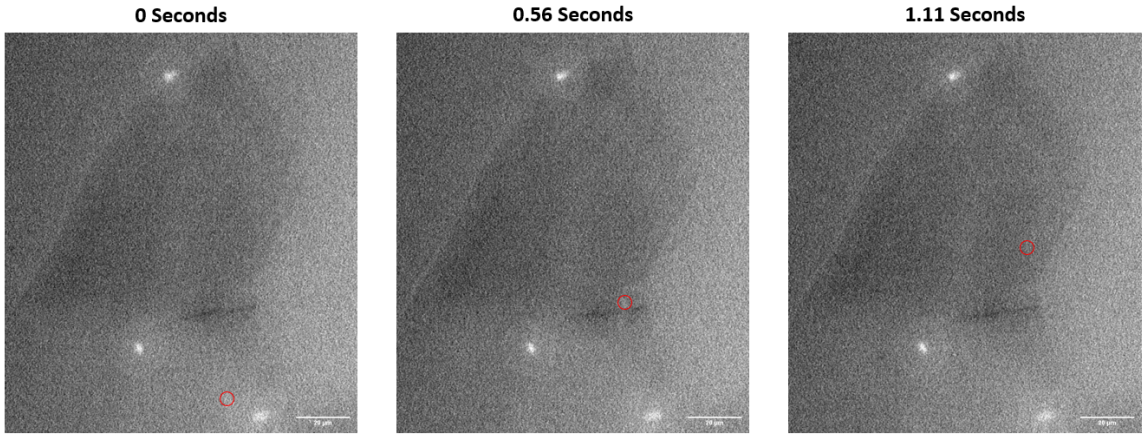

Figure 53: 5 dBm standing wave actuation of lambda DNA with one molecule tracked.

It was found that the molecule that was visible in this actuation was most likely near to, or on the surface. While the molecule was traveling over in the bulk solution, it had a speed of approximately 31.17 $\mu m/s$. While the molecule was traveling over the hBN flake, the molecule had an average velocity of around 20.86 $\mu m/s$. This may indicate that the molecule is slowed due to an interaction with the hBN surface. It is also possible that the molecule is slowing as it approaches the geometric center of the delay line. An illustration of the measured velocities of the molecule can be seen below if Figure 54.

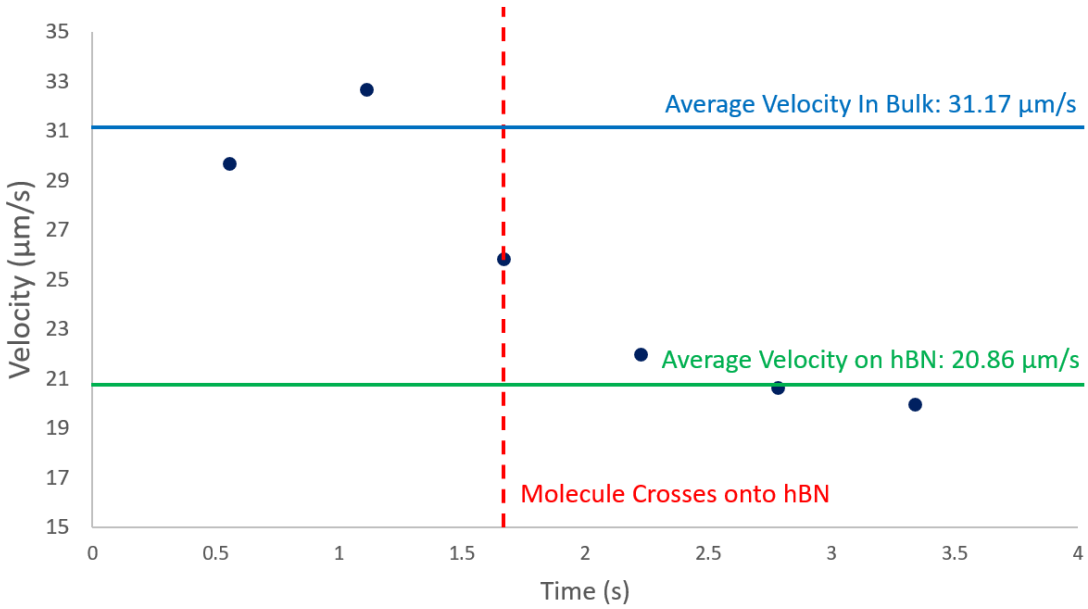

Figure 54: Velocity profile of molecule moving from bulk to hBN under 5 dBm standing wave actuation.

A second experiment was conducted in which the relative phase of the input signals was shifted by 60 degrees. The SAW device was then actuated with a power level of 5 dBm. In this experiment it was found that both molecules in the bulk solution as well as potentially on the hBN surface were manipulated. By comparing the speed and orientation of these molecules, it is possible to determine if lambda DNA interaction with hBN is slowing the transport speed of the molecules. A time sequence of one of the molecules that was found to be moving in the bulk solution can be seen below in Figure 55.

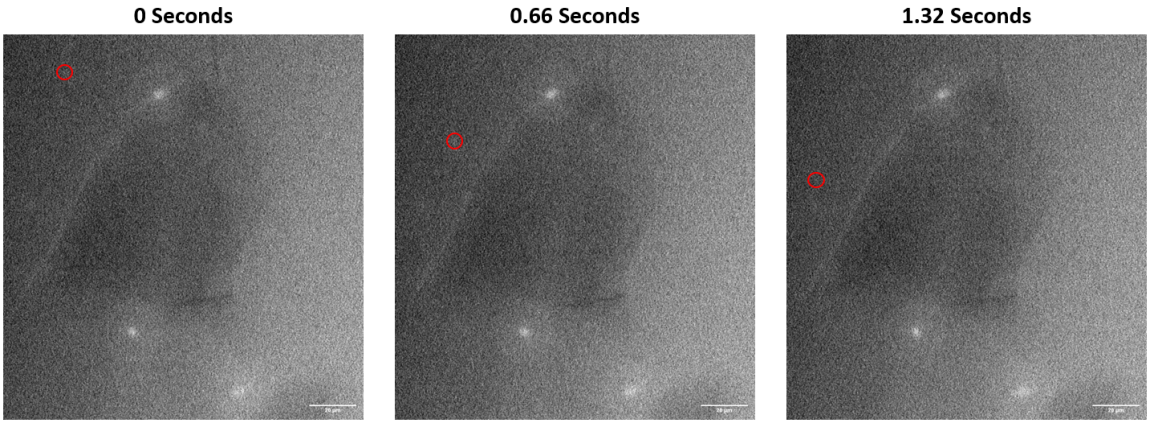

Figure 55: 5 dBm 60 degree phase shift beating wave actuation of lambda DNA with one molecule tracked in bulk solution.

It was found that the molecule being tracked in the bulk solution had an average velocity of 39.11 $\mu m/s$. By comparing this speed to the measured speed of the molecules that are moving across the hBN in the same actuation, it is possible to speculate about the interaction of lambda DNA and the hBN surface. As such, two molecules were tracked as the moved across the surface of the hBN flake during the same 5 dBm actuation at 60 degrees relative phase difference. A time sequence of these two molecules can be found below in Figure 56.

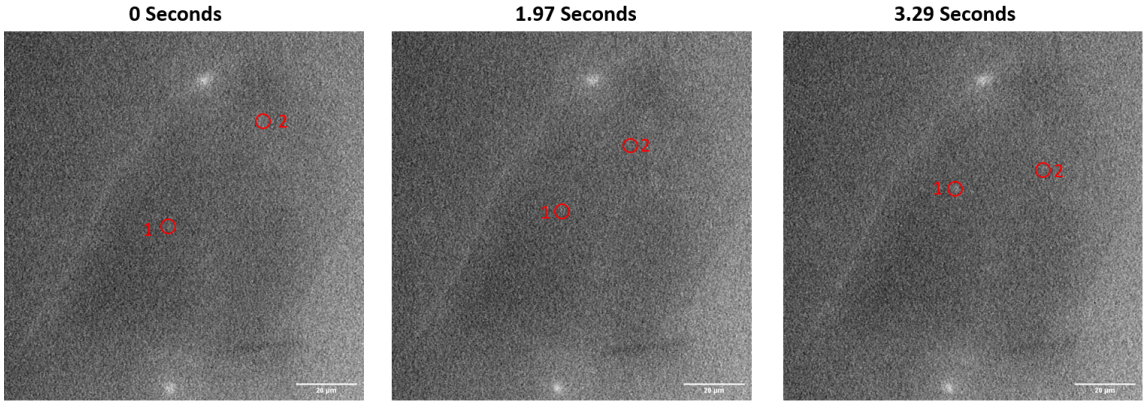

Figure 56: 5 dBm 60 degree phase shift beating wave actuation of lambda DNA with two molecule tracked on hBN surface.

The two molecules that were tracked on the surface of the hBN were observed to travel at about the same speed of 4.64 $\mu m/s$. It was also noticeable that these molecules are moving in opposite directions towards the geometric center of the delay line. A comparison of the velocity profiles between the molecule tracked in bulk and the two molecules tracked on hBN can be seen below in Figure 57.

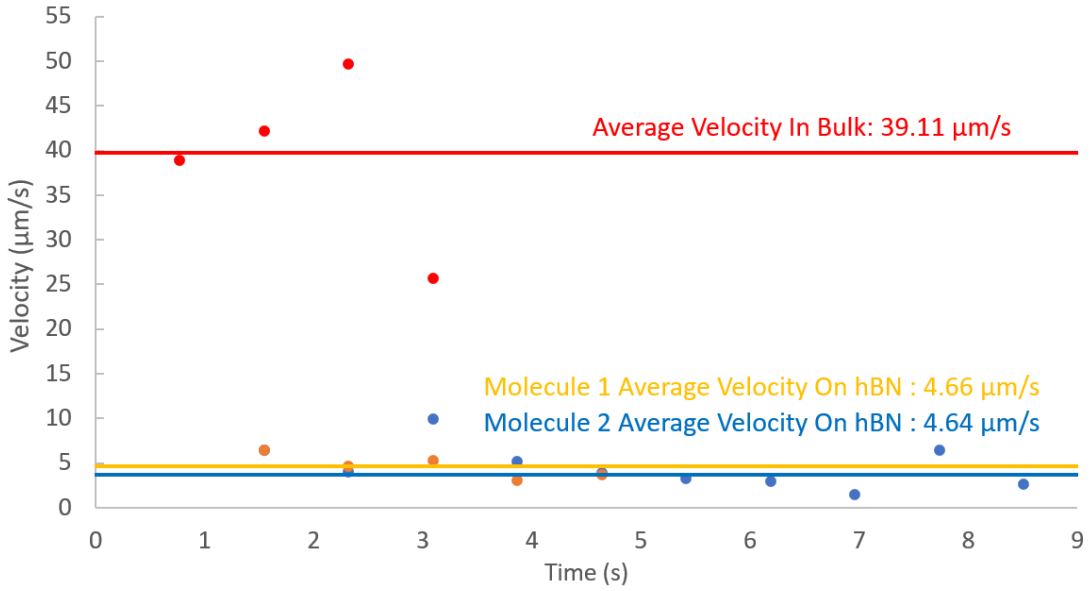

Figure 57: Velocity profiles of molecule moving in bulk and two molecules on hBN 5 dBm 60 degree phase shift beating wave actuation.

It can be speculated that the reduction in the speed of the molecules is a result of surface interaction with the hBN flake. Most likely, only a segment of the lambda DNA is interacting with the hBN as was seen in the diffusion analysis discussed in section 7.1. However, even if only a single segment of DNA is attached to the surface, this result still shows promise for the use of SAW actuation to transport biomolecules on hBN surfaces.

8 Conclusions and Outlook

This report strives to investigate and improve the understanding of localized transport of biomolecules on an hBN surface. The goal of this research was to investigate the possible application of hBN as a sequencing platform for proteins and other difficult to sequence biomolecules. We hypothesized that that SAW actuation of biomolecules could be an inexpensive non-contact method for the manipulation of molecules. The behavior of biomolecules on hBN surfaces as well as the manipulation of molecules on these surfaces has not been experimentally investigated before this report.

In order to conduct research into the SAW manipulation of molecules, it was first necessary to design and fabricate a SAW device. These devices were designed with a 10 μm acoustic wavelength and an operational frequency of 416 MHz. We successfully fabricated these devices and subsequently characterized them using a vector network analyzer to determine the frequency behavior. It was found that the thickness of the SiO_2 protective layer caused the SAW to have a slightly larger acoustic wavelength then originally designed. These SAW devices were characterized in both air and buffer solution, and it was found that the resonance frequencies and transmission powers of the SAW remained similar for both cases, as desired for measurements in liquid. This shows that the SAW device used is generating mostly in-plane shear horizontal waves with minimal fluid coupling. The results of the SAW characterization were in good agreement with literature.

Flakes of hBN were prepared through the use of mechanical exfoliation onto a SiO_2 substrate. Flakes with large surface areas and low thicknesses were then selected from this SiO_2 substrate for transfer onto SAW devices and glass cover slips. These flakes were transferred onto the final substrates through the use of a PPC bubble transfer process. Using this transfer method, we were successful in deterministically placing the selected flakes in the delay line region of the SAW device, with no visible damage to the flakes and with high reproducibility. Having the ability to select and deterministically transfer flakes onto SAW devices was key to this research.

Once the SAW device was prepared and the hBN surface was transferred onto the surface, we began experiments to analyze the behavior of biomolecules on the surface. The goal of these experiments was to answer the research questions posed in section 5. Each of these questions and the relevant conclusions from the experimental results can be seen below.

1. *How are the diffusion dynamics of single molecules affected by the interaction with hBN surfaces?*

   In section 7.1, the diffusion dynamics of various biomolecules adsorbed to hBN were analyzed. In these experiments, three different biomolecules were deposited onto hBN flakes and were allowed to incubate. The behaviour of these molecules was then measured and recorded.

   In the measurement of α-synuclein, it was not possible to observe the individual biomolecules due to low fluorescence and experimental limitations. It was found that fluorescence from these molecules appeared to be highest near the edges of the hBN flakes and at apparent defect regions of the hBN. Details regarding changes to the experimental setup that will potentially allow for single molecule measurements can be found in section 8.1.

   The behavior of M13mp18 DNA on hBN was also evaluated. These molecules were found to be evenly distributed on the hBN surface. However, it was not possible to observe any clear diffusion motion of these molecules on the hBN surface. It is possible that surface contamination or surface crowding resulted in the lack of motion of these molecules on the hBN surface. These molecules experienced rapid photo bleaching when adsorbed to the hBN surface. The cause of this photo bleaching is currently unknown, as hBN is a dielectric and not a fluorescence quencher.[69]

   The behavior of lambda DNA presented the most promising results of the three molecules. Fragmented lambda DNA molecules were observed freely diffusing on the surface of the hBN flake. This diffusion was similar to the random walking diffusion shown in many molecular dynamic simulations of single stranded DNA. However, when full molecules of lambda DNA came into contact with the hBN surface, no free diffusion was observed. It was found that many of these molecules appeared to have one piece of DNA attached to the surface while the remainder moved above the surface. At high concentrations of lambda DNA clumps of molecules were observed very slowly diffusing from regions of high concentration to low concentration.

   Overall, it was found that the various molecules had different behaviors when adsorbed to the hBN surface. It was expected that the molecules would adsorb to the hBN surface and freely diffuse. However, this behavior was only observed for fragmented lambda DNA. The other molecules became stuck on the hBN when they became adsorbed to the surface or were not observable. Further experiments will need to be conducted in order to determine the exact reason for this behavior.

2. *Can we manipulate single molecules using non-invasive acoustoelectronic forces generated with SAW devices?*

   In the actuation experiments conducted, it was found that the current manipulation approach had limited success in the manipulation of biomolecules on an hBN surface. In literature, it was found that under standing wave actuation molecules would often pattern onto the nodes or antinodes of the SAW. In this experiment, this behavior was not observed for any of the three test molecules. This lack of clear patterning is most likely a result of the acoustoelectric interaction of the biomolecules with the SAW. This behavior is strongly dependent on many design elements such as SAW wavelength, particle size, and buffer composition.[44]

   It was possible to observe the manipulation of both M13mp18 DNA, as well as lambda DNA that was in the bulk solution. When under actuation, it was found that both molecules tended to move towards the geometric center of the delay line and then towards one of the SAW IDTs. It is uncertain if this behaviour was a result of fluid coupling with the SAW or if it was true acoustoelectric manipulation.

3. *Can we demonstrate unidirectional single molecule transport and using combined hBN/-SAW devices?*

   In the manipulation of lambda DNA, it was possible to move molecules across the surface of hBN. Many lambda DNA molecules were observed moving near or on the surface of the hBN during actuation. As these molecules moved from the $SiO2$ surface to the hBN flake, it was found that the velocity of the molecules was decreased. This provides strong evidence to support the possibility that these molecules are interacting with the hBN surface while being transported.

   It was also found that the motion for molecules located in the delay line of the SAW device tended to always be in a uniform direction. Often these molecules were shown to only move horizontally towards one of the SAW IDTs and did not show shifts in the vertical direction. This did not hold true for molecules initially located outside of the delay line. These molecules tended to rapidly move towards the delay line and then begin moving towards one of the IDTs. As such it can be claimed that molecules located on the hBN surface inside of the SAW delay line were observed to experience unidirectional transport.

The results of this research will serve as a baseline for further research into the behavior of molecules on hBN surfaces. This research also provided preliminary support for the use of SAW devices and hBN surfaces for the manipulation of biomolecules. Through further work, it is believed that both of these processes can be understood and utilized for future protein sequencing applications. This technology presents a small step towards the ability to sequence new proteins, overcoming some limitations of existing protein sequencing methods.

8.1 Future Work

The current preliminary results found in this report are useful for setting a baseline for the manipulation of biomolecules on hBN with a SAW device. However, there were a number of challenges that were faced during experiments that restricted the quality of data that could be gathered. Along with this, many of the processes used to conduct this research are not

well investigated or modeled. By conducting further research into these processes, it will be possible to conduct more controlled measurements. In order to improve upon the processes and experimental results, there are a number of unknowns that can be investigated. These unknowns are outlined below.

8.1.1 Modeling of SAW Device

In order to more fully understand the behavior seen in the preliminary result, it was deemed necessary to model the behavior of the SAW device in this system. Currently it is not well understood how the mechanical and electrical fields are affected by the presence of the hBN flake and SiO_2 layer on the surface of the device. Understanding the acoustoelectric effect may be critical for developing a more advanced control scheme for the manipulation of bio molecules with a SAW device.

Currently one of the best methods for modeling these fields is through the use of a software such as COMSOL Multiphysics. Many different models of lithium tantalate-based SAW devices have been simulated using COMSOL.[70,71] The SAW devices in these simulations often have a very similar design to the design seen in Section 6.1. Often these simulations use a standard two IDT device with a delay line between the IDTs. These models enable the simulation and visualization of both the mechanical and electrical waves present during actuation. An example of this visualization for a SAW device on lithium tantalate can be seen below in Figure 58.

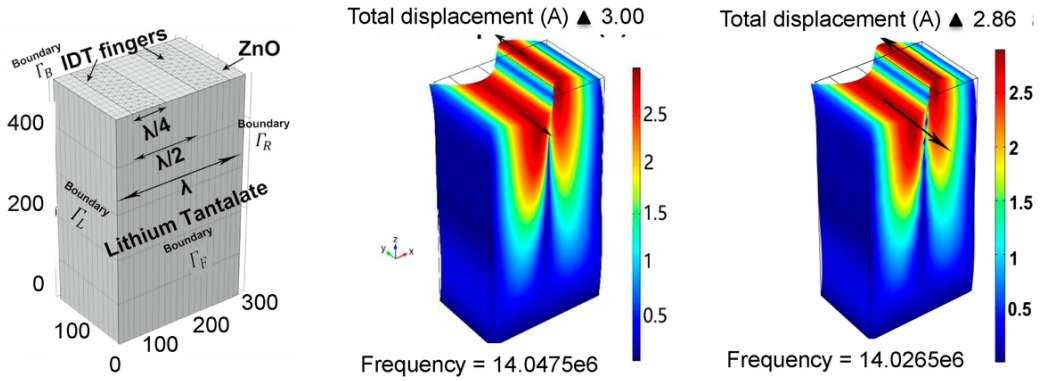

Figure 58: COMSOL visualization of acoustic wave on lithium tantalate SAW device under actuation.[72]

Using this simulation, it may be possible to correlate the motion of molecules under actuation to the acoustoelectric fields generated by the SAW device. Some modification to existing COMSOL models is necessary in order to include a hBN flake on the surface of the SAW device. This may prove challenging, as some of the properties of thin hBN are not fully modeled.

By more thoroughly understanding the behavior of the SAW device, it is possible to begin to develop a more empirical understanding of the behavior seen in this report. As such, the development of these simulations are a clear next step to understand the manipulation of biomolecules adsorbed to an hBN surface with SAW devices.

8.1.2 Investigation into hBN Surface Contamination

A critical component of the manufacturing process used in this research is the PPC transfer process. This process is what allows for the selection of optimal hBN flakes and facilitates the transfer of these flakes onto the SAW device. As such, it is important to fully understand this process and how it affects the quality of the hBN. It is possible that this transfer may cause some contamination transfer from the surface of the PPC film onto the surface of the hBN during the transfer process. This residue may be one factor that is limiting the diffusion of biomolecules on the surface of the hBN. Those contaminants are not visible in either bright field or fluorescence images. This makes it difficult to determine if the flakes are in fact being contaminated by the PPC transfer process.

To determine if the PPC transfer process is contaminating the hBN flakes, it may be necessary to use Raman spectroscopy. Raman spectroscopy would enable the evaluation of the exact chemical composition on the surface of the hBN flake.[73] Using this composition, it could be determined if significant contamination occurs during the PPC transfer process. The Raman spectra of a direct transfer hBN flake would be compared to the Raman spectra of a PPC transferred flake in order to determine the level of contamination. If a significant difference in spectra is found it would be known that this transfer method causes significant contamination.

If it were found that the PPC transfer process causes surface contamination, it would be necessary to remove this contamination before conducting diffusion or actuation experiments. One possible method for the removal of these contaminants is through the use of annealing. It has been found that high temperature annealing of the hBN flakes can remove most organic residues created by adhesives.[28,73] An example of the Raman spectra of an exfoliated hBN flake before and after annealing can be seen below in Figure 59.

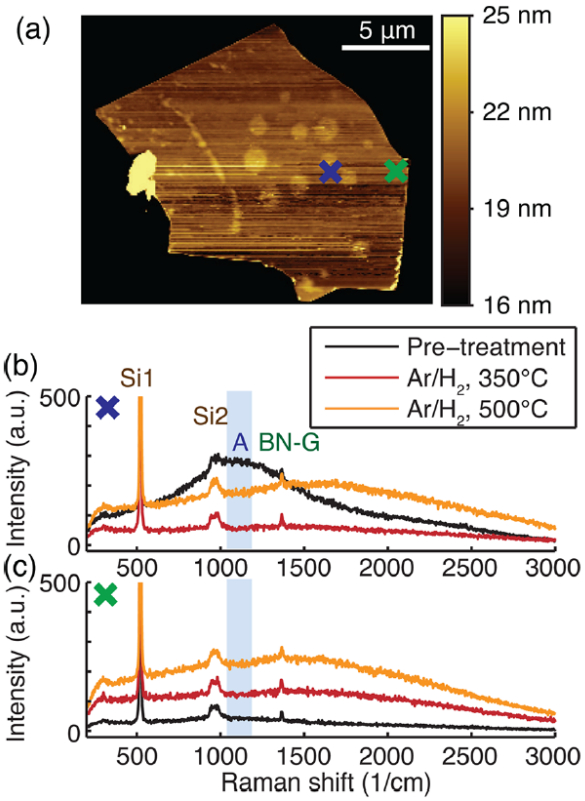

Figure 59: a) An hBN flake with adhesive residue b) The Raman spectra before and after annealing at two temperatures showing a reduction of organic materials on the surface in the two regions marked with an X.[73]

There is a range of environments and temperatures that can be used in this annealing process. It would be necessary to select a temperature and environment that limits potential damage to the SAW device. In order to find this temperature, multiple experiments will need to be conducted to make sure the SAW IDTs do not melt or crack.

By investigating and removing surface contamination on the hBN flake, it is possible to eliminate one major unknown variable from future experiments. Once this surface contamination is removed, it would be of interest to conduct diffusion experiments such as those seen in section 7.1. If the results found in these new experiments differ greatly from the previous experiments, then it can be concluded that PPC transfer contamination significantly affects the biomolecule interaction with hBN.

8.1.3 Optical and Experimental Setup Improvements

During the experiments conducted for this research, both the optical and mechanical experimental setup could be improved upon. One main challenge that was detrimental to the quality of measured data was the loss of light due to the optical stack presented in Figure 23. In order to measure fluorescence from biomolecules, it was necessary for the excitation laser to pass through water, glass, air, lithium tantalate, silicon dioxide, and finally hBN. It was also necessary for the much lower intensity fluorescence from the molecules to pass through the same materials in order to return to the objective. Because of this long optical path through many materials, the emitted fluorescence most likely lost much of its intensity and experienced

refraction effects. This results in a low intensity image with optical aberration's to be measured. Multiple different optical stacks were tested in order to reduce these effect with minimal success.

In order to improve the measurement of the fluorescence from the biomolecules, it is necessary to take a different optical approach. To reduce the amount of loss fluorescence and decrease aberrations, it is necessary to reduce the amount of materials the light passes through. One promising approach to achieve this is to flip the SAW device so that the surface of the hBN is facing the objective. This approach would mean that the fluorescence would only need to pass through water, glass, and buffer to be measured.

By flipping the SAW device the experimental setup must be redesigned. One major change is the need for a smaller, thinner flow cell that is made of glass. One possible solution is to use a simple flow cell made using double sided kapton tape and a glass cover slip. An illustration of this proposed flow cell can be seen below in Figure 60.

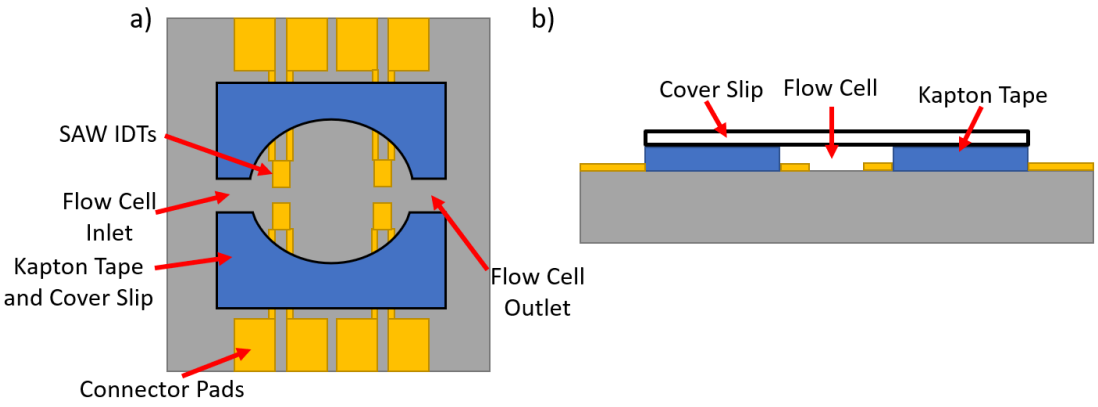

Figure 60: a) Top view of flow cell on SAW device, b) Side view of flow cell on SAW device.

It can be seen that this new flow cell design is very different from the previous design. It is also possible to see that it is not compatible with the current SAW device design. Currently, with this SAW design, it would not be possible to interface the IDTs with the macroscopic electronics due to the short IDT leads. This configuration also presents challenges for wire bonding the device.

By increasing the size of the SAW substrate and increasing the length of the SAW IDT leads, it is possible to implement the new flow cell. These changes also allow for the implementation of changes that can decrease time and difficulty involved in the setup of the PCB assembly. Currently, the assembly process speed is restricted by the need to wire bond the SAW device. This is a tedious process that often results in weak connections that break during experiments. An alternative to wire bonding is the use of pressure contacts. By directly contacting the SAW IDT leads to contact pads on the PCB, it is possible to quickly and easily assemble the PCB assembly. The proposed implementation of the flow cell, as well as the contact pins, can be found below in Figure 61.

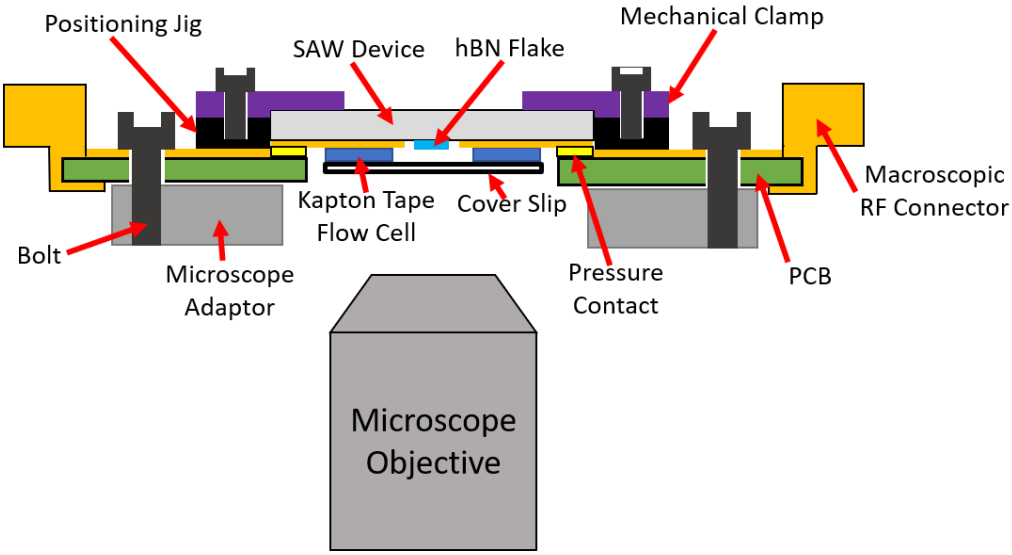

Figure 61: Overview of flipped SAW device with pressure contacts.

The new SAW PCB assembly will first be tested in the wide field epifluorescence microscope described in Section 6.6. If it is found that the new configuration facilitates improved measurements, then the molecule diffusion and actuation experiments will be repeated.

A final change that could be made to the experimental setup is the type of fluorescence microscope used. It was found that when using wide field epifluorescence, it is very difficult to determine with certainty if biomolecules are located on the surface of the saw device or if they are located in the bulk solution. As such, it is necessary to use a microscopy method that has a very narrow focal range. One such microscope is a confocal flourescence microscope. By using this method it would be possible to observe the molecules that are on the hBN surface more precisely. As such, this microscope is being considered for implementation into future experiments.

Appendices

A Material Properties of Y-36° Cut Lithium Tantalate

Material Property	Symbol	Value
Density	ρ	7.465 x 10^3 kg / m^3
Thickness	τ	500 µm
Transmissivity	*T*	5.9×10-11<s<2.0*10-10 at 25°C
Cut Orientation	°	Y-36°
Coupling Coefficient	k^2	5%
Surface Wave Velocity	*v*	4160 m/s
Refractive Index at 632.8 nm	n_0	2.1787

Figure 62: Properties of lithium tantalate used in this research.

B Control of 1.5 μm Fluorescent Beads with SAW Actuation

Before conducting the SAW actuation experiments seen in Section 7.2, a test of the SAW device was conducted with 1.5 μm fluorescent polystyrene beads. The beads were mixed with buffer and then introduced into the flow cell, where they were allowed to settle for five minutes. An initial fluorescence image of these beads on the SAW device can be seen below in Figure 63.

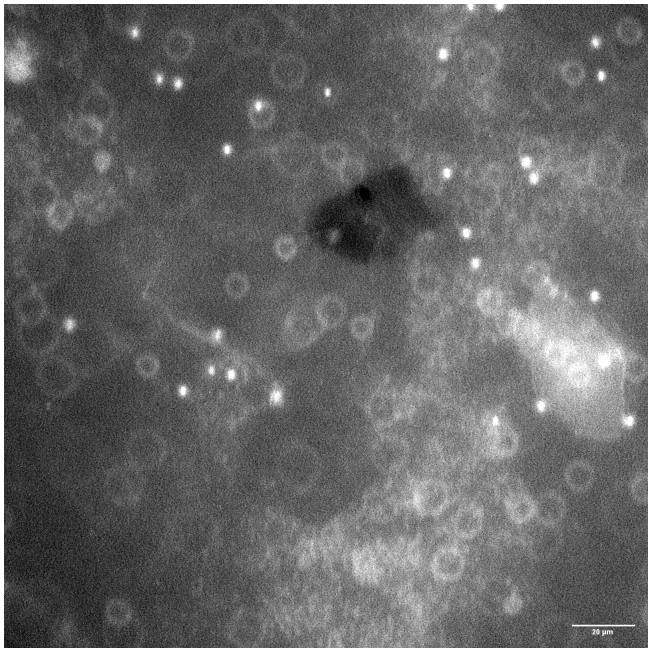

Figure 63: Incubated 1.5 μm fluorescent beads on SAW device.

A -5 dBm actuation power was applied to the SAW device in order to manipulate the beads. A standing wave was the first experiment conducted followed by two beating wave experiments. For the beating wave experiments the phase shift was ±60 degrees. An overview fo the observed motion for all three of these actuations can be seen below in Figure 64.

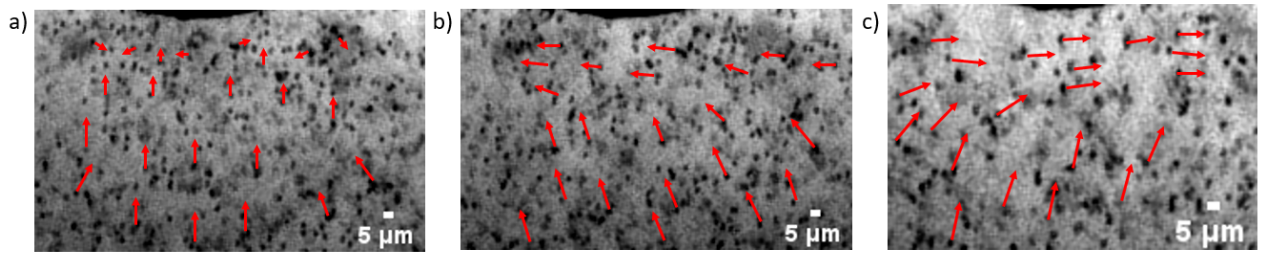

Figure 64: a) Standing wave actuation of SAW device, b) Beating wave actuation with -60 degree phase shift, c) Beating wave actuation with +60 degree phase shift.

During the standing wave experiment the beads were observed to move towards the delay line of the SAW device. Once these beads reached the delay line, most of their directional motions stopped. These beads demonstrated localized random motion once at the geometric center of the delay line.

In both beating wave experiments, the beads were observed to first approach the geometric center of the delay line. Once they reached the center, the beads were found to unidirectionally move either left or right depending on the phase shift. For the -60 degree phase shift the beads moved to the left and for the 60 degree phase shift the beads moved to the right. These bead actuation experiments showed that it was possible to unidirectional manipulate objects in the bulk solution.

References

(1) Restrepo-Pérez, L.; Joo, C.; Dekker, C. Paving the way to single-molecule protein sequencing, 2018.

(2) Breda, A.; Fonseca Valadares, N.; Norberto De Souza, O.; Garratt, R. C. *Chapter A06. Protein Structure, Modelling and Applications 1. Why Is It Important to Study Proteins?*; tech. rep.; Bethesda: National Center for Biotechnology Information (US), 2006, pp 261–272.

(3) Callahan, N.; Tullman, J.; Kelman, Z.; Marino, J. Strategies for Development of a Next-Generation Protein Sequencing Platform, 2020.

(4) Alfaro, J. A. et al. The emerging landscape of single-molecule protein sequencing technologies, 2021.

(5) Wilhelm, M. et al. *Nature* **2014**, *509*, 582–587.

(6) Zubarev, R. A. *Proteomics* **2013**, *13*, 723–726.

(7) Edman, P. *Acta Chemica Scandinavica* **1950**, *4*, 283–293.

(8) Solier, C.; Langen, H. Antibody-based proteomics and biomarker research-current status and limitations, 2014.

(9) Brett, G. M.; Chambers, S. J.; Huang, L.; Morgan, M. R. A. *Design and development of immunoassays for detection of proteins*; tech. rep.; Colney: Institute of Food Research, 1999, pp 401–406.

(10) Venkatesan, B. M.; Bashir, R. Nanopore sensors for nucleic acid analysis, 2011.

(11) Venkatesan, B. M.; Polans, J.; Comer, J.; Sridhar, S.; Wendell, D.; Aksimentiev, A.; Bashir, R. *Biomedical Microdevices* **2011**, *13*, 671–682.

(12) Restrepo-Pérez, L.; John, S.; Aksimentiev, A.; Joo, C.; Dekker, C. *Nanoscale* **2017**, *9*, 11685–11693.

(13) Biswas, S.; Song, W.; Borges, C.; Lindsay, S.; Zhang, P. *ACS Nano* **2015**, *9*, 9652–9664.

(14) Varongchayakul, N.; Song, J.; Meller, A.; Grinstaff, M. W. Single-molecule protein sensing in a nanopore: a tutorial, 2018.

(15) Asandei, A.; Di Muccio, G.; Schiopu, I.; Mereuta, L.; Dragomir, I. S.; Chinappi, M.; Luchian, T. *Small Methods* **2020**, *4*, DOI: 10.1002/smtd.201900595.

(16) Ohayon, S.; Girsault, A.; Nasser, M.; Shen-Orr, S.; Meller, A. *PLoS Computational Biology* **2019**, *15*, DOI: 10.1371/journal.pcbi.1007067.

(17) Luan, B.; Kuroda, M. A. *ACS Nano* **2020**, *14*, 13137–13145.

(18) Min, S. K.; Kim, W. Y.; Cho, Y.; Kim, K. S. *Nature Nanotechnology* **2011**, *6*, 162–165.

(19) Lin, Q.; Zou, X.; Zhou, G.; Liu, R.; Wu, J.; Li, J.; Duan, W. *Physical Chemistry Chemical Physics* **2011**, *13*, 12225–12230.

(20) Wang, J.; Ma, F.; Sun, M. Graphene, hexagonal boron nitride, and their heterostructures: properties and applications, 2017.

(21) Zhang, S.; Li, J.; Wu, H.; Li, X.; Guo, W. *Advanced Materials Interfaces* **2018**, *5*, DOI: 10.1002/admi.201800208.

(22) Liu, Z.; Ma, L.; Shi, G.; Zhou, W.; Gong, Y.; Lei, S.; Yang, X.; Zhang, J.; Yu, J.; Hackenberg, K. P.; Babakhani, A.; Idrobo, J. C.; Vajtai, R.; Lou, J.; Ajayan, P. M. *Nature Nanotechnology* **2013**, *8*, 119–124.

(23) Castellanos-Gomez, A.; Buscema, M.; Molenaar, R.; Singh, V.; Janssen, L.; Van Der Zant, H. S.; Steele, G. A. *2D Materials* **2014**, *1*, DOI: 10.1088/2053-1583/1/1/011002.

(24) He, Z.; Zhou, R. *ACS Nano* **2021**, *15*, 11704–11710.

(25) Luan, B. *Nano Futures* **2020**, *4*, 1–11.

(26) He, Z.; Zhou, R. *Nanoscale* **2020**, *12*, 13822–13828.

(27) Zhan, Y.; Yan, J.; Wu, M.; Guo, L.; Lin, Z.; Qiu, B.; Chen, G.; Wong, K. y. *Talanta* **2017**, *174*, 365–371.

(28) Ziegler, J.; Klaiss, R.; Blaikie, A.; Miller, D.; Horowitz, V. R.; Alemán, B. J. *Nano Letters* **2019**, *19*, 2121–2127.

(29) Mackoit-Sinkevičienė, M. Point defects as single-photon emitters in hexagonal boron nitride: theoretical study, Ph.D. Thesis, Lithuania: Vilnius University, 2020.

(30) Nan, Z.; Hao, C.; Ye, X.; Feng, Y.; Sun, R. *Spectrochimica Acta - Part A: Molecular and Biomolecular Spectroscopy* **2019**, *210*, 348–354.

(31) Li, S.; Aphale, A. N.; MacWan, I. G.; Patra, P. K.; Gonzalez, W. G.; Miksovska, J.; Leblanc, R. M. *ACS Applied Materials and Interfaces* **2012**, *4*, 7069–7075.

(32) Tian, F.; Lyu, J.; Shi, J.; Yang, M. Graphene and graphene-like two-denominational materials based fluorescence resonance energy transfer (FRET) assays for biological applications, 2017.

(33) Gaudreau, L.; Tielrooij, K. J.; Prawiroatmodjo, G. E.; Osmond, J.; De Abajo, F. J.; Koppens, F. H. *Nano Letters* **2013**, *13*, 2030–2035.

(34) Wilson, J.; Sloman, L.; He, Z.; Aksimentiev, A. *Advanced Functional Materials* **2016**, *26*, 4830–4838.

(35) Luan, B.; Zhou, R. *Nature Communications* **2019**, *10*, DOI: 10.1038/s41467-019-12584-w.

(36) Shankla, M.; Aksimentiev, A. *Nature Nanotechnology* **2019**, *14*, 858–865.

(37) Banerjee, A. G.; Chowdhury, S.; Losert, W.; Gupta, S. K. *Journal of Biomedical Optics* **2011**, *16*, 051302.

(38) Keyser, U. F.; Koeleman, B. N.; Van Dorp, S.; Krapf, D.; Smeets, R. M.; Lemay, S. G.; Dekker, N. H.; Dekker, C. *Nature Physics* **2006**, *2*, 473–477.

(39) Bustamante, C. J.; Chemla, Y. R.; Liu, S.; Wang, M. D. *Nature Reviews Methods Primers* **2021**, *1*, DOI: 10.1038/s43586-021-00021-6.

(40) Smith, A. *Surface acoustic wave-induced dielectrophoresis: Lab on a Chip cell sorting technology for autologous cell therapies*; tech. rep.; 2017.

(41) Rocha-Gaso, M.-I.; March-Iborra, C.; Montoya-Baides, Á.; Arnau-Vives, A. *Sensors* **2009**, *9*, 5740–5769.

(42) Connacher, W.; Zhang, N.; Huang, A.; Mei, J.; Zhang, S.; Gopesh, T.; Friend, J. Micro/-nano acoustofluidics: Materials, phenomena, design, devices, and applications, 2018.

(43) Hennig, M.; Wolff, M.; Neumann, J.; Wixforth, A.; Schneider, M. F.; Rädler, J. O. *Langmuir* **2011**, *27*, 14721–14725.

(44) Zhang, P.; Rufo, J.; Chen, C.; Xia, J.; Tian, Z.; Zhang, L.; Hao, N.; Zhong, Z.; Gu, Y.; Chakrabarty, K.; Huang, T. J. *Nature Communications* **2021**, *12*, DOI: 10.1038/s41467-021-24101-z.

(45) Cular, S.; Branch, D. W.; Bhethanabotla, V. R.; Meyer, G. D.; Craighead, H. G. *IEEE Sensors Journal* **2008**, *8*, 314–320.

(46) Neumann, J.; Hennig, M.; Wixforth, A.; Manus, S.; Rädler, J. O.; Schneider, M. F. *Nano Letters* **2010**, *10*, 2903–2908.

(47) Chen, Y.; Ding, X.; Steven Lin, S. C.; Yang, S.; Huang, P. H.; Nama, N.; Zhao, Y.; Nawaz, A. A.; Guo, F.; Wang, W.; Gu, Y.; Mallouk, T. E.; Huang, T. J. *ACS Nano* **2013**, *7*, 3306–3314.

(48) Morgan, H.; Hughes, M. P.; Green, N. G. *Biophysical Journal* **1999**, *77*, 516–525.

(49) Romero-Creel, M. F.; Goodrich, E.; Polniak, D. V.; Lapizco-Encinas, B. H. *Micromachines* **2017**, *8*, DOI: 10.3390/mi8080239.

(50) Kurosawa, O.; Suzuki, S.; Nishizaka, T.; Shinohara, T. *IEEE Transactions on Industry Applications* **1994**, *30*, 835–843.

(51) Walter, N. G.; Bustamante, C. Introduction to single molecule imaging and mechanics: Seeing and touching molecules one at a time, 2014.

(52) Weiss, S. Fluorescence spectroscopy of single biomolecules, 1999.

(53) Anthony, S.; Zhang, L.; Granick, S. *Langmuir* **2006**, *22*, 5266–5272.

(54) Ganji, M.; Kim, S. H.; Van Der Torre, J.; Abbondanzieri, E.; Dekker, C. *Nano Letters* **2016**, *16*, 4699–4707.

(55) Sankaranarayanan, S. K.; Singh, R.; Bhethanabotla, V. R. In *Journal of Applied Physics*, 2010; Vol. 108.

(56) Collins, D. J.; Morahan, B.; Garcia-Bustos, J.; Doerig, C.; Plebanski, M.; Neild, A. *Nature Communications* **2015**, *6*, DOI: 10.1038/ncomms9686.

(57) Rimeika, R.; Čiplys, D.; Shur, M. *Acta Physica Polonica A* **2015**, *127*, 52–54.

(58) Van Der Knijff, I. C. *Moved by sound Design and characterization of SAW devices for acoustic actuation of biomembranes using network analysis and atomic force microscopy*; tech. rep.

(59) Van Der Knijff, I. C. *Moved by sound Design and characterization of SAW devices for acoustic actuation of biomembranes using network analysis and atomic force microscopy*; tech. rep.

(60) Barié, N.; Wessa, T.; Bruns, M.; Rapp, M. *Talanta* **2004**, *62*, 71–79.

(61) Zhang, K.; Feng, Y.; Wang, F.; Yang, Z.; Wang, J. Two dimensional hexagonal boron nitride (2D-hBN): Synthesis, properties and applications, 2017.

(62) Fournier, C.; Plaud, A.; Roux, S.; Pierret, A.; Rosticher, M.; Watanabe, K.; Taniguchi, T.; Buil, S.; Quélin, X.; Barjon, J.; Hermier, J. P.; Delteil, A. *Nature Communications* **2021**, *12*, DOI: 10.1038/s41467-021-24019-6.

(63) Blackstone, T. *Improving localization confidence in electron beam induced super-resolution of fluorescent probes in iCLEM*; tech. rep.; Delft: TU Delft, 2018.

(64) Cho, S.; Jang, J.; Song, C.; Lee, H.; Ganesan, P.; Yoon, T. Y.; Kim, M. W.; Choi, M. C.; Ihee, H.; Heo, W. D.; Park, Y. *Scientific Reports* **2013**, *3*, DOI: 10.1038/srep01208.

(65) Ganji, M.; Kim, S. H.; Van Der Torre, J.; Abbondanzieri, E.; Dekker, C. *Intercalation-based single-molecule fluorescence assay to study DNA supercoil dynamics*; tech. rep.

(66) Messing, J., *Methods in Enzymology*; Academic Press: 1983; Vol. 101, pp 20–78.

(67) Stefanis, L. *Cold Spring Harbor Perspectives in Medicine* **2012**, *2*, DOI: 10.1101/cshperspect.a009399.

(68) Pethig, R. *Electrophoresis* **2019**, *40*, 2575–2583.

(69) Gan, W.; Tserkezis, C.; Cai, Q.; Falin, A.; Mateti, S.; Nguyen, M.; Aharonovich, I.; Watanabe, K.; Taniguchi, T.; Huang, F.; Song, L.; Kong, L.; Chen, Y.; Li, L. H. *ACS Nano* **2019**, *13*, 12184–12191.

(70) Wang, T.; Green, R.; Guldiken, R.; Wang, J.; Mohapatra, S.; Mohapatra, S. S. *Sensors (Switzerland)* **2019**, *19*, DOI: 10.3390/s19081749.

(71) Zhang, Q.; Chen, Z.; Chen, Y.; Dong, J.; Tang, P.; Fu, S.; Wu, H.; Ma, J.; Zhao, X. *Micromachines* **2021**, *12*, 1–14.

(72) Wang, T.; Green, R.; Nair, R. R.; Howell, M.; Mohapatra, S.; Guldiken, R.; Mohapatra, S. S. *Sensors (Switzerland)* **2015**, *15*, 32045–32055.

(73) Garcia, A. G.; Neumann, M.; Amet, F.; Williams, J. R.; Watanabe, K.; Taniguchi, T.; Goldhaber-Gordon, D. *Nano Letters* **2012**, *12*, 4449–4454.